

**An Ultrasonic Investigation of the Effect of Voids on the
Mechanical Properties of Bread Dough and the Role of
Gas Cells in Determining the Cellular Structure of
Freeze-dried Breadcrumb**

By

Hussein Mohamed Elmehdi

A thesis submitted to the Faculty of Graduate Studies as a
requirement for the degree of
Doctorate of Philosophy

Faculty of Graduate Studies
Department of Physics and Astronomy/ Food Science
University of Manitoba
Winnipeg, Manitoba, Canada
R3T 2N2

October 2001



National Library
of Canada

Acquisitions and
Bibliographic Services

395 Wellington Street
Ottawa ON K1A 0N4
Canada

Bibliothèque nationale
du Canada

Acquisitions et
services bibliographiques

395, rue Wellington
Ottawa ON K1A 0N4
Canada

Your de Votre référence

Our de Notre référence

The author has granted a non-exclusive licence allowing the National Library of Canada to reproduce, loan, distribute or sell copies of this thesis in microform, paper or electronic formats.

The author retains ownership of the copyright in this thesis. Neither the thesis nor substantial extracts from it may be printed or otherwise reproduced without the author's permission.

L'auteur a accordé une licence non exclusive permettant à la Bibliothèque nationale du Canada de reproduire, prêter, distribuer ou vendre des copies de cette thèse sous la forme de microfiche/film, de reproduction sur papier ou sur format électronique.

L'auteur conserve la propriété du droit d'auteur qui protège cette thèse. Ni la thèse ni des extraits substantiels de celle-ci ne doivent être imprimés ou autrement reproduits sans son autorisation.

0-612-62634-2

THE UNIVERSITY OF MANITOBA
FACULTY OF GRADUATE STUDIES

COPYRIGHT PERMISSION

AN ULTRASONIC INVESTIGATION OF THE EFFECT OF VOIDS ON THE MECHANICAL
PROPERTIES OF BREAD DOUGH AND THE ROLE OF GAS CELLS IN DETERMINING
THE CELLULAR STRUCTURE OF FREEZE-DRIED BREADCRUMB

BY

HUSSEIN MOHAMED ELMEHDI

A Thesis/Practicum submitted to the Faculty of Graduate Studies of The University of
Manitoba in partial fulfillment of the requirement of the degree

of

DOCTOR OF PHILOSOPHY

HUSSEIN MOHAMED ELMEHDI © 2001

Permission has been granted to the Library of the University of Manitoba to lend or sell copies of this thesis/practicum, to the National Library of Canada to microfilm this thesis and to lend or sell copies of the film, and to University Microfilms Inc. to publish an abstract of this thesis/practicum.

This reproduction or copy of this thesis has been made available by authority of the copyright owner solely for the purpose of private study and research, and may only be reproduced and copied as permitted by copyright laws or with express written authorization from the copyright owner.

بِسْمِ اللَّهِ الرَّحْمَنِ الرَّحِيمِ

Abstract

This thesis is an analysis of voids in the breadmaking process, more specifically the effect of gas cells entrapped in the dough during mixing, their expansion during fermentation, and their relationship to the breadcrumb structure in the final product. This is important to food scientists because the voids ultimately influence the structural integrity of bread and hence its quality. Understanding how voids affect the viscoelastic properties of dough is also a challenging problem in soft condensed matter physics. Longitudinal ultrasonic velocity and attenuation measurements, performed at 54 kHz, investigated changes in the mechanical properties of dough and bread as void concentration was varied.

In the first part of the thesis, the effect of voids on the properties of unyeasted dough at the end of mixing was investigated. As ϕ is increased, the attenuation coefficient increased linearly with ϕ ; hence the change in attenuation is proportional to the number of voids, allowing the combined effects of scattering and absorption by single voids to be directly determined. By contrast, the ultrasonic velocity decreased dramatically with increasing ϕ in the range $0.012 < \phi < 0.03$, while at higher ϕ , the velocity decrease was less rapid. An effective medium model successfully modeled the viscoelastic behavior of the dough at all void fraction values, provided that the shear modulus of the matrix was permitted to vary. The same ultrasonic technique was also used to monitor the increase in gas cell size due to CO_2 production during fermentation of yeasted dough. A large decrease in velocity and an increase in the attenuation coefficient were observed as the gas cells grew. In addition, at early fermentation times, a substantial contribution to the velocity decrease arises from a reduction in the shear

modulus of the dough matrix. This occurs because the pH drops as CO₂ molecules dissolve in the matrix and intermolecular interactions are weakened due to protein chain charge repulsion effects.

In the second part of the thesis, freeze-dried breadcrumb structure was investigated. To change the size of the air cells, the dough was proofed for various times. Ultrasonic velocity and amplitude decrease with increasing ϕ . The experimental data were found to be in reasonable agreement with theoretical models for the elasticity of isotropic cellular foams and tortuosity. The effects of anisotropy in breadcrumb structure were studied by compressing samples uniaxially, thereby transforming the shape of the air cells from approximately spherical to elongated ellipsoids. Ultrasonic measurements were taken in the directions parallel and perpendicular to the strain. These results indicated that the path by which sound propagates is critical. The data were interpreted using the same two theoretical models, taking into account anisotropy effects. The tortuosity model was able to interpret the void fraction dependence of the velocity along the two orthogonal directions, thus giving a way of relating changes in ultrasonic velocity to changes in breadcrumb structure.

This thesis demonstrates the potential for using ultrasound as a non-destructive, cheap and accurate tool for studying the effect of voids (and their expansion) on dough properties. These ultrasonic techniques can also be used to investigate the effect of air cells on the structural integrity of breadcrumb and hence be a useful tool for quantitatively assessing bread quality.

Acknowledgments

I would like to express my appreciation to my supervisors Dr. J. H. Page and Dr. M. G. Scanlon for the valuable advice, guidance and extreme patience throughout the course of this work. I also would like to thank Dr. S. Narine and M. Sumner for agreeing to be members of my Ph.D. examining committee.

Thanks also go to G. Roy, M. Cowan, Department of Physics and Astronomy, and R. Zillman, Department of Plant Science, for all the help they provided.

I would like to gratefully acknowledge the financial assistance provided by the Canadian Bureau for international Education and Natural Sciences and Engineering Research Council of Canada (1998-2001)

Last but not least, I would like to thank my father, mother and the rest of my family for supporting me throughout the course of this work. Special thanks go to my wife and son for their emotional support and for putting up with my long working hours. I also would like to thank my brother Elmehdi who made the trip from back home to attend my defense.

To: Othman M. Elmehdi (1971 – 1999)

الاجـداء

بِقِيَّتِ ذِكْرِي أَنْفَائِكَ الطَّاهِرَةِ أَخِي
مَعَنَا أَيْنَ مَسَاكِنًا وَسَتَضَلُّ مَعَنَا إِلَى أَنْ نُلْقَاكَ فِي جَنَّاتِ
الْفِرْدَوْسِ انْشَاءً اللَّهُ وَمَالَنَا إِلَّا الدُّعَاءُ لَكَ بِالرَّحْمَةِ
وَالْمَغْفِرَةِ، فَيَارِبِ اغْفِرْ لِأَخِي مُحَمَّدٍ وَارْحَمَهُ وَأَدْخِلْهُ فِيسِيحِ
جَنَّاتِكَ وَأَلْحِقْنَا بِهِ مُؤْمِنِينَ شَاهِدِينَ بِاللَّهِ رَبِّاً وَمُحَمَّدٍ
صَلَّى اللَّهُ عَلَيْهِ وَسَلَّمَ نَبِيّاً وَرَسُولاً. أَلَيْكَ أَخِي
أَهْدِي هَذَا الْعَمَلُ الْعِلْمِيَّ وَجَزَاءَهُ وَجَزَاءَ
مَنْ اسْتَفَلَ مِنْهُ السِّي
يَوْمَ الدِّينِ.

Table of contents

Chapter one: Introduction

1.1 Historical background	1
1.2 Aeration of bread dough and the importance of gas cells in determining the structural integrity of breadcrumb	3
1.3 Ultrasound as a tool for investigating the effect of air bubbles on viscoelastic properties of bread dough and the effect of gas cells on the mechanical properties of breadcrumb	9
1.4 Motivation	11
1.5 Aim of the thesis	12
1.6 Thesis outline	14

Chapter two: Sample ingredients and sample preparation

2.1 Dough constituents	16
2.1.1 Flour and its composition	17
2.1.1.1 Carbohydrates	19
2.1.1.2. Proteins	21
2.1.1.3 Lipids	22
2.1.1.4 Minerals	24
2.1.1.5 Vitamins	25
2.1.2 Water	25
2.1.3 Yeast	27
2.1.4 Salt	29
2.2 Dough formation and baking	30
2.2.1 Mixing	31
2.2.1.1 Hydration and the formation of the continuous protein matrix	31
2.2.1.2 Occlusion of air	35
2.2.2 Dough fermentation	37
2.2.2.1 Carbon dioxide production and chemical changes during fermentation	37
2.2.2.2 Effect of time, temperature and humidity on fermentation	39
2.2.2.3 Changes in pH of the dough during fermentation	40

2.2.3	Final dough structure	41
2.2.4	Interactions between components in the continuous phase ...	44
2.3	Heat treatment of dough (Baking)	47
2.4	Final crumb structure	50
2.5	Dough and bread preparation, freeze drying, cutting and bonding	51
2.5.1	Dough and bread preparation	51
2.5.2	Freeze drying	54
2.5.3	Sample cutting and bonding	54

Chapter three: Ultrasonic waves in liquids and solids: basic theory and experimental methods

3.1	Introduction to ultrasound and its relation to food systems	57
3.2	Propagation of ultrasound	59
3.2.1	Homogeneous single-phase materials	60
3.2.2	Multi-phase inhomogeneous media	63
3.2.3	Velocity and attenuation in a system containing bubbles	66
3.3	Apparatus and experimental procedure	67
3.3.1	Apparatus	68
3.3.1.1.	Pulse generator and receiver	68
3.3.1.2.	Transducers	70
3.3.1.3.	Sample holder	71
3.3.1.4.	Data acquisition and signal averaging	74
3.4	Velocity and amplitude measurements	74

Chapter four: Results and discussion part I: dough mixing and fermentation

4.1	Aeration of dough during mixing: Unyeasted dough	78
4.1.1	Introduction: mixing under reduced pressure	79
4.1.2	Density of unyeasted dough	84
4.1.3	Effect of reducing mixing pressure on the attenuation coefficient of the ultrasonic signal	87
4.1.4	The effect of reducing the mixing pressure on ultrasonic velocity.....	92
4.2	Aeration of dough during fermentation: yeasted dough.....	110

4.2.1 Density of fermenting dough	111
4.2.2 Ultrasonic velocity as a function of fermentation time	118
4.2.3 Ultrasonic attenuation coefficient as a function of fermentation time	129

**Chapter five: Results and discussion part II: evaluation of the
mechanical properties of freeze-dried breadcrumb**

5.1 Mechanical properties of freeze-dried breadcrumb proofed at different proofing times	137
5.1.1 Density of breadcrumb as a function of proofing time	137
5.1.2 Phase velocity	140
5.1.3 Interpretation of the mechanical properties of freeze-dried breadcrumb	143
5.1.3.1 Gibson and Ashby's cellular structure model	143
5.1.3.2 Tortuosity model	149
5.2 Compression experiments: Investigating the effects of anisotropy	152
5.2.1 Introduction	152
5.2.2 Investigating the anisotropy effects on the mechanical properties of the breadcrumb by probing the samples along the two orthogonal directions	162
5.2.2.1 Modified Gibson and Ashby's cellular structure approach to anisotropy	162
5.2.2.2 Tortuosity model	171
5.3 Attenuation results	175

Chapter six: Summary and conclusions

6.1 Investigating the effect of air bubbles on the mechanical properties of dough at the end of mixing and during fermentation	181
6.2 The effect of air cells on the mechanical properties of breadcrumb	183
6.3 Recommendations for future work	185
References	188

Chapter one: Introduction

1.1 Historical background:

Bread is one of the oldest foods known to man and it has had a great impact on man and history (McGee, 1984; Morse *et al.*, 1988). Bread has been made since Neolithic times nearly 12000 years ago, when coarsely crushed grain was mixed with water, with the resulting dough placed on heated plates and baked by covering with hot ashes. Later, Egyptians discovered that by allowing wheat doughs to ferment, a leavened loaf was produced which had better flavor (Encyclopedia Britannica, 1997). Egyptians also were the first to discover baking ovens (Encyclopedia Britannica, 1997). Since then, bread has had an impact on humanity not only as a food staple, but also as a social, linguistic, spiritual and economic factor throughout history. Socially, the control of production (Coulton, 1925) and distribution (Veyne, 1990) of bread has been used as means for exercising political influence on people for the last 200 years. In the nineteenth century, the development of the baking industry in the United Kingdom and the decline in home baking was denounced by moralists as inducing laziness among the population (Campbell, 1991). Bread is also used to exert political pressure in many countries as people prefer to eat bread that is made using expensive imported wheat flours rather than those produced from local cheap harvests (Satin, 1988). Linguistically, we find bread's influence on many of the words and the proverbs we use. For example, in Arabic the word bread is commonly used as a metaphor for life. In Russian, the word hospitality is a combination of the words salt and bread (Smith, 1977). Spiritually, bread was mentioned in Genesis 3. Bread was also believed to transform into a divine state (Powers, 1967).

Economically, bread is the backbone of the baking industries in many countries. For example, in the past five years, wheat production in the USA averaged 64.6 million tons. Domestic consumption averaged about 35 million tons and the USA is among the world's primary wheat exporters. As another example, last year the average Russian ate 120 kilogram of bread, keeping the country firmly at the top of the list in the world consumption chart, (Cordonier,1999).

The significance of bread has inspired research communities around the world to attempt to refine and improve the production of such a widely used food commodity. Scanlon and Zghal (2001) counted 16 periodicals, currently received in the Canadian Grain Commission Library in Winnipeg, Canada, devoted to the studies of cereal sciences and technology. This affirms the demand for research efforts applied to studies of factors affecting bread quality.

In the following sections, some of the research pertaining to the two systems studied in this thesis will be reviewed, namely bread dough and breadcrumb. Also, the techniques that have been used to investigate the properties of these systems, including studies done using ultrasound, will be summarized. This will be done in sections 1.2 and 1.3 respectively. In sections 1.4 and 1.5 the motivation and the aim of the thesis will be stated. Finally, in section 1.6, the outlines of the thesis and the material covered in each chapter will be presented.

1.2 Aeration of bread dough and the importance of gas cells in determining the structural integrity of breadcrumb

Bread at its essence is a baked mixture of finely ground cereal flour and water. Baking causes the partial gelatinization of the starch, which is the major component of cereals, and that permits the bread to be digestible and thus an important source of energy for humans. Baking also dries out the dough mixture to render it temporarily stable against microbial attack. Therefore, the practical values for bread lie in its merit as 1) a nutritious product, satisfying the physiological needs of the body, and 2) a shelf-stable commodity in a convenient form for a useful period of time, satisfying the needs of society. However, these two factors alone do not count for the success of bread as a foodstuff. Other factors such as its desirable flavor, which results from baking, and its use as a vehicle for consumption of other foods (e.g. in sandwiches) contribute to its importance as well. An equally important factor for consumer acceptability of bread is its attractive and palatable texture, which is due to its aerated structure. The versatility of bread in its presentation is enhanced by the fact that it rises during processing. Thus, loaves of different shapes, characteristics and sizes may be produced, adding to its appeal. Aeration of bread therefore is a distinctive aspect of its popular appeal and is a central aim of the breadmaking process. The aerated structure of bread is made possible by the ability of the gluten proteins, which are found almost uniquely in wheat flour, to form a gas-trapping network when mixed with water and developed into a dough. With the addition of yeast, which metabolizes sugars to produce carbon dioxide, this gas trapping ability allows production of the aerated dough which is set by baking to give raised bread.

When the loaf of bread is taken out of the oven, it consists of crust and breadcrumb. The main difference between the crust and the breadcrumb is the difference in the temperature they attain during baking. The high temperature of the crust causes the evaporation of water so that the water content of the crust is very low compared to that of the breadcrumb. From the structural point of view, the breadcrumb is a pore structure consisting of the gas cells and pore walls. Often the pore wall is referred to as the matrix (Zghal *et al.*, 1999; Zghal, 2000). It is this material that is the contributor to the mechanical strength and structural architecture of the baked matrix. The pore surface is considered to consist of a monolayer lipid film with patches of polymerized high molecular weight storage protein units dispersed within it (Eliasson and Larson, 1993). The pore walls consist of the partly gelatinized starch. The crust on the other hand, is a hard, vitreous surface layer formed of collapsed crumb pore walls. It is a continuum of dried starch gel with protein and lipid aggregates (Eliasson and Larson, 1993).

Research on different aspects of breadmaking has taken many different approaches. For example, flour characteristics and their effect on the properties of dough strength and loaf volume (e.g. Elion, 1940; Collatz, 1943) are recognized, and wheat varieties undergo continual improvements in breadmaking potential through plant breeding. The processing factors and ingredients affecting bread aeration and texture are well characterized empirically, and are skillfully manipulated by bakers according to experience and to changes dictated by the consumer (references here are numerous from the pioneering work of Baker and Mize (1939) to more recent studies on mixing dough under reduced pressure by Campbell and Shah (1999). Yeast microbiology and the many aspects of bread chemistry have been studied extensively (e.g. Matsumoto, 1973:

Matsumoto and Nishiyama, 1973; Thorn and Ross, 1960). Without a doubt, the one area of research that has been studied thoroughly, is dough rheology. The focus of this area of research is the viscoelastic properties of bread dough, which are of great importance in the baking industry. For example, the rate at which the internal stress induced by mechanical treatment relaxes during the rest period depends on both on the viscosity and the elasticity of the dough (Matsumoto and Nishiyama, 1973; Matsumoto *et al.*, 1971). It is therefore understandable that many workers have devoted a great deal of effort to characterizing dough elasticity using rheological approaches such as creep (constant stress) and recovery or stress relaxation (constant strain). Several studies have also been made using uniaxial extension (Schofield and Scott-Blair, 1932, 1933a, 1933b; Halton and Scott-Blair, 1936). Simple shear has been used more recently to study creep and recovery (Bloksma, 1962, 1972; Yoneyama *et al.*, 1970; Bloksma and Meppelink, 1973; Hibberd and Parker, 1979) and for stress relaxation measurements (Launay and Bure, 1974, 1987; Bohlin and Carlson, 1981). These studies were all based on the conviction that rheological properties of the dough affect its behavior during processing and consequently the quality of the finished loaf of bread. The methods used to study dough rheology have relied on instruments such as dough recording mixers like the farinograph, which provides information about the behavior of the dough during the mixing stage. Load-extension instruments like the extensigraph (in one direction) and Alveograph (in two directions) yield information on the dough's resistance to extension, which is then related to gas retention or gas holding capacity during fermentation. Rheology experiments give information about the shear modulus, Young's modulus as well as the viscosity of the dough. Bloksma (1990a,b) gives an extensive summary of numerical

values for different moduli and their cited references. His summary will be presented in chapter four of this thesis.

Even though these instruments and methods investigate the properties of the dough as a whole, they fail to depict the contribution of the air bubbles to dough rheology. The air bubbles are present in considerable number and in the final product, the loaf, they represent much more than half of the total volume. In fact, studies on flour types, baking technology, chemistry and dough rheology have viewed aeration as a dependent variable, but not as an area of study by itself (Campbell, 1991). By contrast, Campbell *et al.* (1998) have pointed out that the breadmaking process may be viewed as a set of aeration stages, with the bubbles being incorporated in the dough during mixing, and then being inflated with carbon dioxide during proofing. Campbell's study concentrated on the size, the number and number-density of the bubbles rather their contribution to the rheological properties of the dough. It follows from this, and is the contention of this thesis, that the breadmaking process will be better understood if the role of the gaseous phase is investigated directly. That is, knowledge is required of the effect of air bubbles on the properties of the dough during mixing and during proofing, so as to gain an understanding of the effect of the gas cells on the mechanical properties of breadcrumb.

From the point of view of breadcrumb (and almost all baked goods), the final character depends significantly on the extent, the creation and the control of gas bubble structures in the unbaked matrix, and the retention of those gas bubbles in a suitable form until such time as the matrix becomes set or baked. In the baked product, the distribution and size of the small holes or voids in the crumb is commonly referred to as "crumb cell structure" (Zghal, 1999). The crumb structure contributes to texture, grain quality,

mechanical strength and perceived product freshness as well as visual appearance. Each of these particular product attributes varies with numbers, sizes and uniformity of distribution of these small bubbles which may be determined and controlled in the breadmaking process as early as the mixing stage. In general the holes have a relatively small size; for example, at the end of mixing their mean diameter is 75 micrometers and they expand to reach a mean diameter of as large as few millimeters (Bloksma, 1990a). It is generally accepted by consumers that small holes, which are uniformly distributed throughout the crumb, are required in bakery products and that large voids or irregular cell distributions are undesirable (Cauvain, 1999). In fact the holes themselves are not the most important issue, rather the space that they occupy and the extent to which they influence the character of the surrounding matrix. For a good product, the pore wall or the matrix is required to be as thin as possible, yet it must be resilient enough to recover from modest deformation, such as squeezing and pressing, the two most common ways by which consumers assess product freshness. The air cells in the bread crumb have been studied by several research groups. For example, Zghal *et al.* (1999) and Sapirstein (1999) have used a digital imaging technique to analyze the crumb grain (another term for breadcrumb structure). Their studies have centered on an objective characterization of the cellular structure of the breadcrumb. Their measured parameters included mean cell area, cell wall thickness, cell density, specific cell area, uniformity of the cell size as well as crumb brightness. A second example is the study of Cauvain *et al.* (1999), in which they investigated the effect of different stages of the breadmaking process (mixing, moulding, etc.) on the effect of the resulting breadcrumb cellular structure.

The mechanical properties of the breadcrumb are known to be complex. Their complexity is attributed to the difficulty in determining the stress strain curves and the heterogeneity of the system (Scanlon and Zghal, 2001). The former is attributed in part to the porous structure of the breadcrumb, which gives rise to complex combinations of stresses when the specimen is tested (Ponte and Faubion, 1987; Lasztity, 1980). The heterogeneity of the breadcrumb causes potential differences in the mechanical properties of the breadcrumb not only between different loaves, but even within the same loaf of bread (Ponte and Fabion, 1987). Despite these difficulties, quantification of the mechanical properties of the breadcrumb is essential because the elastic properties of breadcrumb have been considered to be the determinant factor of bread quality (Nussinovitch *et al.*, 1990; Piazza and Masi, 1995; Wassermann, 1973).

Mechanical properties of breadcrumb have been investigated using: 1) compression methods which include indentation (AACC, 1983; Ponte and Ovidia, 1996), compressive loading (Cornford *et al.*, 1964) and uniaxial compression (Chuah and Scanlon, 2001; Piazza and Masi, 1995), 2) Tensile testing (Nussinovitch *et al.*, 1990; Chen *et al.*, 1994; Peleg, 1997), and 3) Shear measurements (Persaud *et al.*, 1990). The numerical values for Young's and shear moduli found from these experiments have been summarized by Scanlon and Zghal (2001).

1.3 Ultrasound as a tool for investigating the effect of air bubbles on viscoelastic properties of bread dough and the effect of gas cells on the mechanical properties of breadcrumb

Although ultrasonic techniques are commonly used in materials science for investigating the mechanical properties of inorganic materials, their application to biological systems is less well established. In part, this reflects the fact that biological materials, such as foods, have generally complex, heterogeneous and highly variable structures; for foods, these features can result both from their origins in living tissues or the traditional processing methods that have been used to create/modify them. Therefore, ultrasound propagation in foods is a complicated function of a large number of physical, chemical and biological properties, so that interpreting data from ultrasound measurements can be a challenging problem. To overcome these difficulties, it is important that experimental conditions of the laboratory studies are precisely controlled, and that information on the structure and the mechanical properties of the foods are simultaneously acquired. This is a necessary first step in establishing procedures for eventually using ultrasound measurements in the food industry to determine and control textural quality. Despite these challenges, ultrasonic techniques have considerable potential for assessing the quality of foods. One important advantage is the ability of ultrasonic experiments to probe the physical properties of complex fluids and solids at various degrees of structural resolution.

The types of mechanical information obtainable from ultrasonic measurements can be quite extensive. Ultrasonic velocity measurements determine the stiffness or rigidity of the material, as can be most clearly seen by expressing the velocity in terms of

the (dynamic) elastic modulus. (The bulk, shear and Young's moduli can *all* be determined from measurements of the longitudinal and shear ultrasonic velocities.). Ultrasonic attenuation is especially sensitive to the structure of inhomogeneous materials at a resolution determined by the wavelength. A crucial question here is the relative importance of scattering and absorption, an issue that can be resolved by examining the frequency dependence of the attenuation, measuring both the ballistic signal that propagates straight through the medium and the signals that are scattered out of the main beam, and interpreting the data using appropriate physical models.

Despite its potential, the use of ultrasound in investigating the properties of bread dough and breadcrumb is very limited. As far as we know, besides our research group, there are only three research groups in the world today that have used ultrasound to investigate the mechanical properties of bread dough. Among the three groups, only one group has explored the potential of ultrasound in evaluating the mechanical properties of breadcrumb. Moorjani (1984) was the first to use ultrasound to investigate the properties of bread dough (with and without yeast). She measured the ultrasonic velocity of dough and fresh breadcrumb using 25 kHz transducers. Her measurements were limited to ultrasonic velocity. In 1992, Lee *et al.* used ultrasonic shear measurements as a technique to investigate the rheological properties of bread dough. They demonstrated that rheological properties of bread dough can be measured non-destructively at ultrasonic frequencies ranging between 0.3 to 1 MHz. The third research group is that of Letang *et al.* (1996), who investigated the acoustic properties of water-flour mixtures as a function of water content. Their range of frequencies was between 2 MHz and 8 MHz, which corresponds to a very short wavelength. None of these research groups have investigated

the elastic properties of the dough, nor the breadcrumb, in light of the presence of the air bubbles or gas cells. This will make the results presented in this thesis the only study, using ultrasound or other methods, that gives numerical characterization of the role of the air bubbles/gas cells.

1.4 Motivation

The view taken by many researchers today is that "Breadmaking may be viewed as a series of aeration stages: bubbles are incorporated during mixing, the bubbles are inflated with carbon dioxide during proofing ..." Campbell *et al.* (1998). In light of this view, the motivating question then becomes: can ultrasound be used to characterize these aeration stages?

Our hypothesis to examining these systems is to treat them as aerated cellular solids. This approach is facilitated by models developed by Gibson and Ashby (1982a,b; 1997). These models are based on the elastic deformation of idealized cell structures. A second theoretical approach is to use an effective medium model developed by Sheng (1988) and a tortuosity model (Johnson and Sen, 1981). The complication not usually encountered in industrial cellular solids, for which the cellular solids models were initially developed, is that the dough system is highly hydrated. Therefore the expected relationships between stiffness (which can be determined from ultrasonic velocity measurements) and density may no longer hold. For example, in porous materials such as bread crumb, greater water content means greater density, but when the material is polymeric (as is the case for most foods including bread crumb) the effect of water's plasticising action is to cause the material to become more compliant. In bread we are

dealing with a homogeneous 'cytoplasm' (inside of cell) comprised of air, and a heterogeneous wall material (starch granules in a somewhat homogeneous protein matrix). One of the key problems, to which ultrasound can provide answers, is the extent to which the mechanical properties of the wall material dominate the overall mechanical properties of the structure. One approach is to investigate the effects of air holes on the structural integrity of the bread dough and breadcrumb. Therefore, while the Gibson and Ashby approach will be used to model the breadcrumb results, the effective medium models are used to model the dough results. The two approaches will provide a solid theoretical basis for interpreting the dependence of ultrasound velocity on porosity in foods. Experimentally, we measured both the longitudinal velocity and attenuation in 1) un-yeasted dough mixed at various reduced pressure values, 2) fermenting dough, and 3) freeze-dried bread (compressed and non-compressed). The results obtained from ultrasound in dough and breadcrumb are compared to the behavior predicted by theoretical models. Variants on these models, which account for non-sphericity of the air spaces, are tested. Differences between measurements obtained on dough compared to those on bread will provide important information to baking scientists on how product texture is affected by starch gelatinisation and protein denaturation: there is currently a paucity of information on the textural link between dough and bread (Scanlon *et al.*, 1997).

1.5 Aim of the thesis

Understanding the role of air bubble/cells in determining the mechanical properties of bread dough and breadcrumb is fundamental to understanding aeration of

the bread as a whole. However, there have been no studies to investigate such a role. This is due to the lack of investigative tools and techniques that supply quantitative information. This lack is partly attributed to the fact that bread research has tended to concentrate on the chemistry of breadmaking, at the expense of the physics, and partly due to the difficulty of measuring the effect of air bubbles in the dough or breadcrumb. The latter is caused by the complex nature of these materials. Therefore, the aim of this thesis is to present a comprehensive ultrasonic investigation of the effect of air bubbles on the mechanical properties of dough as a result of the aeration stages (mixing and fermentation). We also extend our ultrasonic investigation to the effect of gas cells on the end product, the breadcrumb.

To accomplish our goal, we have performed three separate sets of experiments: while the first two experiments deal with dough exclusively, the third set of experiments is devoted to breadcrumb. In the first set of dough experiments, the mixing pressure was varied to control the amount of air occluded into the dough. This allowed us to investigate the effect of mixing on the aeration process and monitor its effect on the properties of the dough. In the second set of experiments, the addition of yeast to the dough allowed direct measurements to be made of the change in dough mechanical properties as the bubbles expanded. By relating the ultrasonic velocity and attenuation results to the void fraction (calculated from the dough density and the matrix density), the effect of voids on the elastic properties of the dough was revealed. An additional effect that was studied is the effect of interactions between the matrix components and the yeast cells in the dough matrix at early fermentation times.

In the third set of experiments, the mechanical properties of breadcrumb were studied as the size and the shape of gas cells was changed. The size of the gas cells was controlled by varying the proofing times from 0 to 108 minutes. To change the shape of the gas cells, the samples were compressed using a uniaxial compression. The results of these experiments are then related to the properties of breadcrumb.

1.6 Thesis outline

Chapter two presents the necessary breadmaking background: the basic ingredients of bread and the breadmaking process, which includes mixing, proofing, the interactions between the different constituents of the dough, and baking. Chapter three describes the experimental techniques used in the work presented in this thesis. This chapter also includes an outline of the theory of ultrasonic wave propagation, the ultrasonic parameters and their relationship to food properties. The second part of this chapter describes the experimental set-up and how the ultrasonic measurements were carried out. Chapter four is divided into two main sections. In the first section, the results of the ultrasonic velocity and attenuation of unyeasted dough mixed at various pressures will be presented. The second section is devoted to the results of experiments done on yeasted dough. For both systems, the behavior of ultrasonic parameters is investigated as a function of void size/concentration. The results obtained from these experiments will be compared to those predicted by theoretical models.

In chapter five we turn our attention to the second system studied in this thesis, the breadcrumb. Results of ultrasonic velocity and attenuation measurements performed

on freeze-dried breadcrumb samples are presented and interpreted. These results include experiments done on both compressed and non-compressed samples.

Chapter six presents the conclusions of this work, indicates its relevance and implication for the baking industry, and identifies suggestions for future work and areas requiring further attention.

Chapter two

Sample Ingredients and Sample Preparation

In this chapter, the sample ingredients and sample preparation are discussed in detail. The essential ingredients of dough and bread, namely flour, water, yeast and salt, will be covered in section 2.1. After that, the transformation of these components into dough will be investigated. This will include mixing, gas cell occlusion and the expansion of these cells during fermentation. After that, the heat treatment of dough and the final structure of the breadcrumb will be discussed. The final section will deal with the preparation of breadcrumb sample for ultrasonic measurements, in which we will discuss how the samples were freeze dried, cut and waterproofed.

For the dough experiments, unyeasted and yeasted, some of the ingredients which are normally used in the breadmaking process were omitted. These ingredients included improvers and additives such as sugar, shortening and oxidants. The reason for omitting these ingredients was to eliminate additional complexity effects they may introduce to ultrasonic measurements of the dough structure. In addition, in the bread section, we investigate only the bread crumb structure and ignore the loaf crust and its structure.

2.1 Dough constituents

In this section we examine the different components of dough and their relative importance in dough development, fermentation and final structure of the dough, as well as their effect on the final product, i.e., the breadcrumb. The carbohydrates, which include

starches, sugars and both soluble and insoluble polysaccharides are the most abundant. Perhaps the most important component is the protein fraction, which includes the wedge and adhering proteins in the intact grain and the derived fractions such as gluten, albumin, globulins, prolamins and lipoproteins. The lipids form a small but significant part of the flour. Finally there are minor components, which are present in minute amounts, including minerals and vitamins.

The second group of dough constituents include water, which plays a key role in dough fermentation, air which forms the nuclei of the gas cells and oxygen which acts as an improver. The final group comprises the various substances that are added to the dough. These include yeast, salt and other improvers and conditioners.

2.1.1 Flour and its composition

Wheat flour is one of the most widely used food ingredients in the world today. For example in the United States 15 M tonnes of flour is used every year (Kent and Evers, 1994). Among the many reasons for this high consumption, the one that is most relevant to this study, is the unique property of wheat flour proteins to yield a continuous, extensible matrix upon wetting and mixing. This permits the production of yeast-leavened light bread that has served mankind as a principal food since the dawn of history. In the following subsections, the chemical composition of wheat flour and its relative components will be examined. The main components of flour are carbohydrates, proteins, lipids, minerals and vitamins. The relative percentage of each of these ingredients is shown in table 2.1 (Kent, 1983).

Table 2.1 Flour Components (Kent, 1983).

Component	(%)
Protein	11.8
Carbohydrate	74.7
Fat	1.1
Moisture	12
Other	0.4

2.1.1.1 Carbohydrates

The main carbohydrate of wheat flour is starch, which represents about 74-90% on a dry basis, of wheat flour (Hoseney *et al.*, 1971). Other minor carbohydrate components include dextrins, cellulose and various other free sugars and pentosans (Pylar, 1988). The starch granule is almost 100% composed of the polysaccharides amylose and amylopectin. Wolforn and Elkhadem (1975) have reviewed the developments which have established that both polysaccharides are polymers of D-glucose, one linear and one branched in a bushlike structure. The glucose units in the linear molecules comprise the amylose molecule. The units are joined by alpha-1, 4-glucosidic bonds, see figure 2.1a. The branched molecules comprise the amylopectin molecule, figure 2.1b. In these units, alpha-1,4-bonds are also predominate, but the branching is introduced by alpha-1,6-bonds, see figure 2.1b. Some other minor amounts of linkages other than these two have been reported, but the quantity is too small to change the general picture (Manners and Matheson, 1981).

The starch granule that has been damaged during milling (damage includes fracture, cracking, and shearing) exhibits a marked susceptibility to attack by α -amylase, and thus it plays an important role in fermentation during the proofing and baking processes (Eliasson and Larsson, 1993). Tipples (1960) suggested that the starch granule plays an important role in the formation of sufficient fermentable carbohydrate to sustain adequate gas production by the yeast during dough fermentation. The starch also contributes to the structure of the bread crumb. Gelatinization (swelling of the starch granule that occurs when it is heated in an aqueous medium) is another important

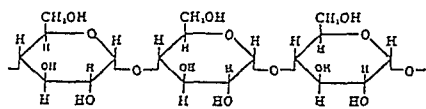


Figure 2.1a. Section of amylose molecule. (taken from D'Appolonia, *et al.*, 1970).

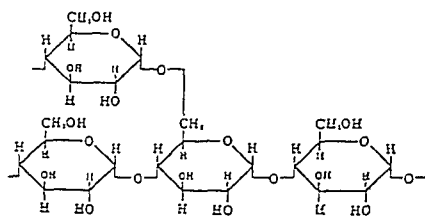


Figure 2.1b. Point of branching of amylopectin molecule (taken from D'Appolonia, *et al.*, 1970).

characteristic of starch during baking. The ability of the starch granule to retain water is important for prolonging the shelf life of the loaf.

2.1.1.2 Proteins

The composition of proteins is 50-55% carbon, 20-25% oxygen and 12-19% nitrogen (Pylar, 1988). The proteins in wheat flour are crucial in determining the flour's breadmaking quality, both quantitative and qualitative characteristics being important (Finney, 1943). The ability of wheat flour to be baked into bread is attributed to the physico-chemical properties of its gluten protein fraction (Booth and Melvin, 1979). It is the gluten proteins that are recognized generally as being important in breadmaking. They represent about 90% of the total proteins of wheat flour and are comprised of two major groups: gliadins and glutelins. These two groups are present in approximately equal amounts and differ in their chemical and physical characteristics (Bietz and Wall, 1975). Gliadins are a heterogeneous range of proteins with an average molecular weight of *ca* 40,000, composed of single polypeptide chains (Kasarda *et al.*, 1971). Intramolecular disulphide bonds are present which confer stability on folded random coil structures. Glutelins are also a heterogeneous range of proteins with molecular weights of 10^7 . They consist of polypeptide subunits ranging in molecular weight from *ca.* 40,000 to 150,000 which are capable of forming both intra- and inter-polypeptide disulphide bonds. The two fractions also have different physical properties when hydrated. The gliadin fraction behaves as a viscous liquid and the glutinin fraction as a cohesive elastic solid. The rheological properties of gluten (i.e. its combination of viscous, elastic and cohesive properties) are generally considered to be responsible for conferring breadmaking quality on wheat flour, and both the gliadin and glutelin fractions contribute to the viscoelastic

nature of gluten (Miflin *et al.*, 1983). Glutelin is considered as the major contributor to the elasticity and the cohesive strength of the dough. However, doughs that are too elastic and inextensible give poor breadmaking performance compared to doughs with a balance of elasticity and extensibility. Therefore, the tenacity of a dough produced by an appropriate balance of glutelin and gliadin is such that it allows expansion of bubbles to proceed during fermentation and baking. Expansion of doughs containing too low a proportion of gliadin will be inhibited, while doughs containing too high a proportion of gliadin will expand excessively with consequent rupturing of gas cell walls and collapse of the walls (Payne *et al.* 1984).

2.1.1.3 Lipids

The composition of lipids in wheat has been studied by several investigators (Acker *et al.*, 1968; Hosney *et al.*, 1969; Nelson *et al.*, 1963; Pomeranz *et al.*, 1966, to name a few). Figure 2.2 show a graphical description of the main lipids of wheat flour (Hosney *et al.*, 1969). In the cereal literature, lipids are defined as *free* or *bound*; this distinction is based upon solubility. If the lipid is soluble in a non-polar solvent such as petroleum ether, it is considered free; if it requires a polar solvent for extraction, it is considered bound (Hosney *et al.*, 1969). Another distinction is that of *polar* and *non-polar* lipids (Hosney *et al.*, 1969). The common definition of a non-polar lipid is the material that can be eluted from a silicic acid column with chloroform. On the other hand, polar lipids are defined as the materials eluted from the column with methyl alcohol.

Using the above definitions, the free lipids in wheat flour can be separated into two fractions according to their elution from silicic acid column. The total lipids in wheat flour

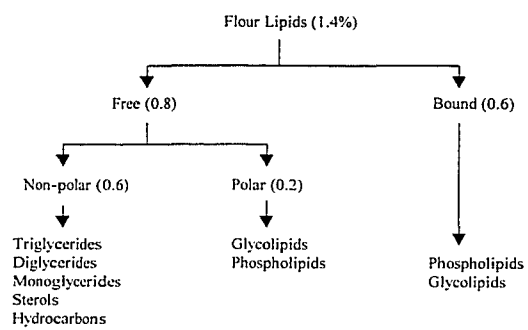


Figure 2.2. A schematic description of the main lipids of wheat flour (from Kilborn and Dempster, 1965).

are found in small amounts, 1.4% (Kilborn and Dempster, 1965). The non-polar fraction of about 0.6% lipids can be eluted with chloroform (Bloksma, 1971). This fraction contains mainly triglycerides and smaller amounts of hydrocarbons, sterols, steryl esters, monoglycerides and free fatty acids. The second fraction (0.2% free lipids) is a mixture of free polar lipids. Free polar lipids are rich in glycolipids, and contain relatively small amounts of phospholipids. In addition to 0.8% free lipids, wheat flour dough contains about 0.6% bound lipids (mainly polar), which can be extracted from flour with water-saturated butanol, after the petroleum ether extraction. This fraction (0.6%) contains mainly phospholipids and glycolipids.

It has been suggested that lipids may affect baking in many ways. During progressive stages of the baking process, the lipids may (Bloksma 1971, 1974; Glass, 1960; Wehrli and Pomeranz, 1970): 1) modify gluten structure at the mixing stage; 2) act as lubricants; 3) improve gas retention by sealing gas cells; 4) prevent gas interaction between starch granules during gelatinization; 5) give some structural support to the gluten; 6) retard water transport from protein to starch; 7) retard starch gelatinization; 8) act as an antistaling agent. In order to keep the dough samples as simple as possible, shortening was not included.

2.1.1.4 Minerals

The wheat kernel contains 1 to 2% various mineral substances. These comprise the ash content within the kernel. After milling, the end result flour should contain an ash content of about 0.44 to 0.48%. On average, the mineral composition of wheat flour is, expressed as mg/100 g flour (Cornell and Hovelung, 1998):

Cationic forms	Potassium	98
	Magnesium	21
	Calcium	16
	Sodium	2
	Zinc	1
	Iron	1
	Copper	0.2
Anionic forms	Phosphate	92 (as total phosphorus)
	Chloride	47

2.1.1.5 Vitamins

Vitamins are organic substances which are present in very small quantities in wheat flour. The main vitamins are of the B and E groups. Vitamin A is also present but in minute quantities (Bailey, 1944).

2.1.2 Water

As a swelling agent, water has two important functions in dough making (Ablett *et al.* 1986): 1) when mixed with flour, it gives a material whose mechanical behavior allows the mechanical formation of desirable structure during bread making, and 2) some of this water will be present within the end product (bread), which will play a large role in determining its texture. In this section our main concern will be with the influence of water on the mechanical behavior of dough. The effect of water on storage and staling of the final product is outside the scope of this thesis and will not be discussed in this chapter. Flour doughs contain about 0.6-0.8 g water per gram of dry flour and approximately half of it is non-freezable water, i.e. bound water. In breadcrumb, the

water content is between 40 and 50% of the weight of the bread (Longton and LeGrays, 1981).

Water, which is first introduced into the flour during the mixing stage, plays a big role in determining the tensile mechanical properties of the dough. Webb *et al.* (1970) found that the energy required to produce a given deformation of the dough falls exponentially with increasing water content, that the rupture stress also decreases with increasing water content, and that the elongation to rupture ratio increases with water content.

The gluten phase controls the mechanical properties of dough, and in many respects protein networks have properties that are similar to those of rubber (Schofield and Scott Blair, 1937). Protein networks are capable of large reversible elongation and it appears that the retractive force produced on stretching is similar to that of rubber, i.e. it is due to entropy changes rather than internal energy changes during deformation (Funt Bar-David and Lerchenthal, 1975). We therefore will look at the effect of water on the protein networks in terms of the influence of swelling agents on the rubbery-like materials.

When water (the swelling agent) is introduced to this rubbery network it reduces the material's stiffness. This is due to the reduction in the number of macromolecules crossing a unit area and the reduction in the number of cross-links per unit length (Muller, 1969). The gluten phase (sometimes referred to as the continuous phase of the dough) determines the elastic properties of dough and contains about twice its actual weight of water in the average dough (Chui and Mark, 1977). As swelling increases, the energy required to cause rupture is reduced. This reduced strength is due to the reduction in the number of load bearing macromolecules per unit area (Gent and Tobias, 1982). The

swelling agent pushes the macromolecules apart, thus minimizing the intermolecular energy dissipative mechanisms which are known to be a major influence on the strength of the rubbery-like material (Treloar, 1958). As swelling increases, this continuous phase becomes weaker and it tends to fracture at lower strains (Blokma, 1971). Another mechanism whereby increasing water addition could allow increased elongation to fracture is that the soft continuous phase of dough will swell in direct proportion to the free water, whereas the hard particulate phase (starch granules) will not (Nielsen, 1974). Thus added free water will effectively increase the volume fraction of the soft phase.

In summary, we see that the addition of water acts to soften the dough (lower its modulus) and increase its flexibility (increase its elongation to fracture) (Ablett *et al.*, 1986). Undoubtedly, when water is added in excessive amounts the effect is a “soggy” material which will not be strong enough to retain gas (Flory and Rehner, 1943).

2.1.3 Yeast

Baker’s yeast is a unicellular, eukaryotic microorganism. It is a strain of the species *Saccharomyces cerevisiae*. It may be found commercially in two forms, dry and compressed (sometimes called fresh). Table 2.2 summarizes some of the main characteristics of commercial yeast (Pylar, 1988).

In bread making, yeast has two main functions: 1) leavening of the dough and 2) contributing to the taste, flavor, aroma and nutritional value of the bread (Thorn and Ross, 1960). The leavening activity (gas production) of yeast in dough is the result of its fermentation of sugars. Starting with glucose, the fermentation process may be formulated using the following equation:

Table 2.2 Yeast components (Pylar, 1988).

	Dry matter (%)	Protein (%)
Compressed yeast	27-34	42-56
dry yeast	92	40-43



According to this equation, about 0.49 grams of CO₂, the leavening gas, is produced per gram of glucose fermented, which at a dough temperature of 30 °C and at atmospheric pressure, would be 276 ml of CO₂ per gram of glucose (van Dam, 1986). If bread with only flour and water is baked, the loaf volume will correspond to roughly the dough volume after mixing. The addition of 3.5-5.5% of yeast to this water-flour suspension will lead to an increase in the volume by a factor of about 2.4 (Finney, 1984). The gas producing power of the yeast depends on the temperature of the dough, pH level, alcohol concentration, nature of the carbohydrate supply, osmotic pressure and yeast concentration (Pylar, 1967).

2.1.4 Salt

In chemistry, salt refers to compounds that are produced by the interaction of a base with an acid in which part or all of the hydrogen of the acid is replaced by a metal or a metal-like radical. In baking, the common salt used is sodium chloride (NaCl). The functions of salt in dough are (Eliasson and Larsson, 1993): 1) adding flavor to the baked product, 2) masking off-taste and improving the flavor balance, 3) inhibiting yeast activity, 4) inhibiting potential spoilage micro-organisms, and 5) strengthening and tightening the gluten matrix. Gross *et al.* (1966) showed that salt may be used to inhibit yeast activity, i.e. it works to reduce the gassing rate. Miller and Johnson (1946) added that the reason for the strengthening and tightening effects of salt is due to its inhibitory effect on proteolytic enzymes. The amount of salt which is added to the bread dough ranges from 1.5 to 2% based on the flour weight (Holmes and Hosenev, 1987; Finney, 1984).

2.2 Dough formation and baking

To transform the above ingredients into dough and bread, they have to go through several stages. The first stage is mixing in which all ingredients are put into the mixing bowl and blended together. During the mixing stage, the dough is developed and air is occluded into the dough. The second stage is the fermentation stage, in which the dough is placed in a proofing cabinet where the temperature and the humidity are well controlled. During fermentation, the air bubbles are inflated with carbon dioxide and the volume of the dough increases as a result. The second stage involves three intermediate steps which the dough goes through. These steps will be discussed briefly in this thesis as they are only important for the second part of the experiments, i.e. the freeze-dried bread experiments. These three intermediate steps include rounding, sheeting and moulding. The main function of these steps is to subdivide the air bubbles and redistribute them through the dough (Pylar, 1988). The third step in the breadmaking process is the proofing stage. The function and the conditions under which the proofing stage is carried out are similar to those of the fermentation stage. However, in proofing the cells are more uniform as a result of rounding, moulding and sheeting. For the purpose of the presentation of the ultrasonic results, it is important to make the distinction between the two terms. In the yeasted-dough experiments, the dough was transferred directly from the mixer to the experimental measuring devices and hence the ultrasonic parameters will be measured as a function of fermentation time. However, for the breadcrumb experiments, where the dough has gone through fermentation, rounding, sheeting, moulding, and proofing, the ultrasonic parameters will be measured as a function of proofing time. The

forth and final stage in the breadmaking process is the heat treatment of the dough which serves to transform the viscoelastic dough into bread.

2.2.1 Mixing

During mixing, the dough ingredients are first blended together (incorporated) and then the ingredients are hydrated or solubilized. The second event that happens during mixing is the occlusion of air nuclei in the dough. The occlusion of air is vital for the production of bread as these air nuclei will serve as sites for the CO₂ produced during fermentation. To gain a full understanding of those two important events, this section will be divided into two subsections. In subsection 2.2.1.1, we discuss the hydration of the flour particles and the production of the gluten phase. We will also discuss the interactions that take place during the hydration of the flour particles. In subsection 2.2.1.2, we will discuss the mechanism by which the air nuclei are occluded into the dough.

2.2.1.1 Hydration and the formation of the continuous protein matrix

Mixing is the process of converting flour and water into dough by both blending and disrupting the dough ingredients and developing the gluten protein into a continuous phase. When water is added to flour, the particles are wetted and slowly hydrated. As water penetrates the flour particles it weakens the starch-protein bonds. With no mechanical energy (mixing) the process stops at that point. Upon mixing, several changes occur: the flour-water mass gradually becomes coherent, loses its wet and sticky appearance, and becomes a smooth homogeneous-appearing dough (Schofield, 1986). Further mixing produces wet and sticky dough with "overmixed" characteristics. In addition to the above visual changes, other physical changes occur during mixing.

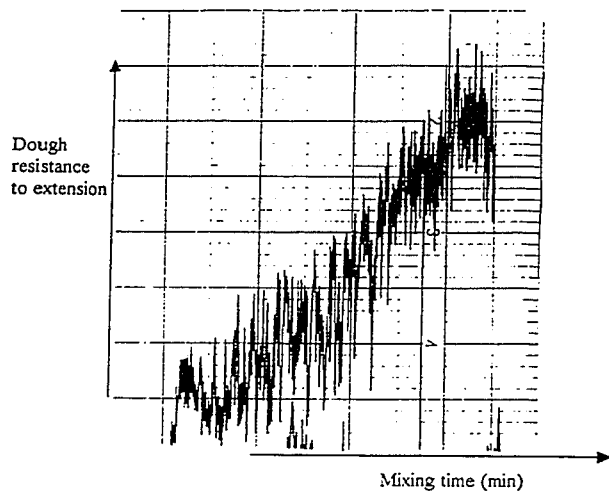


Figure 2.3: Mixograph curve showing the resistance of the mixer pins as a function of mixing time in minutes. Each square on the scale represents a minute.

In dough rheology, mixing is often investigated using an apparatus called the mixogram. The apparatus measures the dough's resistance, measured in arbitrary units, to extension. A typical mixograph curve is shown in figure 2.3, in which the resistance increases with mixing until a peak is reached, then it starts to decrease. The y-axis in figure 2.3 is a measure of the dough's resistance to extension (torque) caused by the passage of the mixing pins. The x-axis represents the time over which the dough has been mixed. The peak point is the "mixing time" of the flour. It has also been called the point of minimum mobility or the point of optimum mixing time (Bushuk and Tsen, 1968). The optimum mixing time has to be achieved for good quality bread. Continued mixing beyond this time will result in an increase in dough mobility and extensibility, which breaks down the viscoelastic properties of the dough and its ability to retain gas (Kilborn and Tipples, 1972). Hydration also occurs at the molecular level (Bloksma, 1990a). Hydration is a slow process that is accelerated by mixing and is also related to the speed of the mixer. To visualize this, one must be reminded that flour is composed of discrete particles of endosperm. As the protein and other dough constituents become hydrated the free water in the system is decreased. As the level of free water in the system decreases, the dough feels drier, resistance to extension increases, consistency increases and dough mobility decreases. In the last sentence the term dough consistency refers to the height of the mixing curve at the peak, which is also referred to as the point of minimum mobility or optimum mixing time (Hoseney and Finney, 1974).

Mobility, fluidity and resistance to extension are not properties of a wetted mass of flour particles (Hoseney and Finney, 1974). The original molecular structure of the starch-protein complex of wheat endosperm probably is not altered during hydration.

Rather, as the water penetrates the flour particles, the mixing action promotes removal of the hydrated layers from the flour particles. The hydrated mass loses some of its excess free water to the remaining unhydrated flour particles. The outer layer of those particles hydrates and the process is repeated, until all of the particles are hydrated and form a homogeneous-appearing dough.

As the dough becomes a coherent mass, continued mixing begins to alter the protein structure, stretching it and developing it into a continuous phase capable of retaining gas. If mixing is terminated before the optimum development of the protein matrix, the dough structure is less able to retain gas even though hydration appears complete. Additional mixing beyond the point of maximum mobility radically alters the structure of the dough and leads to breakdown of the dough. The phenomenon of dough breakdown is explained by Hlynka (1970) as follows: as a result of mixing there is an orientation of long-chain molecules; associated with this is the decrease in the chain entanglement which results in a condition of more nearly laminar flow in the dough, making it less resistant to extension. Hlynka also suggested that the orientation of the protein molecules would greatly increase the probability of protein-protein interaction (H-bonding), the result of which would be the release of water. The increase in free water would further decrease the dough's resistance to extension and result in the wet sticky appearance normally associated with an overmixed dough.

Experimental evidence supports the idea that increased free water is not the only important factor in overmixed dough (Bushuk and Mehrotra, 1977). An overmixed dough which appears to be too slack cannot be structurally equated with the same flour mixed to optimum condition with an excess amount of water. Some overhydrated doughs produce

bread with loaf volumes higher than those produced at normal optimum water absorption levels (Kilborn and Tipples, 1972). However, few overmixed doughs can be handled, few completely recover during fermentation and most produce bread with loaf volume below optimum (Finney and Shogren, 1972). In overmixed doughs, the protein network is altered and gas retention is reduced.

2.2.1.2 Occlusion of air

For baked goods, the occlusion of air during mixing is a vital step and it plays an important role in the quality of the final product. As the gluten layers are being sheared and folded by the mixing blades, air gets entrapped within these layers. Baker (1941) and Baker *et al.* (1946) established the fact that air bubbles were incorporated into doughs during the mixing stages and that these bubbles form the nuclei for the gas cells. These gas cells will expand due to the production of carbon dioxide that diffuses into the gas cells during the fermentation stage. It should be emphasized that no new cells can be produced beyond these stages, but the existing cells may be subdivided during the moulding and sheeting operations. Therefore, the gas bubble structure (which is incorporated during mixing) and the volume potential of the final product (crumb) are largely determined by the end of the mixing process (Baker, 1941). The incorporation of the air bubbles within the system depends on the viscosity of the medium, the speed of the mixer and the concentration and types of surface-active agents present (MacRitchie, 1976).

Among the important features of the matrix are its ability to retain gas and its ability to accommodate the expansion of the gases during the fermentation process. If we

treat the gas cell as a bubble embedded within a continuous medium, we may define the pressure within the bubble as follows:

$$\Delta P = \frac{2T}{r}$$

where T is interfacial surface tension and r is the radius of the bubble. From the above equation, the pressure required to start a new bubble ($r = 0$) would be infinite, confirming the earlier point we have established, namely air bubbles have to be incorporated during the mixing process. Therefore, after the mixing stage, the gas cells may only be subdivided or made bigger.

Microscopic examination of bread dough showed the presence of occluded gas cells which are spherical in shape and have diameters ranging from 10 to 100 μm (Carlsson and Bohlin, 1978; Junge *et al.*, 1981; Moss 1974; Pomeranz *et al.*, 1984). The number of gas cells per unit volume can be calculated from the total volume of occluded gas and the size distribution or the average size of the cells (Bloksma, 1981). At the end of mixing, the number of the gas cells per unit volume is 10^{11} to 10^{14} / m^3 (Bloksma 1990a). Other researchers reported that at the end of the mixing stage the size of these gas cells is between 3 μm and 300 μm (Shimiya and Nakamura, 1997). To make these gas cells finer, doughs were allowed to ferment for fifteen minutes at 30 °C and then the large bubbles were subdivided into smaller ones by punching, sheeting and/or moulding (Preston *et al.*, 1982). The result of such an operation lead to more bubbles per unit volume.

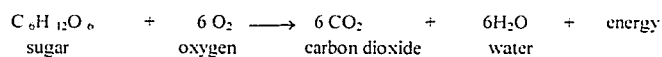
Other ways of mixing include mixing at over pressure (Baker and Mize, 1941a,b) and reduced pressure (Baker and Mize, 1941a; Campbell *et al.*, 1998), Campbell *et al.*

(1998) found that both the void fraction and loaf volume decreased as mixing pressure was reduced. They also found that the bubble size distribution did not appear to vary significantly, but the number of bubbles per unit volume decreased with reduced mixing pressure. Mixing the dough under reduced pressure was used for the first part of the dough experiments to investigate the aeration properties of the unyeasted dough and it will be discussed in more detail in section 4.1.1.

2.2.2 Dough fermentation

2.2.2.1 Carbon dioxide production and chemical changes during fermentation

As discussed in the previous section, the mixed bread dough consists of an insoluble but highly hydrated gluten protein system that acts as the continuous phase containing discontinuous starch granules and air bubbles. Also dispersed throughout the aqueous system are the yeast cells which ferment sugar to produce carbon dioxide. As fermentation commences, the dough slowly changes from a rough dense mass lacking extensibility and with poor gas holding properties, into a smooth extensible dough with good gas holding properties. The yeast uses the sugars in much the same way as we do, that is to break down the carbohydrates (starch and sugars) that are found naturally in the flour into carbon dioxide and water. When there is plenty of oxygen present the following reaction occurs:



The energy released is used by the yeast for growth and activity. In the bread dough system where the oxygen supply is limited, the yeast can only partially break down the sugar. Alcohol and carbon dioxide are produced in this process which is known as

alcoholic fermentation (van Dam, 1986). Enzymes present in the yeast and flour work to speed up fermentation reaction (Pylar, 1988). The carbon dioxide produced in these reactions causes the dough to rise (ferment or proof), and the alcohol produced mostly evaporates from the dough during the baking process. Carbon dioxide is produced in the aqueous phase and saturates the free water first. Once the free water is saturated, newly produced carbon dioxide must find a place to go to. Because it cannot form new bubbles, the only other possibility is the migration of CO₂ to the preexisting air bubbles. Carbon dioxide enters the air bubbles thus increasing their pressure, and because of the viscous flow and elastic properties of the dough, the bubbles will expand to equalize the pressure (Elmer and Reed, 1968). This process will increase the total volume of the dough mass and is referred to as the leavening effect of the yeast (Pylar, 1988).

The gluten matrix forms membranes or sheets that surround the gas bubble. The elastic properties of the gluten matrix allow the gas cells to expand, thereby allowing the gas to be retained with the bubbles. The analogy often used in cereal chemistry is that of a rubber balloon, i.e. a gas cell surrounded by a dough matrix (Pylar, 1988). This is a questionable analogy since it assumes that there is a barrier, which will prevent the gas from reaching the air bubbles. In fact, no barrier is needed since carbon dioxide in the bubbles cannot diffuse out of the bubble because the aqueous phase surrounding the air bubbles is saturated with carbon dioxide, and because the yeast is producing more, it remains saturated (Schofield, 1986). To explain this further: from the diffusion laws we know that materials diffuse from high concentration to low concentration and as the difference in concentration increases, the diffusion flux increases. The concentration of carbon dioxide is greater in the saturated aqueous phase and lower in the gaseous bubble.

Therefore, CO₂ will diffuse from the aqueous phase into the bubble. In doughs the diffusion rate is slow and since the distance between the air bubbles and the surrounding atmosphere is great, carbon dioxide must diffuse into the nearby air bubbles which are at a relatively higher pressure than atmosphere (Tsen, 1973). It is because of these diffusion processes and the characteristics of wheat flour dough, that dough is able to retain gas. As a result of the fermentation process, the dimension of the gas cell grows to the millimeter scale. Using microscopy, Bloksma (1990b) reviewed the results of several experimental investigations of the size of gas cells as compared with their distance apart at different stages of the breadmaking process. He stated that the ratio of the radius of the bubbles and distance between them depends only on the relative volume (defined as the volume of liquid dough phase divided by the total volume of the dough). Since both carbon dioxide and oxygen dissolve in water, this leaves nitrogen as the only choice of gas to form those air nuclei. The diameter of the gas cells at the end of fermentation ranges from 500 μ m to a few millimeters (Cauvain, 1999).

2.2.2.2 Effect of time, temperature and humidity on fermentation

The final stage of fermentation involves placing the dough in a baking pan and transferring it into the proofing cabinet. This stage is often referred to as the proofing stage (Baker, 1941; Eliasson and Larsson, 1993; Pylar, 1988). This procedure is usually preceded by rounding, sheeting and the degassing of the moulding process. Proofing conditions which include time, temperature and humidity are very important and vary in different processes. For example, Holmes and Hosenev (1987) reported that proofing times vary from 41-65 minutes with 55 minutes being the most typical. Similar proofing times were reported by Freilich (1949), who investigated proofing time in the range

between 0-150 minutes and found that the optimum time was between 45 and 60 minutes. Loaf volume increased with the increase in proofing time but crumb grain was unacceptably open for the higher proofing times. Dubois and Vetter (1987) suggested that an optimum proofing temperature is 46 °C (115 °F). Another study by Freilich (1949) on the effect of proofing temperature on loaf volume found that 30-46 °C is the optimum temperature and that 63 minutes is the optimum time. Siffering and Bruinsma (1993) have investigated the proofing temperature effect on loaf volume. They suggest that cooler proofing temperatures gave larger loaf volumes (bearing in mind that the proofing time was longer for low temperature proofing). Using digital image analysis, Zghal *et al.* (1999) have reported that longer proofing times gave loaves with bigger porous structure and larger volume. The density of the dough and bread crumb as a function of proofing time will be one of the subjects studied in detail in this thesis. Finally, if the dough is allowed a longer time to proof, the result will be extra stretching of the cell walls. Therefore the cell walls will be weakened and neighboring gas cells tend to coalesce (Elmer and Reed, 1968; Tsen, 1988). The third factor that affects proofing is relative humidity. Pyler (1988) reported that the typical range is 75-90% relative humidity. Lower humidity was found to produce a dry crusty surface of the proofed product while higher humidity causes surface discoloration or spotting.

2.2.2.3 Changes in pH of the dough during fermentation

The pH of the dough is determined by the wheat proteins through the dissociation of charged amino acid side chains (Garver *et al.* 1966). pH plays an important role in dough fermentation. It exerts its principal effects during fermentation where it controls yeast activity, amylolytic action, gluten characteristics and the survival of rope-producing

organisms (Pylar, 1988). These organisms are of the *Bacillus* species and are capable of forming high resistant spores. They are the causative agent of ropey bread (Pylar, 1988). The dough which has a considerable buffer capacity has an initial pH of about 5.5, which drops as a function of fermentation owing to the saturation of carbon dioxide in the water phase. Values of pH as low as 3.8 can be attained in the first 100 minutes of fermentation (Eliasson and Larsson, 1993). In general, the repulsion of gluten polymer chains over the aqueous zone in the gluten structure will increase with increasing protein charges. Therefore, the swelling of the gluten will increase as we move away from the isoelectric point of the constituents proteins (most of the gliadin-type proteins have an isoelectric point above 6.5 (Eliasson and Larsson, 1993)), and therefore the mechanical strength of the gel will be reduced. The drop in the pH value is expected to increase ion concentration within the matrix; we therefore expect the pH drop to influence the physical properties of the dough, and its elastic characteristics in particular.

2.2.3 Final dough structure

The final structure of the dough is heterogeneous in nature. On the one hand we have the gluten mix which contains the starch granules embedded within the protein matrix and water. On the other hand we have the gas cell structure which was introduced to the dough through mixing and later expanded during the fermentation stage. Figure 2.4 shows a schematic description of the arrangements of these different components. We will first discuss the continuous phase and in the remainder of the section we will look at the assembly of the different phases of the dough.

The continuous phase that surrounds the gas cells has two interpenetrating water-

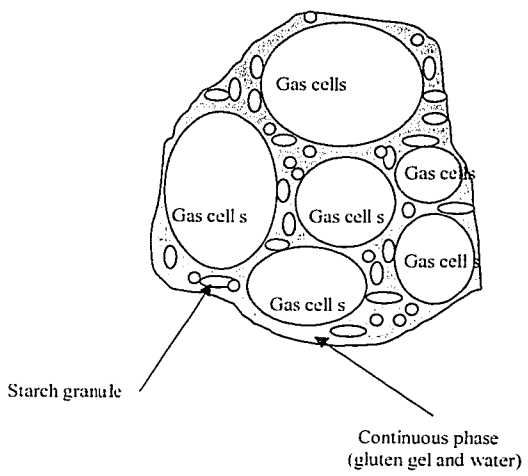


Figure 2.4 Dough Structure.

Table 2.3. Summary of gas cell size and the number of cells distribution at different stages of breadmaking process.

Diameter (μm)	Number of cells ¹	Reference
at the end of mixing		
3 – 300	$3 \times 10^8 / m^2$	Shimiya and Nakamura (1997)
10-100	-	Carlson and Bohlin (1978)
-	$10^{11}-10^{14} / m^3$	Pomeranz <i>et al</i> (1984)
75	$7 \times 10^{14} / m^3$	Campbell <i>et al.</i> (1998)
2- 900	-	Whitworth & Alava (1999)
at the end of fermentation		
2-1500	-	Whitworth & Alava (1999)
100– 5000	$3 \times 10^8 / m^2$	Shimiya and Nakamura (1997)

¹ The number of gas cells measured by Shimiya and Nakamura is a measure of the cells per unit area, i.e., surface measurements.

containing phases, the gluten phase and the free water phase. It also contains the starch granules which, as mentioned above, are embedded within the gluten phase. Free water comprises 17% (w/w) of water in dough (Eliasson and Larsson, 1993). The interface between the protein units and the starch granule is of an aqueous nature. The end result is that the two systems, starch and gluten, will tend to diffuse to form a continuous network.

The gas cells which were first introduced during the mixing process and now are expanded, are expected to account for the other half of the loaf volume. The size and distribution of these gas cells at the beginning and end of fermentation varies within the dough sample. In fact, if we are to cut the sample longitudinally with a razor blade, it is possible to see a structure that resembles a foam with a considerable variation in bubble size. One of the studies that presents a clear picture of the evolution of the size of the gas cells at different stages of breadmaking is that of Whitworth and Alava (1999). The authors studied bubbles of dough at the end of mixing and after the final moulding using a scanning electron microscope (SEM). They also studied the expansion of the bubbles during fermentation using an X-ray computerized tomography (CT) scanner. A summary of their results as well as the results of other researchers is presented in table 2.3.

2.2.4 Interactions between components in the continuous phase

The continuous phase contains the starch granules, which are dispersed throughout the gluten gel. The surfaces of starch granules are coated with a thin film of "free" water. The granules are associated into a network interpenetrating the continuous gel. The granules tend to be fused into the continuous protein network (Eliasson and Larsson, 1993). The fact that the starch granules can easily wash out from the gluten gel is

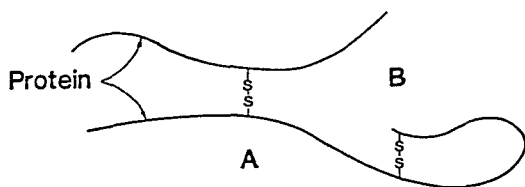


Figure 2.5a Illustration of disulfide bonding between polypeptide chains (A) and within a polypeptide chain (B). Taken from Hosoney, (1986)

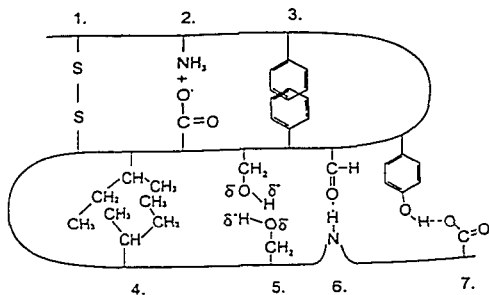


Figure 2.5b The typical interactions that stabilize the tertiary structure of the proteins include: 1. Disulfide bond formation from cysteine residues (intermolecular type); 2. Ionic (electrocovalent) bonding, e.g. from lysine and glutamic acid; 3. Hydrophobic interactions, e.g. from two side chains of phenylalanine; 4. Hydrophobic interactions, e.g. from two side chains of isoleucine; 5. Dipole-dipole (Van der Waals) interactions, e.g. from two side chains of serine; 6. Hydrogen bonding as in α -helix; 7. Hydrogen bonding between side chains, e.g. tyrosine and oxygen of carboxyl side chains. Taken from Cornell and Hoveling (1998).

consistent with such phase separation. If the starch granules were attached directly to the gluten gel, it would not be possible to "dilute" the granules away in an excess of water without the disintegration of the gel. The continuous protein matrix is generally credited with attaining the final objective of the baker, the production of a well-risen loaf of bread of satisfactory texture. In addition, the proteins largely govern the flour's water absorption, oxidation requirement and mixing and fermentation tolerance (Schofield, 1986). The backbone of the protein is flexible and to a limited extent can twist or curl into different forms. The sulfhydryl group on the amino acid cysteine is a reactive group; it can react with another cysteine residue to form a disulfide bond. That linkage contributes with hydrogen bonds to the protein's secondary structure (Cornell and Hoveling, 1998). The two cysteine residues can be on the same protein chain (intramolecular bonding), forming a loop in the protein or they can be on different protein chains (intermolecular bonding), linking two peptide chains together, as shown figure 2.5a (Cornell and Hoveling, 1998). A number of different types are responsible for the tertiary structure of the proteins. In most cases, the individual bonds are weak, but a large number of them creates the overall strength. These bonds include ionic bonds (salt formation between an acidic and basic group) and hydrogen bonds with side chains containing uncharged oxygen, nitrogen and hydrogen (Hoseney, 1986). Another type of bonding is hydrophobic bonding - two hydrophobic side chains associate closely with each other and, because of Van der Waal and other forces, to form a relatively weak bond. Figure 2.5b schematically illustrates the typical interactions that stabilize the tertiary structure of the protein gel.

2.3 Heat treatment of dough (Baking)

The final stage in breadmaking is baking which involves subjecting the dough to a heat treatment for a given period of time. This process, in which the raw piece of dough is transformed into a light, porous, readily digestible and favorable product, is a very important step and directly influences the quality of the final product. Various chemical, biochemical and physical reactions take place which irreversibly alter the structure of the major dough constituents. Some of the apparent effects of this heat treatment are (Pylar 1988): 1) volume expansion, 2) formation of enveloping crust, 3) inactivation of yeast and other enzymatic activities and 4) coagulation of the dough's protein and partial gelatinization of its starch. The end result of these transformations is that new flavorful substances are produced. Such substances include caramelized sugars, pyrodextrins and melanoidins as well as osmotic compounds such as aldehydes, ketones, various esters, acids and alcohols. The factors that vitally affect the baking process include the rate and the amount of heat applied, the relative humidity within the baking chamber and the duration of the bake (Ponte and Faubion, 1987).

The baking process may be divided into three stages. In the first stage, the temperature of the dough rises slowly to accelerate the enzymatic activities and yeast growth which will directly result in an increase in the loaf volume (Pylar, 1988). Hlynka (1972) reported that baking results in an additional expansion of about one-third of the original volume of the proofed dough. This sudden rise may be explained using Charles' Gas Law, i.e., when heat is applied to a gas at constant volume, the pressure of the gas will increase in proportional to the temperature. If this gas is contained in an elastic or expandable cell, the immediate result of this pressure increase is an increase in the volume

of the cell. In this case, the dough system, which contains many gas cells (of various sizes) confined within the elastic cell walls, will indeed expand, resulting in an increase in the total volume of the dough system. Another factor which contributes to oven spring¹ is the effect of heat on carbon dioxide. As the temperature is increased within the dough beyond 49 °C, the carbon dioxide held in solution is released and migrates into the existing gas cells adding to their internal pressure and thereby increasing their size. Moore and Hosney (1985) have determined that the total expansion as a result of the baking process cannot only be attributed to carbon dioxide but also to the ethanol at elevated temperatures. They have reported that carbon dioxide only accounts for half of the increase during oven spring. They suggested that of the carbon dioxide expansion, 57% is as a result of expansion of gas that already exists in the cell, 39% is due to release of carbon dioxide from the aqueous phase and 4% is due to the effect of the temperature increase on activity of the yeast.

Another event that takes place during the first stage of baking is the effect of heat on enzymes and bacteria. Walden (1959) reports that when the dough temperature reaches 50 °C to 60 °C most of the enzymes undergo a thermal inactivation so that yeast and bacteria are killed. He found that inactivation of malt α -amylase takes place between 65-95 °C, that β -amylase inactivates in the range 57 to 72 °C, and that fungal α -amylase is inactivated at 60 °C. The surface skin of the dough starts to thicken, loses its elasticity and begins to show a browning coloration. According to Hlynka (1972), the duration of the first stage of baking is about half of the baking time.

¹ The term oven spring refers to the sudden expansion of the dough when it is placed in the oven. It is caused by the expansion of the gas entrapped in the cells due to the increase in temperature.

The second stage of baking covers the rest of the baking time. In this stage, the crumb reaches a temperature of 98.9 °C which coincides with the temperature of maximum evaporation rate, starch gelatinization and protein coagulation. The interior of the dough progressively transforms into a crumb from its outer to inner portions by the penetrating heat. As the temperature of the outside regions of the loaf reaches 205 °C, a crust of brown color starts to form. The final stage, in which the temperature of the crumb crust reaches the maximum oven temperature serves to firm up the cell walls and develop the final crust color and a volatilization of certain organic substances. This volatilization is referred to as "bake-out loss" (Eliasson and Larsson, 1993).

As mentioned in the beginning of this section, one of the important factors that has to be kept in mind is the relative humidity within the oven or as it is sometimes called, the "oven steam" (Pyle, 1988). This plays an important role during the first stages of baking and in particular it acts to preserve the extensibility of the surface of the dough piece over the critical period of the oven rise. In addition to promoting heat penetration into the interior of the loaf, it also imparts desirable gloss to the crust. Marston and Wanna (1976) reported that lack of sufficient moisture will have a negative effect, in which the starch layer will undergo pyrolysis rather than partial gelatinization and the crust will not acquire its desired glossy look. The moisture will also penetrate the surface into the porous portion thus keeping it flexible.

2.4 Final crumb structure

As the crumb temperature reaches 70 °C, the protein begins to undergo thermal denaturation that reduces its water-binding capacity to practically zero (Baker, 1957). Baking thus causes the transfer of the water from the proteins to the starch in the course of gelatinization. In dough, the protein films provide the dough with its structural integrity that sustains the loaf volume. As the temperature rises these films transform into a semi-rigid structure, within which swollen starch is embedded. The final baked product, bread, consists of two somewhat different structures: crust and crumb. Their relative percentage depends on the experimental conditions such as oven temperature and baking time. Westerlund *et al.* (1989) reported that the crumb percentage represents about 41% of the total weight of the dry weight of the loaf. For the purpose of the experiments presented in this thesis, we will only consider the structure of the bread crumb and ignore the structure of the crust.

The most noticeable changes result, from the microscopic point of view, in the opening of the foam type of gas cell to give pores and the solidification of the aqueous bulk medium. The solidification is a result of the loss of cohesiveness when the gluten is transformed into coagel and partly due to the gelatinization of the starch granule in a regime in which there is no excess of water outside the starch granules. Figure 2.6 shows a cross section and the microstructure of the crumb as taken by a digital camera. The pore surface is considered to consist of a monomolecular lipid film with only a few patches of polymerized high molecular weight storage protein units dispersed within it (Eliasson and Larsson, 1993). The remainder of the pore wall consists of the continuous phase of the dried aqueous phase of the partly gelatinized starch. In figure 2.6 we also see that the

pores differ in sizes as we move across the plane of the crumb. This is due to the expansion that occurs during the oven spring in which the temperature of the center of the crumb is not the same as that of the outer regions. This temperature gradient will result in a pressure gradient which in turn will influence the cell structure of the crumb. Also, the cells in the lower region of the baking pan appear to be smaller which is a direct result of the confining effect of the baking pan walls (Kulp, 1991). The pan walls limit the expansion of the gas cells during fermentation and baking (Ponte and Faubion, 1987).

2.5 Dough and bread preparation, freeze drying, cutting and bonding

2.5.1 Dough and bread preparation

For all of the experiments investigated in this thesis the type of the flour used was milled from Canadian Western Red Spring (CWRS) hard wheat grade No. 1, with a protein content of 12.4%. The wheat was milled in the Canadian International Grains Institute (CIGI) pilot mill at the Grain Commission located in Winnipeg, Manitoba, Canada. Except when it is specified otherwise, the dough and breadcrumb samples were prepared using the Canadian Short Process Method (Preston *et al.* 1982) which was carried out using the following constituents: flour (200 g), yeast (3.0%), salt (2.4%) and water (63% to give optimum absorption). For the bread samples, in addition to these ingredients, the following ingredients were added: sugar (4.0%), phosphate (0.1%), shortening (3.0%), whey (4.0%), malt (0.2%), potassium bromate (30 ppm) and ascorbic acid (37.5 ppm). The ingredients were then added to the mixing bowl of the GRL-200 mixer. The dough was mixed at 165 rpm to 10% past peak consistency at 30°C. The dough was then

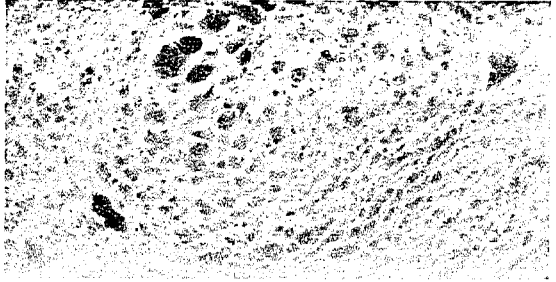


Figure 2.6. Digital image of an optimum proofed breadcrumb.

allowed to rest for 15 minutes in the proofing cabinet at 30°C and 83% R.H., then rounded by hand and given a further 15 minutes rest time at 30°C and 83% R.H. Doughs were then sheeted, moulded and panned, as described for the Remix procedure (Irvine and McMullen, 1960; Kilborn and Tipples, 1981a,b), proofed at 37.5°C for 70 minutes, and baked for 30 minutes at 205 °C. Note that 70 minutes is the optimum proofing time. To vary the density of the breadcrumb, the proofing time was also varied for the bread samples.

In preparation for the ultrasonic experiments the breadcrumb samples had to be cut, freeze dried and bonded to a thin transparency sheet. The latter was necessary to protect the freeze dried sample from the coupling gel. For experiments performed on the dough (unyeasted and yeasted), the procedure was straightforward. After mixing, the dough was cut into small pieces weighing about 4-gram masses and transferred into the sample holder to be placed between the two transducers for subsequent measurements. However, for the experiments involving freeze dried bread, the samples had to go through several preparatory steps before measurements were performed on them. These steps include: 1) cutting the fresh baked loaf into slices of 1 to 5 cm thickness using an electric slicer (Tefal, model 220) and removing the crust using an electric knife (Van Wyck, model 0601), 2) freeze drying the slices and 3) cutting the freeze dried samples to achieve parallel sides. Each of these steps was important and had to be done with extra caution to eliminate any errors that might arise from such factors as non-parallelism and density variations in the compressed bread samples.

2.5.2 Freeze drying

Freeze drying the sample was a useful and important procedure in the ultrasonic experiments for the following reasons (Potter, 1986): 1) to fix the structure of the bread crumb with minimal structural changes due to shrinkage, thus making the task of achieving samples with parallel sides relatively easy, and 2) rapid complete dehydration of the breadcrumb so that the sample is rigid and easy to handle. The latter was important because fresh bread was found to be absorbent to most bonding agents that could be used.

The principle behind freeze-drying is that under certain conditions of low vapor pressure, water can sublime from the ice without the ice melting to a liquid (Potter, 1986). Dry ice sublimates at atmospheric pressures and room temperatures. Frozen water will sublime if the temperature is 0°C or below and the frozen water is placed in a vacuum chamber at pressure of 4.7 mm-Hg or less (Potter, 1986). Within the vacuum chamber, heat is applied to the frozen food to provide the energy for sublimation. If a sufficiently high vacuum is maintained, usually within the range of about 0.1-2 mm-Hg, and the heat is controlled just short of melting the ice, moisture vapor will sublime at a maximum rate. Sublimation takes place from the surface of the ice and so as it continues, the ice front recedes towards the center of the food piece: thus the food dries from the surface inwards. Finally, the last of the ice sublimates and the food is below 5% moisture content (Potter, 1986)

2.5.3 Sample cutting and bonding

After the samples were freeze-dried, they were cut to the desired thickness, which depends on the ultrasonic frequency used. For the compressed breadcrumb samples, where the attenuation was found to be high, the sample thicknesses had to be very thin

(about 4 mm). However, for the non-compressed samples, where the attenuation was not as high, the thickness was as large as 1 cm. In both cases, the freeze-dried breadcrumb samples had to be cut and machined to achieve perfect parallelism of the sides perpendicular to the ultrasonic propagation direction. To cut the freeze-dried samples, we first mounted the sample on a 1-cm-thick acrylic plate using a silicone sealant. After the sealant dried, the sample was then transferred into a precision cutting machine (Micro-Matic Precision Wafering Machine made by Micromech MFG Corp. Model No. WMSA 2269) that uses a 2mm-thick steel plate rotating at 3450 r.p.m. After the sample was cut, the two sides perpendicular to the ultrasonic propagation direction were polished using fine (600 grit) silicon carbide waterproof paper made by Carborundum Abrasives. Once parallelism of the two faces was achieved, the sample was then mounted into a custom made holder shown in figure 2.7. The sample holder was machined so that it had the same thickness as the sample. The sample was then bonded to a pair of thin transparencies using a two component and low viscosity epoxy made by Emerson and Cuming (model STYCAST 1266). After that, the sample was fixed into the custom made sample holder and water proofed using a silicone rubber sealant (made by General Electric). These steps were necessary to ensure that the sample does not absorb any water from the surroundings and, protect the sample against cracking and other mechanical damages that might arise from handling the sample.

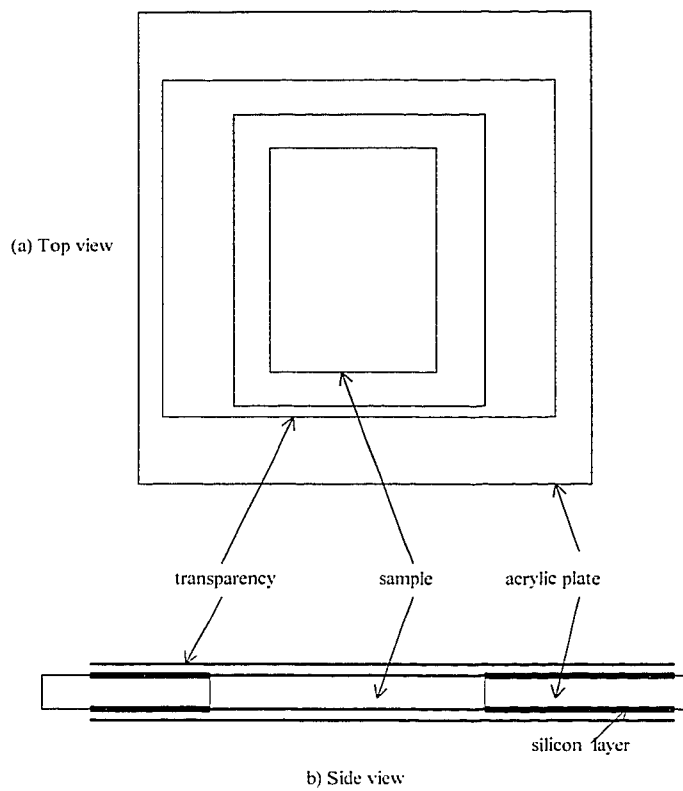


Figure 2.7 Sample holder, bonding and water proofing.

Chapter three

Ultrasonic waves in liquids and solids: basic theory and experimental methods

3.1 Introduction to ultrasound and its relation to food systems

Ultrasonics is the name given to the study and application of mechanical sound waves propagating at frequencies greater than the upper limit of audibility heard by the human ear (larger than 16-20 kHz). Evaluation of inorganic materials by ultrasonics is an established and successful technique. The study of ultrasound wave propagation has been used in a wide variety of applications. One of the first important applications of ultrasound technology was its use for military purposes as a mean for detecting submarines underwater during the first world war (Kinsler *et al.*, 1982). Manufacturing industries and medicine have used ultrasound to monitor metals and biological tissues respectively. Ultrasound is very sensitive to the presence of internal defects and structural flaws, such as air pockets and fractures. Between 20 kHz and approximately 100 kHz, high power ultrasonic devices are used to initiate or speed up chemical reactions. This branch of ultrasonics is known as sono-chemistry (Mason and Lorimer, 1989).

To date, however, ultrasound has found relatively little application in food materials, even though ultrasonic methods ranging in frequency from 50 kHz up to the MHz range can be used to examine food and related systems. Some examples of the applications include the use of ultrasound in emulsification (McClements *et al.*, 1993).

cleaning (Lambert, 1982) and animal backfat thickness estimation (Lister, 1984). Other more recent applications include the homogenization of food materials (Fairley, 1992), the disaggregation of gluten proteins (Singh *et al.*, 1990), determination of solid and fat content in foods (Povey, 1997), enhanced sterilization (Campbell and Schoenleber, 1994) and particle sizing in food emulsions (McClements, 1994). There is also a growing interest in the use of ultrasonic methods to provide data on-line and non-destructively on the bulk properties of food materials (Agricultural Research Council, 1982).

The emphasis of these applications is the use of ultrasound to probe the food material non-destructively. The great advantage of ultrasound compared with other non-intrusive methods such as light scattering is that the majority of food materials do transmit ultrasound even though they may be optically opaque. Therefore, there remains a wide range of liquid based foods, and even certain solids, which are amenable to analysis using ultrasonic methods.

In general, the propagation of ultrasound through a system depends upon its response to rapid pressure fluctuations; in principle all its mechanical properties, and indirectly some of its thermal properties, have an effect on the propagation of sound through the material. Foods are rarely homogeneous, and the transmission of ultrasound through a multi-phase material is influenced not only by the properties of the various phases in isolation, but also by the physical structure. These structural features include the concentration, size and distribution of phases or particles, and ultrasound sensitivity to these features depends on the mismatch in the acoustic properties of the constituents. The full picture is very complex but the corollary is that the ultrasonic response is sensitive to many of the key mechanical properties of foods. Therefore, there is considerable interest

in using ultrasound in the food industry to monitor food properties, provided that the samples are otherwise well characterized.

In the following subsections, the fundamentals of ultrasonics, and in particular their relevance to food materials are presented. Initially the principles of ultrasonic wave propagation, with special reference to multi-phase materials are summarized. The manner in which these measurements may be done in practice are then described.

3.2 Propagation of ultrasound

The principle of wave propagation through a single-phase material can be presented in a simple way, provided that certain assumptions are made. When the propagation of ultrasound through materials containing two or more phases are being considered, even the simplest treatment is already complex. This is the case whatever the nature of the multi-phase material. However, for certain combinations of material properties, simplifications of the treatment may be possible, especially if the internal structures occupy particular size ranges relative to the wavelength of ultrasound.

The features of ultrasonic wave propagation of which most use has been made experimentally are the velocity and attenuation of the wave. To gain a better understanding of these two quantities, we will first discuss their behavior in single-phase materials. After that, we will discuss their expected behavior in multi-phase materials such as dough and freeze-dried bread. We begin by considering ultrasound that is produced at single frequency, f , and is in the form of a plane wave. The former constraint means that continuous waves are considered, while the later means that the wave extends to infinity in planes normal to the direction of propagation. It is further essential to restrict the power

carried by the wave, so that the maximum induced change in the density of the medium at any point in space is much smaller than the average density at that point.

3.2.1 Homogeneous single-phase materials

Subject to the above restrictions, it can be shown (Coulson, 1955) that a longitudinal ultrasonic wave, propagating through the medium in the x -direction with an amplitude A , is given by

$$A = A_0 \exp(-\alpha x / 2) \exp\{i(kx - \omega t)\} \quad (3.1)$$

Here A_0 is the amplitude at $x = 0$, α is the attenuation coefficient in m^{-1} , $k = 2\pi / \lambda$ is the wave number, λ is the wavelength and ω is the angular frequency ($= 2\pi f$).

The phase velocity at which the sound travels is $v = \omega / k$. The velocity of propagation, the phase velocity, in a solid material is related to the longitudinal modulus, β , of the material and its density, ρ , by

$$v_l = [\beta / \rho]^{1/2} \quad (3.2)$$

where

$$\beta = B + \frac{4}{3}\mu \quad (3.3)$$

Here B is the bulk modulus (equal to the inverse of the compressibility), μ is the rigidity modulus (shear modulus) and the subscript l in equation 3.2 refers to longitudinal velocity. A derivation of this expression is given in Kinsler *et al.* (1982) who also give an introduction to the theory of ultrasonic propagation. In homogeneous materials, the compressibility and the shear modulus are determined by the interatomic or intermolecular forces.

For most purposes, it is only necessary to appreciate that a measurement of the ultrasonic velocity provides information about the ratio of a elastic modulus to the density of the material through which it propagates. Thus independent measurements of density and velocity enable a value of the combined elastic modulus $B + \frac{4}{3}\mu$ to be determined.

For liquids, equation 3.2 becomes

$$v = \left(\frac{B}{\rho} \right)^{1/2} \quad (3.4)$$

since liquids have no rigidity. The speeds of longitudinal sound waves through liquids and solids at room temperature are typically in the ranges 1000-2000 ms⁻¹ and 2000-7000 ms⁻¹ respectively. Some food systems have a rigidity modulus that is much smaller than the bulk modulus. Examples of such systems are gels (Povey, 1998), in which case equation 3.4 provides a good approximation.

In foods with non-zero shear modulus, a different type of ultrasonic wave may also propagate, called a shear wave, in which the material moves transversely to the propagation direction of the wave, thereby inducing a shearing action in the material. The velocity of propagation is generally less than that of a compressional wave and is given by:

$$v_s = \left(\frac{\mu}{\rho} \right)^{1/2} \quad (3.5)$$

where v_s is the shear wave velocity.

Many foods and food related materials do not behave ultrasonically as either simple liquids or solids; instead they display viscoelastic properties. Such properties can be accounted for by attributing a frequency dependence to the bulk and shear moduli of

the material. These moduli are a mathematical expression of the fact that such materials flow when subjected to a slowly applied stress, although under a rapid blow they behave like solids, some even fracturing.

Whereas knowledge of the wave speed provides information about the modulus of the material, the attenuation coefficient depends on other material properties. Even in pure homogeneous materials, there are many possible causes of attenuation. For fluids these can generally be divided into three main types: absorption due to viscous losses, heat conduction losses and molecular relaxation processes (Kinsler *et al.*, 1982). All of these processes are characterized by a relaxation time τ , which represents the time for local equilibrium to be re-established following the perturbation caused by the ultrasonic wave. When the ultrasonic frequency is sufficiently low that $\omega \ll \tau^{-1}$, the attenuation due to all these mechanisms is proportional to ω^3 . The first of these processes, absorption due to viscous losses, results from viscous dissipation due to the relative motion of the fluid during the compression and rarefaction cycles of the ultrasonic wave. At low frequencies, the attenuation due to these viscous losses is given by (Kinsler *et al.*, 1982)

$$\alpha_v = \frac{2\omega^2 \eta_s}{3\rho v^3} \quad (3.6)$$

where η_s is the shear viscosity. Longitudinal ultrasonic waves also cause temperature gradients to exist in the medium through which the waves propagate, since at normal ultrasonic frequencies there is not enough time for heat to flow from the regions of compression to those of rarefaction so as to maintain thermal equilibrium. As a result, ultrasonic wave propagation is adiabatic, and heat conduction along the direction of the thermal gradients gives rise to thermal losses, given by

$$\alpha_i = \frac{1}{2} \frac{\omega^2}{\rho v^3} (\gamma - 1) \frac{K}{C_p} \quad (3.7)$$

where γ is the ratio of the heat capacities at constant volume and pressure, K is the thermal conductivity and C_p is the heat capacity at constant pressure (Kinsler *et al.*, 1982). For liquids that are non-metallic, the attenuation due to this thermal conduction mechanism is generally much less than that due to viscosity. For non-monatomic fluids, it may also be necessary to account for relaxation effects due to the internal degrees of freedom of the molecules and/or association or disassociation of different ionic complexes. These relaxations involve the exchange of energy at the molecular level, giving rise to a third attenuation mechanism that also depends quadratically on frequency in the low-frequency limit. The details of these effects are reviewed in more detail by Kinsler *et al.* (1982). Apart from heat conduction, solids generally possess different loss mechanisms from liquids, but a detailed discussion of these effects is beyond the scope of this thesis.

3.2.2 Multi-phase inhomogeneous media

In this section, we will present a brief discussion of the propagation of sound waves in multi-phase materials. This is a subject of great complexity, and as such presents enormous theoretical challenges. Nevertheless, theoretical treatments have been devised. For example, Ishimaru (1978) presents a detailed mathematical approach, which is also applicable to electromagnetic wave propagation as well as mechanical wave propagation.

When an ultrasonic wave propagates through a heterogeneous system, the wave may be scattered as well as absorbed. Scattering occurs whenever the constituent materials have different densities and/or phase velocities. Relatively simple examples of

such heterogeneous systems consist of spherical particles, voids or inclusions distributed throughout a second material, with the second medium forming a continuous phase. Dough, one of the two main food materials investigated in this thesis, is an important example of this type of system. In dough, the gluten matrix encompasses a high volume fraction of another phase - the starch granules. A third phase is also contained within the gluten matrix, but initially at a lower volume fraction- and these are the air bubbles. The largest difference in both density and velocity is between the air bubbles and the gluten matrix, so that the strongest scattering is from the air bubbles. In common with all such systems, the magnitude of the scattering at a given frequency is strongly dependent on the size of the dispersed bubbles; thus the scattering can be either enhanced or reduced by suitable choice of the ultrasonic frequency in a given experiment. However, one crucial point here is that the presence of scattering can produce a distortion of the wavefront when a plane wave propagates through the material. This occurs because, in addition to the ballistic component that travels straight through the material without scattering out of the forward direction, there is also a scattered component, which in general varies in both amplitude and phase across the output face of the sample. In the case where scattering dominates over absorption, Page *et al.* (Page *et al.* (1996), Schriemer *et al.* (1997), Cowan *et al.* (1998) and Zhang *et al.* (1999)), have shown how these two components to the total transmitted wave can be separated experimentally; this was achieved by taking advantage of the fact that the ballistic component is coherent, both spatially and temporally with the input pulse, whereas the scattered component varies incoherently across the detection plane. For both of the systems (dough and breadcrumb) investigated in this thesis, however, the opposite limit holds, where absorption dominates over scattering. Thus we

were not able to measure the scattered component of the transmitted waves independently in these experiments, so that we have focussed on measurements of the ballistic component only. This ballistic signal was measured reliably in our experiments, because the area of the detecting transducer was large enough that any incoherent scattered component was cancelled out in the phase sensitive piezoelectric transducers used, and therefore did not make a significant contribution to the measured signal. Since the ballistic signal propagates according to equation (3.1), its measurement allows quantitative information to be obtained on how both absorption and scattering influence the attenuation and phase velocity.

To interpret the velocity and the attenuation coefficient that describe the propagation of the ballistic component, we use effective medium theories. The simplest approach to this problem, originally due to Wood (1941), assumes that both the density and compressibility of the multi-phase material are simply volume fraction averages of their values in the separate media. Thus, for a two phase material

$$\rho_c = \phi\rho_1 + (1-\phi)\rho_2 \quad (3.8)$$

and

$$B_c = \left(\frac{\phi}{B_1} + \frac{1-\phi}{B_2} \right)^{-1} \quad (3.9)$$

Here ϕ is the volume fraction of the phase with density ρ_1 and bulk modulus B_1 . Substituting equations 3.8 and 3.9 into equation 3.4 leads to the following expression for the velocity of sound in a two-component composite material.

$$v^2 = \frac{v_2^2}{\left[1 - \phi \left(1 - \frac{\rho_1}{\rho_2}\right)\right] \left[1 - \phi \left(1 - \frac{v_2^2 \rho_2}{v_1^2 \rho_1}\right)\right]} \quad (3.10)$$

Here ρ_1, v_1 and ρ_2, v_2 are the velocities and the densities of the dispersed and continuous phases respectively. This equation is also called the Urick equation after Urick (1947).

Equation 3.10 may be written in a form which easier is to read as

$$\frac{1}{\rho v^2} = \frac{\phi}{\rho_1 v_1^2} + \frac{1-\phi}{\rho_2 v_2^2} \quad (3.11)$$

where ρ is given by equation 3.8. Other more sophisticated effective medium models, which give better descriptions of the behavior of the ultrasonic velocity as it propagates through the systems studied in this thesis, will be discussed in the relevant sections of chapters 4 and 5.

3.2.3 Velocity and attenuation in a system containing bubbles

If the density of the dispersed phase is much less than that of the continuous phase, i.e. $\rho_1 \ll \rho_2$, then resonant scattering may occur (Gaunard and Uberall, 1981). One important example is a liquid containing gas bubbles. Near the resonant frequency of the bubbles, given approximately by

$$\omega_o = \left[\frac{3\rho_1 v_1^2}{\rho_2 a_1^2} \right]^{1/2} \quad (3.12)$$

the ultrasonic attenuation is sharply peaked, and enhanced attenuation appears from zero frequency up to just above the resonant frequency, ω_0 ¹. Here ρ_1 and v_1 are the density and ultrasonic velocity in the gas bubble, respectively, ρ_2 is the density of the surrounding medium and a_1 is the bubble radius. For $\omega < \omega_0$ the velocity is considerably less than its value in the surrounding matrix and it is highly frequency dependent in the resonant region. At frequencies well above the resonant region, the velocity is expected to be same as in the matrix.

3.3 Apparatus and experimental procedure

The structural properties of dough and freeze-dried bread were investigated by studying the behavior of the longitudinal ultrasonic signal as it propagates through the samples. The ultrasonic parameters that characterize the propagation of the ultrasonic signal are the phase velocity and attenuation coefficient. The numerical values of these two parameters change as the structure of the material is altered, thereby providing a tool for monitoring these internal changes in the structure of the material.

To perform the velocity and attenuation measurements, the sample was sandwiched between two piezoelectric transducers. An electromagnetic (EM) pulse was generated and transmitted to one of the transducers which transformed the EM signal to an acoustic pulse with a central frequency determined by the resonant frequency of the transducers, 54 kHz. At the transducer/sample interface, the pulse was partially transmitted into the sample and partially reflected back into the generating transducer.

¹ For air bubbles in water, the resonance frequency is approximately 75 kHz for a bubble diameter of 75 μm .

The pulse that traveled through the sample was then detected by the transducer at the opposite side of the sample. The receiving transducer reconverts the acoustic pulse back into an EM pulse and the output signal was amplified and displayed on the oscilloscope. In order to measure the time taken by the acoustic pulse to travel across the sample, a separate reference signal was taken with the two transducers in direct contact. Another alternative was to measure the signal through a material with well-known acoustic properties. Ideally the reference and the transmitted pulses should have identical shapes and they should differ only in their time of arrival and their amplitude.

3.3.1 Apparatus

A block diagram of the apparatus is shown in figure 3.1, the details of which are described in this section. A Portable Ultrasonic Non-destructive Digital Indicating Tester (PUNDIT 6) was used to generate a short (+ ve) voltage pulse (or spike). The pulse was then sent through 50Ω BNC cables to the generating transducers. The generated ultrasonic signal traveled through the sample and was detected at the other face of the sample with a similar transducer, which converted the transmitted ultrasonic signal into an EM signal. This EM signal was then amplified at the receiver amplifier (PUNDIT 6) and displayed on a digital oscilloscope (Tektronix TDS 420 A).

3.3.1.1 Pulse generator and receiver

As mentioned above, we used a short pulse generator, PUNDIT 6 (made by CNS Farnell). The pulse generator may be operated at an EHT voltage of either 1.200 V or 500 V, as selected by a switch at the back of the unit, and can output pulses at a pulse

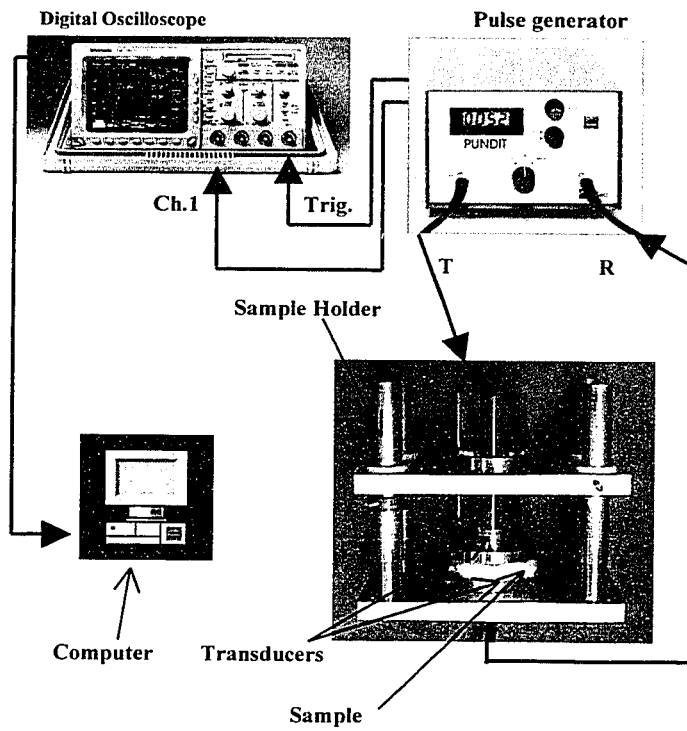


Figure 3.1: Block diagram of experimental set-up. Ch.1 is the viewing channel on the oscilloscope. Trig is signal used to trigger the oscilloscope, T is the generated signal to be sent through the sample. R is the received signal.

repetition rate of either 10 pulses per second (pps) or 100 pps. A 3.5 V positive pulse with a rise time of 2 μ s, synchronized with the main output signal, was used to trigger the oscilloscope. The receiving amplifier has a high input impedance enabling the instrument to be used with piezoelectric transducers over the frequency range 5kHz to 1MHz.

3.3.1.2 Transducers

The transducers used in these experiments have a fundamental frequency of 54kHz. They are made of lead zirconate titanate (PZT4) ceramic piezoelectric elements mounted in stainless steel cases. The elements are very tightly held on the inside face of the stainless steel case to provide highly efficient acoustic transmission. The voltage excitation of the pulse generator causes the transducer to oscillate mechanically at its own natural frequency (54kHz).

The principle of operation of the transducers may be explained as follows: when an EM pulse is applied to a piezoelectric material, the driving voltage oscillations cause mechanical vibrations of the piezoelectric surface. The surface of the piezoelectric element will vibrate at the same frequency as the RF signal (and causes acoustic waves to propagate through the transducer material). Piezoelectric materials can be used to both produce and detect vibrations. They operate most efficiently when the driving frequency excites a mechanical resonance in the transducer: the wavelength of the fundamental resonance is twice the thickness of the transducer, and odd harmonics can be produced by driving the transducer at the appropriate resonant frequency.

One phenomenon that may affect the detected ultrasonic signal is ringing, in which oscillations of the transducer persist after the duration of the initial driving pulse. To understand how ringing might affect the detected signal, consider a pulsed excitation of a

piezoelectric element placed between two materials of different acoustic impedances. The element has an acoustic impedance mismatch with its surroundings, so that reflections occur at the interfaces, causing interference with the desired waveform and increasing the temporal extent of the pulse. In well-backed transducers, ringing effects are minimized using a highly attenuating material as a backing layer to which the piezoelectric element is bonded. The acoustic impedance of the backing material should be comparable to that of the piezoelectric element. The backing absorbs the acoustic energy radiating from the back face (directly) and from the front face (upon reflection) of the element, thus minimizing ringing. The transducers supplied with the PUNDIT unit did not appear to be well backed, with the result that ringing was quite substantial under normal operating conditions. In fact, there were no technical data provided to us by the manufacturer as to what type of materials were used as backing, if any, or how the transducers were assembled.

3.3.1.3 Sample holder

The transducers were mounted in a custom-made sample holder to control the sample thickness precisely and provide support to the transducers while maintaining their front faces parallel to each other. The sample holder is shown in figure 3.2. The transducer support consisted of a top and a bottom aluminum plate of thickness 2 cm. The top plate was allowed to slide up and down the supporting rods, while the bottom plate was fixed in place to the same supporting rods. The bottom transducer was held in place using a tightly fitting aluminum guard ring that was screwed into the 2-cm-thick bottom plate. The top transducer, on the other hand, was tightly held in a hollow acrylic cylinder, which was allowed to slide in the vertical direction with respect to the top 2-cm-

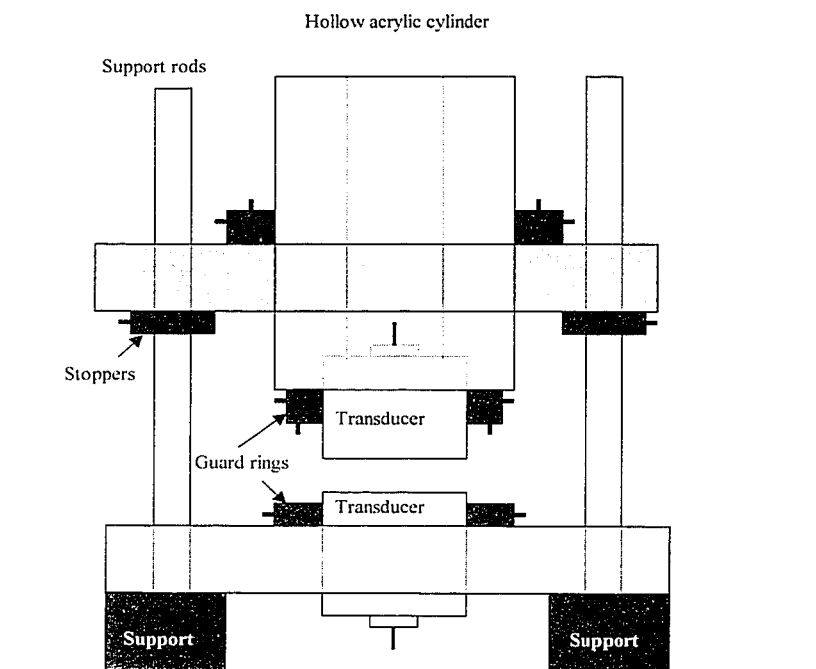


Figure 3.2a. Transducer holders. side view

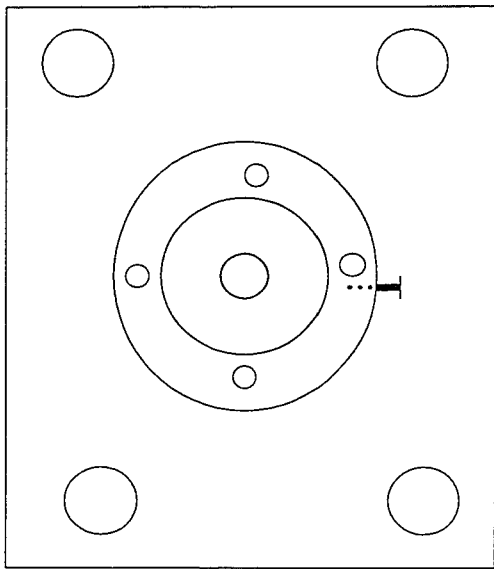


Figure 3.2b. Transducer holders. top view

thick aluminum plate.

To set the sample thickness, we first placed a number of 1-mm glass slides on the lower transducer and then lowered the top transducer until it freely rested on top of the glass slide. After that, the stopper rings on the support rods were screwed in tightly to prevent the top plate from sliding beyond the preset sample thickness. Upon raising the top plate, the sample was then placed on top of the lower transducer, and the top transducer (which was fixed to the top plate) was lowered down. The top plate was not able to slide past the preset thickness because of the stopper rings that were screwed in place on the support rods.

3.3.1.4 Data acquisition and signal averaging

The data were acquired using a computer-controlled digitizing oscilloscope (Tektronic TDS 420 A) which was set in averaging mode. The signal averaging, which consisted typically of 1000 sweeps, greatly improved the signal-to-noise ratio. The triggering of the sweeps was performed by the TB synchronization output on the pulse generator, so as to synchronize the data acquisition with each repetition of the pulse from the signal generator. The oscilloscope was capable of a maximum digitizing rate of 1 GigaSample/s and could acquire record length of up to 50000 points. A general purpose interface bus (GPIB) connection between the oscilloscope and the computer allowed direct control of the data acquisition and enabled the acquired waveforms to be transmitted directly to the hard disk of the computer for subsequent analysis.

3.4 Velocity and amplitude measurements

The velocity and the amplitude were calculated from the waveforms that were stored in the computer, using computer software called Microcal Origin (Microcal

Software Inc.). Typical examples of the reference and sample waveforms are shown in figure 3.3. The amplitude of each waveform was directly measured from the height of the second oscillation in volts. The reason for using the second oscillation rather than the peak of the waveform was to avoid interference effects that arise from the ringing of the transducer and possible scattering effects. The velocity on the other hand was measured by calculating the time taken for the signal to travel from one side of the sample to the other. This was done in two steps. In the first step a reference waveform was acquired. This waveform was taken with the two transducers separated by a material of well-known acoustic properties. In all of the dough experiments, the material used was an acrylic plate of thickness 2 cm. This same plate was used in the density measurements for the yeasted dough experiments. The two transducers were bonded to the plates or each other *via* a thin coupling layer (Ultrasonic Gel II, Diagnostic Sonar Ltd.). After the transmitted signal was acquired, the two waveforms (reference and transmitted) were downloaded to the computer. The transit time Δt was then calculated by measuring the time difference between the first two oscillations of the reference and the sample waveforms as follows. This was accomplished by aligning the two waveforms using the pulse shape as a guide. The delay time introduced by the reference signal (through the acrylic plates) was then subtracted from the measured time, Δt , to give the time taken for the signal to travel through the sample, t . Figure 3.3 shows the reference, the transmitted waveforms and Δt . The transit time in conjunction with the sample thickness, yields the velocity of sound through the sample *via* $v = d/t$, where d is the sample thickness and t is the transit time.

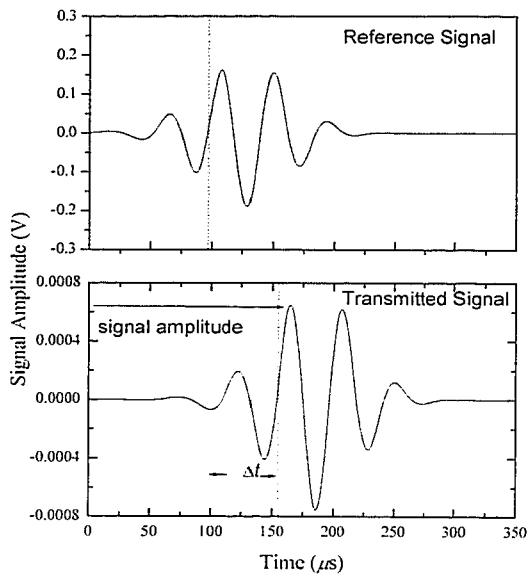


Figure 3.3 Reference and transmitted waveforms

Chapter 4

Results and discussion part I: Dough mixing and fermentation

It was reported in section 2.2 that the air bubbles are introduced into the dough during the mixing stage. These will inflate during the yeast fermentation stage. In this chapter, we discuss in detail the results of a comprehensive experimental study of the mixing and fermentation stages using the ultrasonic technique. In section 4.1, we investigate the aeration of dough during the mixing process and its effect on the structural properties of the dough, as measured by the ultrasonic parameters. To accomplish this, we performed a set of ultrasonic experiments on un-yeasted dough samples in which we varied the mixing pressure. As is discussed in more detail below, the net effect of changing the pressure during mixing is to change the number of air bubbles per unit volume introduced into the dough, but the size of these bubbles stays approximately the same for all mixing pressures. This procedure allowed us to vary the amount of air within the sample, enabling us to investigate the elastic properties of the dough as a function of the amount of air occluded into the dough.

In section 4.2, a discussion of the results of the experiments performed on the dough with yeast will be presented. The yeast cells will generate CO_2 as a result of their fermentation activities. The CO_2 produced will cause the air bubbles to expand during fermentation, leading to an increase in the bubbles' size and expansion of the total dough

volume; hence there is also a decrease in the number of bubbles per unit volume. This provides a different way of changing the void fraction within the sample than that achieved by reducing the pressure. The aim of the experiments on dough with yeast is to investigate the changes in mechanical properties of the dough as a function of fermentation time. The findings of the two sets of experiments done on doughs (yeasted and unyeasted) should provide complementary information that can be used to understand the effects of the structural changes accompanying the two important processes in breadmaking process (mixing and fermentation) and hence predict the quality of the final product. This is true, even though in most plant bakeries, a number of additional ingredients will be added which will influence the manner in which mixing and fermentation proceed.

4.1 Aeration of dough during mixing: Unyeasted dough

In order to investigate the aeration of dough during the mixing stage, we varied the mixing pressure, thereby varying the concentration of the air bubbles within the dough. The structural changes that occur in the dough will be detected *via* the change in the behavior of the ultrasonic velocity and attenuation coefficient. Before we proceed with the discussion of the results of the experiments performed on samples mixed at different pressures, we will introduce the hypothesis by which mixing under reduced pressure reduces the number of bubbles per unit volume. The reader is reminded that throughout all of section 4.1, the ingredients of the dough were limited to flour, water and salt. This was done to eliminate any other complications that might arise from additional ingredients

such as yeast and improvers, which will introduce additional effects that influence the behavior of the ultrasonic parameters.

4.1.1 Introduction: mixing under reduced pressure

As discussed in chapter 3, the gas cells are introduced into the dough during the mixing stage in which mixing beats air bubbles into the dough and subdivides it to produce gas cells of small size. Baker and Mize (1941a,b) showed that when the dough is mixed under vacuum, the air cells can be substantially eliminated. Their results showed that for doughs mixed under reduced pressure, the number of air cells per unit volume is much less than when the dough was mixed at atmospheric pressure and the cell walls were apparently thicker. Also, the density of the dough mixed at reduced pressures was found to be higher than that of dough mixed under ambient (atmospheric) pressure. In fact, this early work provided direct experimental evidence that the air cells originate exclusively during the mixing rather than the fermentation stage. More recently, Campbell (1991) and Campbell *et al.* (1998) studied the effects of mixing under reduced pressure on the aeration of bread dough. In their study, they explain how mixing under reduced pressure reduces the number of air cells. Their hypothesis suggests that mixing under reduced pressure produces fewer bubbles per unit volume in the dough but the size distribution of the bubbles stay the same. The mechanism by which they explained their hypothesis is illustrated in figure 4.1. Three major aeration processes have been identified during mixing (Campbell, 1991): entrainment of air, disentrainment of air and bubble breakup. In addition, the bubbles in the dough will experience extra compression due to the viscoelastic nature of the dough (Fogler and Goddard, 1970). In step (a) in figure 4.1.

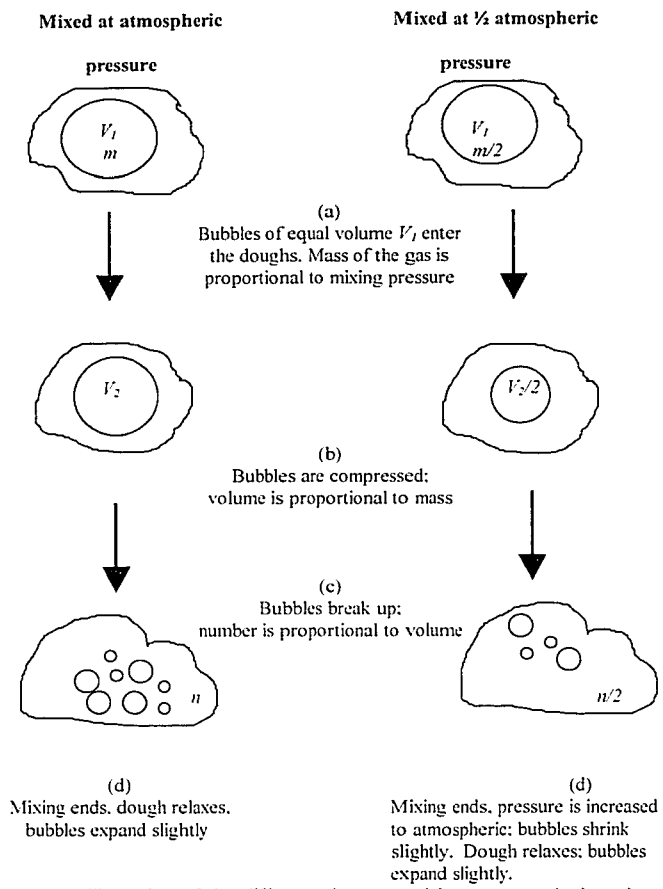


Figure 4.1. Illustration of the difference between mixing at atmospheric and under reduced pressure. Taken from Campbell *et al.* (1998)

two primary bubbles of equal volume enter the doughs which are being mixed at atmospheric pressure and at half atmospheric pressure. The mass of the gas in the bubble in the dough mixed at half atmospheric pressure is half of that mixed at atmospheric pressure, since the ideal gas law, $PV = nRT$, holds to a good approximation (Campbell *et al.*, 1998). Once inside the dough, step (b), both bubbles experience compression due to the stress in the dough. If the compressive stress is large compared to the external pressure and the surface tension contribution, then both bubbles are compressed to a volume approximately proportional to the mass of the gas contained, i.e. the bubble entrained at half atmospheric pressure is half the volume of the bubble entrained at atmospheric pressure. Upon further mixing, step (c), both primary bubbles break up giving the same size distribution of small bubbles. However, there are twice as many bubbles in dough mixed at atmospheric pressure than there are in the dough mixed at half atmospheric pressure. This behavior is predicted under the assumption that the equilibrium bubble size distribution depends on the break-up forces of the mixing action.

At the end of mixing, step (d), the final pressure is one atmosphere, so that the bubbles in the dough mixed at half atmospheric pressure case shrink. However, this shrinkage does not occur immediately, due to viscoelastic properties of the dough. At the same time, the bubbles should expand as the compressive strain that developed during mixing relax. This expansion also should occur in the dough mixed at atmospheric pressure. This mechanism explains why mixing at reduced pressure produces fewer bubbles, but a similar distribution of sizes, than mixing at atmospheric pressure.

To explain this effect mathematically, Campbell, (1990) formulated a mass balance equation of entrainment and disenitainment of air in the dough during mixing. The mass balance maybe stated as

$$\left(\begin{array}{l} \text{Rate of accumulation} \\ \text{of air in dough} \end{array} \right) = \left(\begin{array}{l} \text{Rate of flow of air} \\ \text{into the dough} \end{array} \right) - \left(\begin{array}{l} \text{Rate of flow of air} \\ \text{out of the dough} \end{array} \right)$$

$$\frac{dm_a}{dt} = \dot{m}_i - \dot{m}_o \quad (4.1)$$

where m_a is the mass of air in the dough per unit volume of gas-free dough and \dot{m}_i and \dot{m}_o are the mass flow rates of air into and out of the dough per unit volume of gas-free dough respectively. Entrainment of air into the dough occurs as the surfaces of the dough come into contact with the air during mixing thereby entrapping a volume of air. This volume is independent of the pressure but the mass of the air it contains is proportional to the pressure. The volume of air entrained per unit volume of gas-free dough per second,

\dot{V} , is related to the mass flow rate via the ideal gas law:

$$P \dot{V} = n RT = \frac{\dot{m} RT}{M_w} \quad (4.2)$$

Where n is the number of moles. R is the universal gas constant. T is the temperature and M_w is the molecular weight. Therefore

$$\dot{m}_i = \frac{\dot{V} P M_w}{RT} \quad (4.3)$$

To model disenitainment, it is proposed that the mass flow rate of air out of the dough is proportional to the mass of air already in the dough, m_a .

$$\dot{m}_o = k m_a \quad (4.4)$$

where k is a constant measured in units of s^{-1} representing the mass of gas disentrained per unit mass of gas in the dough per second. Although the above is based on mass conservation, we want to convert this to the volumetric air content of the dough. Let the volume of air per unit volume of gas-free dough, measured at atmospheric pressure be V_a .

From the ideal gas law,

$$\begin{aligned} P_{am} V_a &= nRT = \frac{m_a}{M_w} RT \\ \Rightarrow m_a &= \frac{V_a P_{am} M_w}{RT} \end{aligned} \quad (4.5)$$

Therefore

$$\dot{m}_o = \frac{k V_a P_{am} M_w}{RT} \quad (4.6)$$

Substituting into equation 4.1 for \dot{m}_i and \dot{m}_o we get:

$$\begin{aligned} \frac{dm_a}{dt} &= \frac{\dot{V} P M_w}{RT} - \frac{k V_a P_{am} M_w}{RT} \\ &= \frac{P_{am} M_w}{RT} \left(\frac{P}{P_{am}} \dot{V} - k V_a \right) \end{aligned} \quad (4.7)$$

In terms of volume, we get:

$$\frac{dV_a}{dt} = \frac{P}{P_{am}} \dot{V} - k V_a \quad (4.8)$$

At the steady state flow in which there is no change in the air content of the dough so that

$$\frac{dV_a}{dt} = 0. \text{ Then,}$$

$$V_a = \frac{P}{P_{atm}} \frac{\dot{V}}{k} \quad (4.9)$$

Thus, at a steady state flow, the volumetric air content of the dough at a steady state depends on the mixing pressure and on the balance between the rate of entrainment and disentrainment of air in the dough. Considering the case when the dough is mixed at atmospheric pressure,

$$V_a = \dot{V} R_i \quad (4.10)$$

where R_i is the inverse of k .

The dependence of the dough volume on mixing pressure will cause the density of the dough to change as the mixing pressure is varied. Therefore, the first experiment that had to be performed was the determination of dough density as a function of mixing pressure. This will enable us to represent the ultrasonic parameters as a function of density and hence relate these parameters to the structure of the dough. In the following section, the measurements and results of the density of unyeasted dough as a function of mixing pressure will be discussed in detail.

4.1.2 Density of unyeasted dough

The density of the unyeasted dough was measured using a 25 ml specific gravity bottle with a 2.4-cm-diameter neck (Kimble Glass Inc.). For each mixing pressure, several small samples, each about 4 grams, were cut from the same dough piece. The volume of each sample was calculated by calculating the volume of the water that escaped from the specific gravity bottle when the sample was immersed in the bottle. The density was then

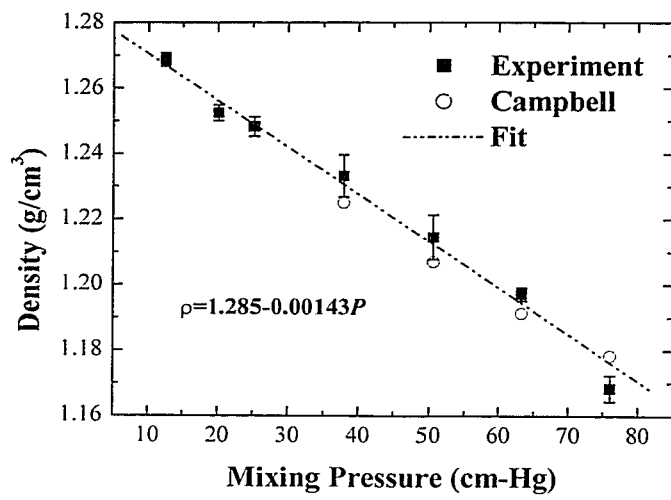


Figure 4.2. The density of unyeasted dough as a function of the mixing pressure.

determined from the simple formula $\rho = m/V$, where m is the mass of the dough and V is the volume of the escaped water. This method was found to be very accurate and gave very reproducible results. Figure 4.2 shows the density of the dough as a function of the mixing pressure. As the mixing pressure is reduced from atmospheric to 10 cm-Hg, the density increases according to the following linear relation

$$\rho = 1.285 - 0.00143P \quad (4.11)$$

Here the density of the mixed dough, ρ , is measured in g/cm^3 and P is the mixing pressure measured in cm-Hg. According to Campbell *et al.* (1998), this decrease in the density as a function of mixing pressure is likely due to the reduction in the number of air bubbles per unit volume as explained in the previous section. They support this hypothesis with their measurement of bubble size distribution using microscopy. In their measurements, 30- μ m-thick slices were cut from dough samples, which were frozen in liquid nitrogen, and mounted onto the microscope. Using this method, Campbell (1991) was able to measure the size distribution of bubbles covering the range 25-1000 μ m.

Figure 4.2 compares our density results to those of Campbell *et al.* (1998), who determined the density of the dough by obtaining neutrally buoyant suspension of the dough mass using a series of calcium chloride solutions. We see that both results agree very well. We have extended the data to lower pressures than those reported by Campbell *et al.* (1998) and the same linear trend is observed. This confirms the linear extrapolation that was used by the same authors to determine the gas-free density. Other dough density measurements were reported much earlier by Baker and Mize (1941a). They reported that

the density for unyeasted dough mixed at atmospheric pressure and in vacuum to be 1.15 and 1.25 g/cm³. Both these values lie below our experimental values.

From the results in figure 4.2, we can establish the relationship between the amount of air introduced into the sample and the mixing pressure. This relationship will be established using the fact that the amount of air, commonly referred to as the void fraction and denoted by the symbol ϕ , is defined as follows:

$$\phi = 1 - \frac{\rho}{\rho_m} \quad (4.12)$$

Here ρ is the density of the material as a function of the mixing pressure and ρ_m is the matrix density, i.e. the gas-free dough density. The density ρ_m is determined from the y-intercept in figure 4.2, which is 1.285 g/cm³. Substituting for ρ and ρ_m we get the following relation between ϕ and the pressure P

$$\phi = 1.113 \times 10^{-3} P \quad (4.13)$$

This relationship will be used throughout this chapter to convert the mixing pressure (in cm-Hg) to void fraction, thereby simplifying the interpretation of the ultrasonic results and their relation to the aeration properties of the dough.

4.1.3 Effect of reducing mixing pressure on the attenuation coefficient of the ultrasonic signal

The attenuation coefficient, α , was found by measuring the amplitude of the transmitted ultrasonic signal for samples mixed at the same pressure but with different sample thicknesses ranging from 1 to 9 mm. The signal amplitudes were then plotted as a function of sample thickness and fitted by a single exponentially decay curve plus a

constant background. These results are shown by the solid symbols and curves in figure 4.3, which indicates that the amplitude of the ultrasonic signal decays exponentially, as predicted by equation 3.1. The constant background term accounts for spurious contributions due to bond losses and interfacial reflections. These spurious contributions could therefore be eliminated from the attenuation measurements using this approach, allowing the true sample attenuation to be accurately measured. This procedure was repeated for all mixing pressures and exponential decay behavior was observed for all mixing pressures, as shown in figure 4.3. It is clear from these exponentially decaying curves that as the mixing pressure decreases the decay rate of the amplitude increases. However, the amplitude of the signals decreases as the mixing pressure is increased, an effect which is due to the presence of more air within the sample, resulting in very small signals, as the mixing pressure approaches atmospheric pressure. This suggests that as the mixing pressure is lowered, the samples become less absorbent and/or that there is less scattering of the ultrasonic signal. This is of course due to the fact that at higher mixing pressures the amount of air entrapped within the sample is larger than at the lower pressure values. Since air is a highly attenuating medium, one expects the attenuation to be higher accordingly. To examine this further, the attenuation coefficient, α , which was determined directly from the decay exponent of these exponential fits was plotted against the void fraction, ϕ . The latter was calculated from the different mixing pressure values using equation 4.13. The results are plotted in figure 4.4, which shows that the attenuation coefficient increases in a linear fashion as the void fraction increases. A linear fit to the data gives,

$$\alpha = 0.245 + 9.8\phi \quad (4.14)$$

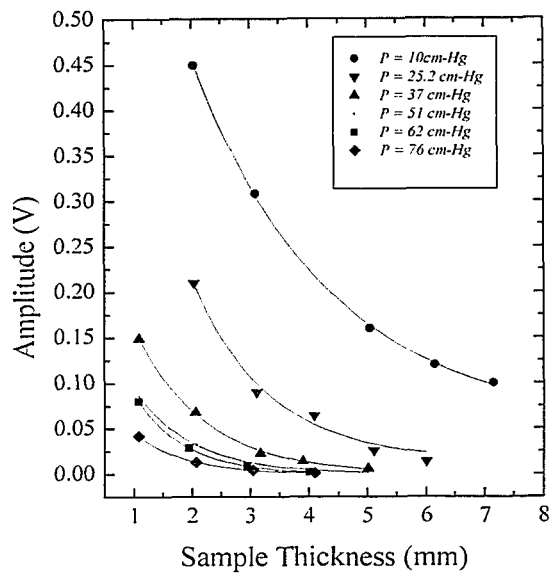


Figure 4.3. A typical set of results for ultrasonic signal amplitude as a function of sample thickness for the different mixing pressures. The symbols represent the experimental data and the solid curves are fits of the decaying exponential function $A(L) = A_0 \exp(-\alpha L/2) + B$, where B represents the background contribution.

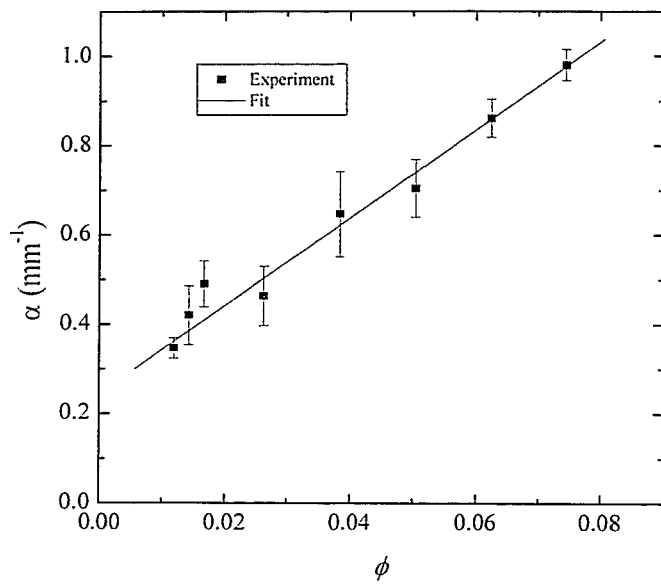


Figure 4.4. The attenuation coefficient of dough as a function of void fraction.

It is clear that the attenuation increases in proportion to the amount of air trapped in the dough, and that the air cells (or voids) make a significant contribution to α for $\alpha > 0$. The y -intercept of the above linear fit gives the background effect to the total attenuation coefficient, i.e., the contribution of the matrix to the attenuation coefficient. To interpret this result, we will compare the behavior of the attenuation coefficient in an aerated dough to a generic system in which bubbles are embedded. An example of such a system is bubbles in water.

For such a system the total attenuation coefficient is written as the sum of two terms: the matrix contribution, α_0 , and a term that depends on the scattering cross section of the bubbles in the matrix, σ , and their number density, n .

$$\alpha = \alpha_0 + n\sigma \quad (4.15)$$

where $n = \phi / \frac{4}{3}\pi a^3$. In this equation ϕ is the void fraction and a is the average radius of the air bubble. From this equation we see that if the radius of the gas cells remains constant (as deduced by Campbell *et al.* (1998)), the number density, n , will be proportional to ϕ . In addition, the scattering cross section will be a constant as well. Therefore, if we take the radius of the gas cells, a , to be $75 \mu\text{m}$, (Shimiya and Nakamura, 1997), we get,

$$\alpha = \alpha_0 + (566\sigma)\phi \quad (4.16)$$

from which we see that the total attenuation coefficient α will be a function of the amount of air introduced into the sample, ϕ , during the mixing stage. Comparing this result to our linear fit to the experimental results, we see that both equations predict the same behavior for the attenuation coefficient as a function of void fraction. In fact, under these

conditions, i.e., the radius of the bubbles remaining constant regardless of the mixing pressure, the scattering cross section may be found by comparing the two equations above:

$$566 \text{ mm}^{-3} \sigma = 9.8 \text{ mm}^{-1},$$

$$\text{then } \sigma = 0.0173 \text{ mm}^2 = 1.73 \times 10^{-8} \text{ m}^2.$$

The geometric cross section σ_g may also be calculated using $a = 75 \mu\text{ m}$,

$$\sigma_g = \pi a^2 = 1.77 \times 10^{-8} \text{ m}^2.$$

We see that the calculated result for the scattering cross section obtained from the ultrasonic measurements is essentially the same as the geometric cross section. Another parameter that is of interest is the ratio of the scattering to that of the geometrical cross section for the gas cells. Using $75 \mu\text{ m}$ for the radius of the gas cell, this ratio is 0.97.

4.1.4 The effect of reducing the mixing pressure on ultrasonic velocity

To determine the ultrasonic velocity of the unyeasted dough mixed at reduced pressures, small samples of thicknesses ranging from 1 mm to 9 mm were cut from the same dough mixed at a certain pressure. For each of these small samples, we first measure the time taken for the ultrasonic signal to travel through the sample, i.e., the transit time, t , as described in section 3.5. After that, the transit time is plotted *versus* the sample thickness; a typical example is shown in figure 4.5. The velocity is then simply the inverse of the

slope of the straight line, i.e. $v = \frac{1}{\text{slope}} = \frac{\Delta d}{\Delta t}$, where d is the sample thickness. Repeating

this procedure for all pressures, we get the velocity dependence on mixer headspace pressure. The relationship between the velocity and the void fraction is shown in figure 4.6. The void fraction was found from mixing pressure using equation 4.13. These data

show that the velocity decreases dramatically in the range of $0.012 < \phi < 0.03$, dropping from a velocity near to that of water to values well below the velocity of sound in air. At higher ϕ values, the velocity decrease is less rapid. In the low void fraction region, the void fraction is changed by only 0.018 whereas the velocity changed by a factor of 15 from its value at $\phi = 0.03$. The more rapid increase at these low void fractions suggests that there are mechanisms other than the void fraction which contribute to the velocity.

To interpret these data, we first look at the simplest effective medium model, for sound propagation in a multi-phase system such as bubbles in a liquid. This simple model was first introduced by Wood in 1941 (Wood, 1941) and was discussed in section 3.2. According to this model, the velocity of sound in two-phase mixtures and suspensions is controlled by the mean density and the mean compressibility, given by

$$\kappa_s = \phi \kappa_i + (1 - \phi) \kappa_m \quad (4.17)$$

Here ϕ is the volume fraction and the subscripts s , i , and m refer to sample, inclusion and matrix respectively; in particular i refers to the dispersed phase (gas cells) and m refers to the continuous phase (cell walls). The velocity of the system is then given by the following expression,

$$\frac{1}{\rho_s v_s^2} = \frac{\phi}{\rho_i v_i^2} + \frac{(1 - \phi)}{\rho_m v_m^2} \quad (4.18)$$

where ρ is the density and v is the velocity of sound. When the inclusion is air, $\kappa_i \gg \kappa_m$, so that equation 4.18 reduces to:

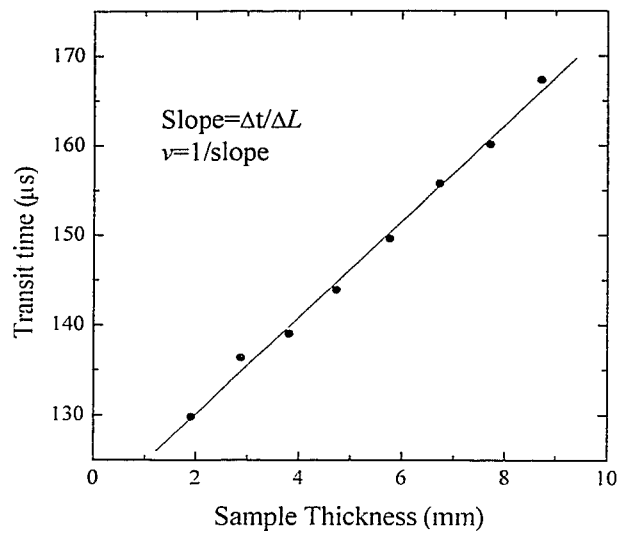


Figure 4.5. The transit time through the sample as a function of sample thickness for samples taken from the same dough piece.

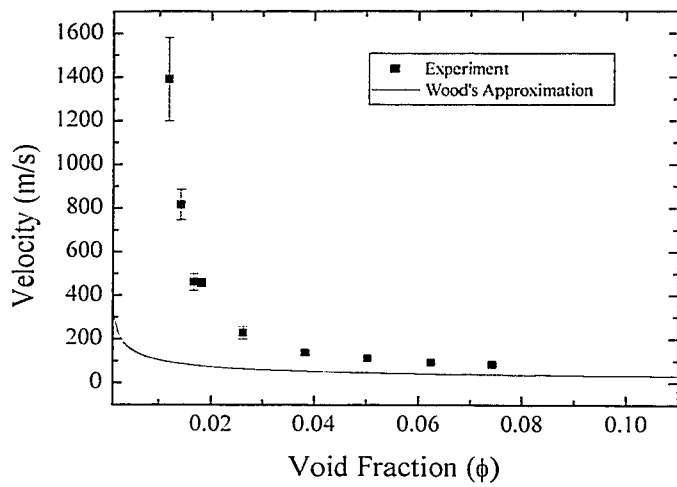


Figure 4.6. The velocity of sound through dough mixed at various pressures. The solid line represents Wood's prediction.

$$\Rightarrow v_s \cong v_{air} \sqrt{\frac{\rho_{air}}{\rho_s \phi}} \quad (4.19)$$

for $\phi \geq 10^{-3}$. If we neglect the change in velocity and pressure within the bubble as the outside pressure is reduced during mixing, Equation 4.18 will then be written as,

$$\Rightarrow v_s \cong 330 \sqrt{\frac{1.29}{1290\phi}} \quad (4.20)$$

This gives the solid curve in figure 4.6. The problem in modeling the experimental data is for the lower void fraction values where the experimental velocity is increasing rapidly, while the theoretical prediction only varies weakly in the region $0.01 < \phi \leq 0.03$. This suggests that there are additional factors affecting the behavior of the velocity that this simple model does not account for. The failure of Wood's model suggests that changes in the properties of the matrix are important and these effects have to be accounted for in more sophisticated models. One such model was developed by Sheng (1988), which is based on the effective medium theory for dispersed inclusions in an elastic medium.

In this model, the effective modulus of an elastic material with dispersed inclusions is found from the condition that the forward scattering amplitude is zero for a scatterer embedded in the effective (homogeneous) medium. A schematic of inclusion geometry for this model is shown in Figure 4.7. The scattering unit is taken to be a coated sphere. This effective medium theory is the elastic analogue of the Maxwell-Garnett theory for electromagnetic waves. The theory is valid in the limit where the wavelength is much

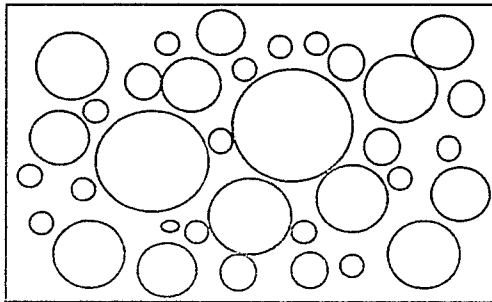


Figure 4.7. Schematic depiction of the dispersed-inclusion microstructure used in the effective medium model.

longer than the scale of the basic structural units, where the inhomogeneities cannot be individually resolved, and the medium appears homogeneous with effective elastic moduli, β_{eff}, μ_{eff} , which are given by

$$\beta_{eff} = \frac{\beta_m \{4(\mu_m - \mu_i) + 3\beta_i\}}{\{4(\mu_m - \mu_i) + 3\beta_i\}(1 - \phi) + 3\phi\beta_m} - \frac{4}{3}(\mu_m - \mu_{eff}) \quad (4.21)$$

$$A \left(\frac{\mu_{eff}}{\mu_m} \right)^2 + B \left(\frac{\mu_{eff}}{\mu_m} \right) + C = 0 \quad (4.22)$$

Here the moduli β and μ are complex, thereby determining the phase velocity and attenuation of the propagating wave. The subscripts i and m refer to inclusions (air) and matrix (matrix) respectively. The parameters A , B and C are defined in terms of the void fraction, ϕ , and the constants k_2 , k_3 , and k_5 which are given by the following ratios of the longitudinal and shear moduli for the matrix and the inclusions.

$$k_2 = \frac{\beta_m}{\mu_m}, \quad k_3 = \frac{\beta_i}{\mu_i}, \quad k_5 = \frac{\mu_m}{\mu_i} \quad (4.23)$$

For more details, including the complete expressions for A , B and C , see Sheng (1988).

In order to use this model to interpret our velocity results, we first have to relate the velocity and attenuation to the complex longitudinal modulus $\tilde{\beta} = \rho \tilde{v}^2$, where $\tilde{v} = v' + iv''$ is the complex velocity. Since for a travelling wave,

$$y(x, t) = A \exp i(\omega t - \tilde{k}x) = A \exp i\omega t - \frac{k'}{\omega} x \exp i(k''x), \quad (4.24)$$

so that complex velocity \tilde{v} is expressed in terms of the complex wave vector \tilde{k} by

$$\tilde{k} = \frac{\omega}{\tilde{v}} \quad (4.25)$$

Therefore

$$k' = \frac{\omega}{v} = \frac{\omega v'}{v'^2 - v''^2}, \quad (4.26)$$

and

$$k'' = \frac{-\omega v''}{v'^2 + v''^2}. \quad (4.27)$$

The attenuation coefficient is then

$$\alpha = -2k'' = \frac{2\omega v''}{v'^2 + v''^2} \quad (4.28)$$

Thus, v and α can be written in terms of the real and imaginary parts of the complex longitudinal modulus, $\tilde{\beta} = \beta' + i\beta'' = \rho(v'^2 - v''^2) + i2\rho v'v''$, as

$$v = \sqrt{\frac{2}{\rho} \left(\frac{\beta'^2 + \beta''^2}{\beta' + \sqrt{\beta'^2 + \beta''^2}} \right)} \quad (4.29)$$

$$\alpha = \omega \sqrt{2\rho \left(\frac{\sqrt{\beta'^2 + \beta''^2} - \beta'}{\beta'^2 + \beta''^2} \right)} \quad (4.30)$$

Equivalently, β' and β'' can be written in terms of v and α as

$$\beta' = \frac{\rho v^2 (1 - \alpha^2 v^2 - 4\omega^2)}{(1 + \alpha^2 v^2 - 4\omega^2)^2} \quad (4.31)$$

$$\beta'' = \frac{2\rho v^3 \alpha - 2\omega}{(1 + \alpha^2 v^2 - 4\omega^2)^2} \quad (4.32)$$

To fit this model to our data, we also need to determine the values of longitudinal and shear moduli for the matrix and inclusions. From the linear extrapolation of the density and attenuation data to $\phi=0$, we get $\rho=1285 \text{ kg/m}^3$ and $\alpha=0.245 \text{ mm}^{-1}$. It is more difficult to extrapolate our velocity data to $\phi=0$, so instead we take the value

$v = 1500$ m/s found by extrapolating the velocity data measured by Letang *et al.* (1996) at much higher frequencies to dough with our moisture content. The justification for this procedure is that we expect at very high frequencies, well above the resonances of the bubbles in dough, that the velocity will approach the matrix value (Leighton, 1994). Using these estimates of the matrix values for ρ , α and v , equations 4.31 and 4.32 give $\beta' = 3 \times 10^9$ N/m² and $\beta'' = 2.5 \times 10^9$ N/m², for the dough. To get an approximate estimate of the dough matrix values for the storage and loss moduli, we use values taken from low frequency rheology measurements in the literature. $\mu_m' = 3 \times 10^4$ N/m² (Faubion *et al.*, 1985; Bloksma, 1990a), and $\mu_m'' \sim 1.0\text{-}4.5 \times 10^4$ N/m² (Bloksma (1990b); Faubion *et al.* (1985)). For the experimental fit, we took the mean of the latter values, i.e., 2.7×10^4 N/m². These values will evidently be lower than those of the true values for the matrix, but they do serve as a starting point for our interpretation of the data. The inclusion is air, for which $\beta_i' = 1.5 \times 10^5$ N/m² and $\beta_i'' \sim 4$ (Anderson, 1989). The shear modulus for air, μ_i , is assumed to be very small and was taken to be 1 (for both real and imaginary parts). Using a Fortran program, the velocity prediction of the effective medium model was calculated for these values of the parameters, giving the solid curve shown in figure 4.8. The model gives reasonable agreement to the data at the higher void fraction values investigated. However, at lower void fractions the model does not describe the data, as the experimental velocity starts to increase at higher void fraction values than predicted. This discrepancy is an indication that mixing under reduced pressure not only removes the

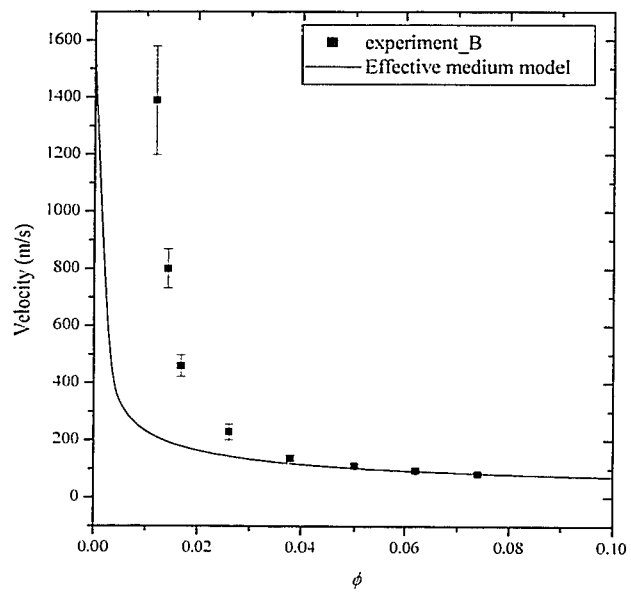


Figure 4.8. Velocity as a function of void fraction along with the effective medium prediction.

bubbles, thereby decreasing the density, but it also increases the stiffness and the rigidity of the matrix. The only way to account for the difference between the predictions of the effective medium model and our data is allow the elastic moduli of the matrix to increase when the dough is mixed at lower pressures. To examine this behavior quantitatively, we fit the data at each mixing pressure to determine the matrix modulus. Unless ϕ is extremely close to zero ϕ , the velocity and the attenuation coefficient are not sensitive to the values of β'_m and β''_m . Therefore, the only parameters which can account for the large increase in the velocity at low mixing pressures are μ'_m and μ''_m . Thus, by fitting the predictions of the effective medium model to our data for both the velocity and the attenuation, we have a unique and unambiguous way of determining how μ'_m and μ''_m of the dough matrix both vary with void fraction.

To facilitate the fitting, it is helpful to also consider the volume fraction dependence of the real and imaginary parts of the longitudinal modulus β' and β'' , determined from our data for the velocity and attenuation. These data for β' and β'' are shown by the symbols in figure 4.9(a). Not only is there a considerable variation in both moduli as ϕ is decreased, but, quite remarkably, the ratio β'' / β' (figure 4.9(b)) changes from a value of about 1/4 at ambient pressure to a value greater than one at the lowest ϕ , indicating that on a percentage basis, losses are large even at the lowest ϕ where the attenuation is the smallest. The considerable increase in the longitudinal modulus may be due to the decrease in the amount of oxygen as $\phi \rightarrow 0$, thereby affecting the intermolecular bonding within the matrix (Baker and Mize, 1937).

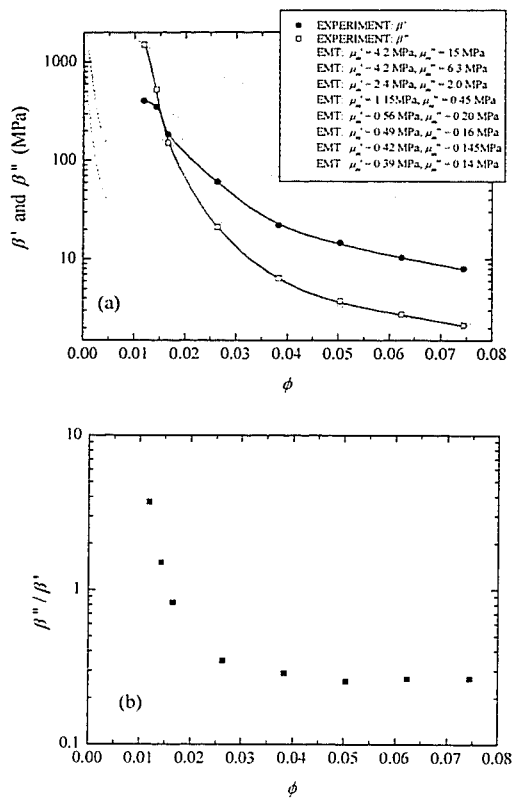


Figure 4.9. The behavior of the longitudinal modulus (a), and the ratio of the imaginary and the real parts (b) as a function of void fraction.

In fitting our data by varying the values of μ'_m and μ''_m , we take advantage of the fact that the best fit for the ratio μ''_m / μ'_m for the matrix is approximately equal to the experimental ratio β'' / β' over the range of the experimental ϕ values. For each value of ϕ , we fit μ'_m and μ''_m to generate four families of curves which pass through the experimental data points for β' , β'' , ν and α , as shown in figures 4.9 and 4.10. For the two lowest ϕ values, the matrix shear moduli have become so large that the effective medium parameters become slightly dependent on the matrix values of β'_m and β''_m . This reflects the fact that such large values of the matrix shear moduli make the matrix sufficiently rigid that the compressibility of the dough is no longer dominated by the compressibility of the gas cells, as it is at high ϕ . Despite this slight sensitivity to the matrix longitudinal moduli at low ϕ , we are still able to determine the shear moduli of the matrix to a fitting precision better than 20% in the worst case. Thus, we are able to use the predictions of the effective medium theory to determine the variation of μ'_m and μ''_m with ϕ . As shown in figure 4.11, the increase in μ'_m and μ''_m at low ϕ is very substantial, with μ''_m varying by approximately two orders of magnitude.

There are two possible mechanisms, which may affect the behavior of the velocity over the experimental void fraction region and account for the increase in μ'_m . These are the stiffening of the matrix due to increasing moisture loss as the mixing pressure is lowered, and stiffening due to the effect of dough relaxation at the end of mixing. These two effects were examined experimentally. Firstly, we examine the effect of dough

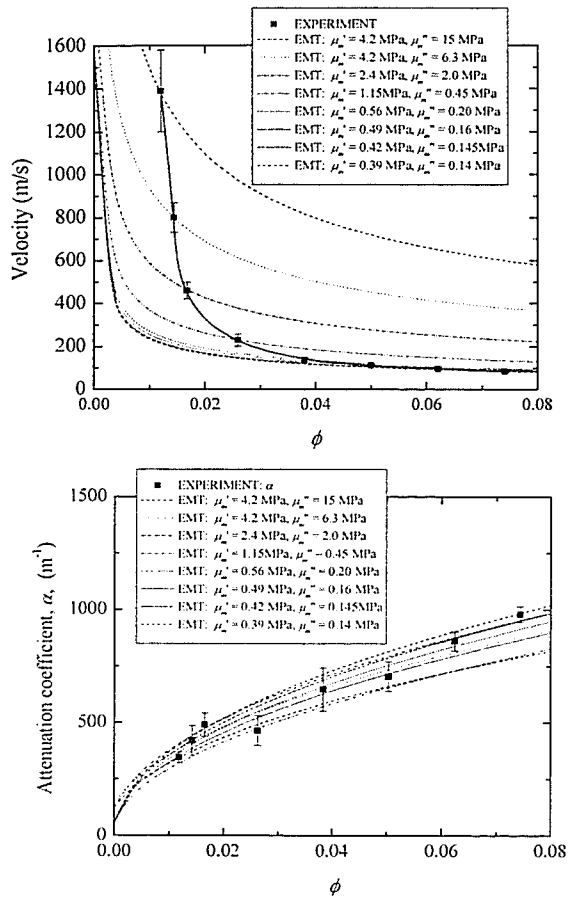


Figure 4.10. The velocity (a) and the attenuation coefficient (b) as a function of void fraction. The curves represent the results of the effective medium theory fitted at the specified μ_m values.

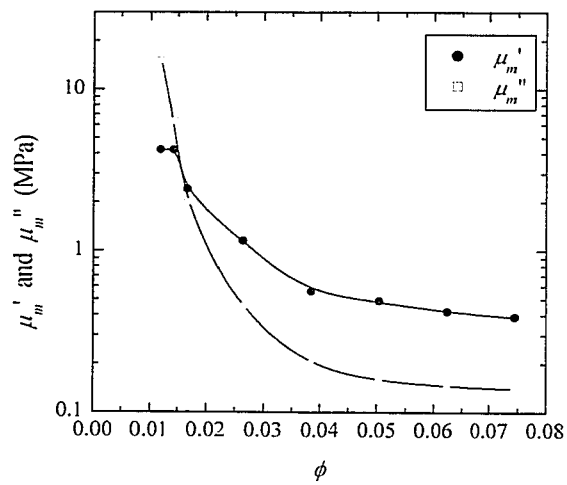


Figure 4.11. The variation in the μ'_m and μ''_m as determined from the effective medium model.

relaxation on the behavior of the velocity, and after that the moisture loss in the dough as the mixing pressure is lowered. When the dough is being mixed, the protein molecules are stretched and folded in all directions which results in a disorientation or misalignment of the protein chains. After mixing, these chains tend to reorient and realign themselves again. The time needed for this process is called the relaxation time and it is believed to last as long as 10 minutes Bushuk (1987). During the relaxation time, the dough should undergo structural changes which may influence the propagation of the ultrasonic signal. To investigate the response of the ultrasonic parameters to such relaxation effects, we measured the ultrasonic velocity of the dough mixed at ambient pressure as a function of time for up to sixty minutes after mixing. The results of these experiments are shown in figure 4.12, which shows that there is very little change in the velocity throughout the experiment. An exponential decay fit to the data showed that the dough relaxation time, τ , is about 12 minutes which is similar to that reported by Bushuk (1972). Hence, the structural changes resulting from relaxation of the dough have only a very small effect (2%) on the ultrasonic velocity.

A second mechanism which may contribute to the dramatic increase in the velocity is the decrease in moisture content of the dough as the mixing pressure is reduced. This will affect the velocity *via* the stiffening of the matrix (Baker and Mize, 1937). To investigate the contribution of the moisture loss to the stiffening of the matrix, we measured the moisture loss as a function of mixing pressure and compared it to the change in the velocity as a result of varying the mixing pressure. The moisture loss was measured by comparing the weight of the sample after mixing to the sum of the individual

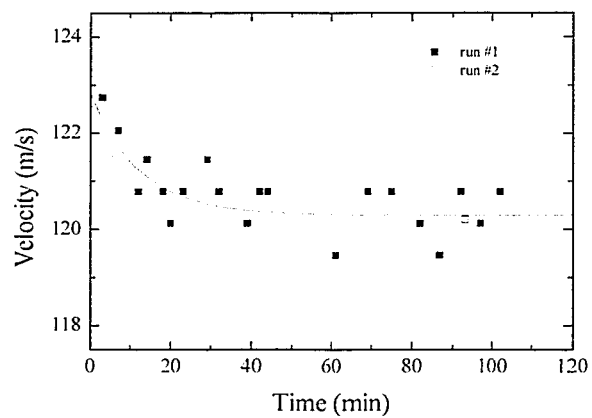


Figure 4.12. Velocity as a function of time. The open and closed symbols represent two replicates and the solid curve represents an exponential decay fit to the data. The relaxation time, τ , was found to be 12 minutes.

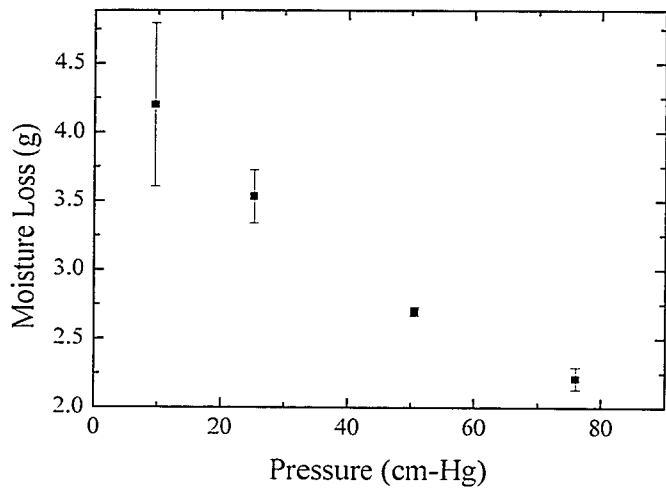


Figure 4.13. Moisture loss as a result of reducing the mixer headspace pressure.

ingredients (flour, water and salt). The results of these measurements are shown in figure 4.13. Moisture loss is small; it ranges from 3.2% when the dough is mixed at atmospheric pressure to 6.7% when mixing at 10 cm-Hg. These results are in agreement with the results obtained by Baker and Mize (1937) who reported dough moisture loss to be 6% when the dough was mixed under vacuum. According to Letang *et al.*, (1996) the ultrasonic velocity change associated with a moisture loss of about 3% is ~ 120 m/s. The observed change in our velocity results between the dough mixed at ambient and vacuum is ~ 1400 m/s. Therefore, we conclude that the moisture loss due to changing the mixing pressure is small and is not likely to be the main cause for the dramatic increase in the velocity. This suggests that there must be other additional interactions, chemical ones included, that affect the bonds between the protein molecules and their interactions in such a way that they cause the shear modulus of the dough to increase as the mixing pressure is reduced. These interactions seem to influence the velocity more in the low void fractions and need to be investigated. Further investigation of their effect is an interesting project for further research.

4.2 Aeration of dough during fermentation: yeasted dough

As discussed in chapter two, the addition of yeast to the dough leads to the inflation of the air bubbles. This is a direct result of the yeast fermenting the sugars to produce carbon dioxide, which diffuses through the dough matrix into the air nuclei that were occluded into the dough during the mixing stage. As a result, the void fraction, ϕ , increases and the density of the dough decreases. In the following sections, I present the results of the ultrasonic experiments done on the dough as a function of fermentation time. These

experiments focus on the effects of the expansion of the gas bubbles on the ultrasonic velocity and attenuation coefficient, giving information about the changes in the structure of the material. Before we can interpret the measurements of the ultrasonic experiments, the density of the fermenting dough must be measured as a function of time. This allows us to correlate the behavior of the ultrasonic parameters with the change in the structure of the fermenting dough as manifested in the expansion of the gas cells and the resulting density reduction.

4.2.1 Density of fermenting dough

The density of the fermenting dough was measured in three different ways: using a graduated cylinder, a specific gravity bottle and by digital imaging and analysis. In the graduated cylinder method, the dough was placed in a graduated cylinder and the volume of the dough was measured by following the rising of the dough in the graduated cylinder. The walls of the cylinder were well lubricated to minimize frictional effects that might arise between the cylinder walls and the dough. The drawbacks of this method lie in the fact that the dough is allowed to expand in one direction only (upwards), and that air pockets may exist underneath the dough when it was placed into the cylinder (the air pockets will act as pressure release sites for the expanding dough, thus introducing errors into the measurements).

In the second method, the yeasted dough was cut into small pieces. These small pieces were allowed to ferment in the proofing cabinet, which was set at normal proofing conditions, i.e. 37 °C and 83% R.H. At the end of each time interval, approximately 5 minutes, a sample was taken out of the proofing cabinet and gently immersed into the specific gravity bottle to measure its volume. In this method the samples had to be very

small in order to fit in the specific gravity bottle. Also, the samples had to be carefully handled to perform the measurements. These factors limited the accuracy of the density measurements.

The third method by which the density of the fermenting dough was measured was a digital imaging method. In this method, the sample was placed between two 3-cm-thick acrylic plates. The thickness of the sample was preset to the desired thickness using a set of 1-mm-glass slides between the two acrylic plates. To restrict the expansion of the dough to the radial direction only, the two plates were clamped together. The sample was then placed in the proofing cabinet and mounted directly below a digital camera as shown in figure 4.14a. To follow the radial expansion of the fermenting dough, digital images of the dough were taken every two minutes. Figure 4.15 shows photographs of the fermenting dough at several fermentation times. These images show the expansion of the dough due to inflation of the air bubbles in the dough as CO_2 is being produced by the yeast. To find the density of the dough as a function of fermentation time, the area of the expanding dough was found using a digital imaging analysis software program called Scion Image, which was downloaded from the web site www.scioncorp.com. Since the distance between the acrylic plates is fixed throughout the experiment and the mass is measured before the sample is placed between the plates, the density can be easily found from the density equation, $\rho = m/LA(t)$, where L is the sample thickness and $A(t)$ is the area of the dough as a function of fermentation time. The advantage of performing the measurements in this manner was to ensure that the dough was fermenting under exactly the same conditions of relative humidity and temperature as in the ultrasonic experiments.

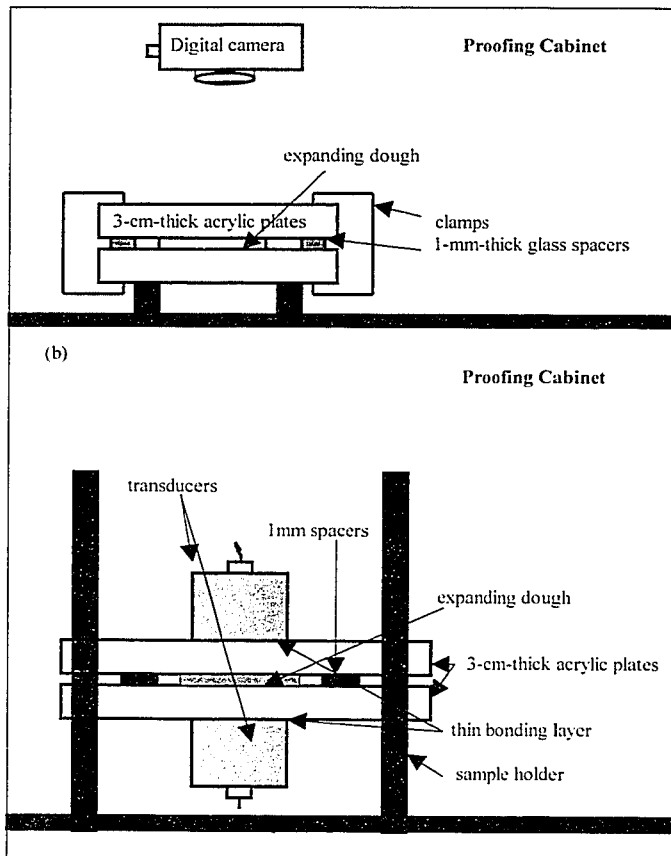
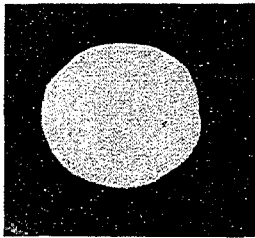
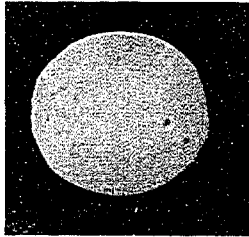


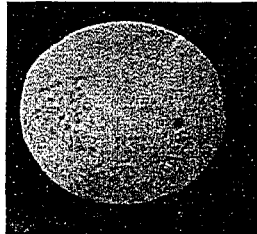
Figure 4.14. (a) Digital imaging setup (b) Ultrasonic setup (both placed in the proofing cabinet at 37°C and 83% R.H.).



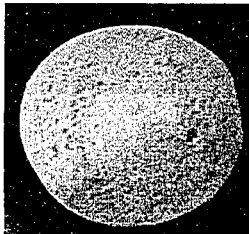
after 4 minutes



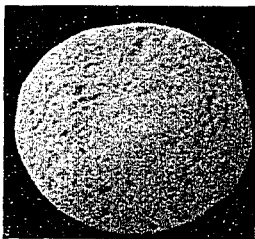
after 21 minutes



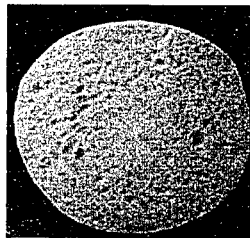
after 33 minutes



after 47 minutes



after 64 minutes



after 85 minutes

Figure 4.15. Digital images of radially expanding dough at various stages of fermentation.

The second advantage of measuring the density this way is that it replicates the ultrasonic experimental situation in which the sample must be placed between the two transducers, which restrict the expansion of the sample to the radial direction only. The use of this method allowed both density and ultrasonic measurements to be performed simultaneously. Figure 4.14b shows the sample holder containing the two acrylic plates, with the sample sandwiched between the two transducers, as they were placed in the proofing cabinet along with the digital imaging equipment (figure 4.14a).

A comparison of the dough density results as measured using the three methods is shown in figure 4.16a. The density results measured using the graduated cylinder are lower, but follow the same trend with time as the other two methods, likely due to the presence of the air pockets which act as pressure release sites when the dough is expanding. On the other hand, the density measured using the imaging method starts at high values because of the initial compression of the sample. The important point which arises from these experiments is that the geometrical constraints and boundary conditions under which the yeasted dough density is measured are important, and have to be taken into account. We therefore conclude that to make a meaningful interpretation of our ultrasonic measurements, the density of the dough has to be measured under the same conditions as the ultrasonic measurements. Hence, the density results found using the imaging method will be used throughout the discussion of the results of the ultrasonic velocity and attenuation of the yeasted dough.

Using the imaging methods, the density as a function of fermentation time was measured for doughs mixed at ambient pressure and under vacuum (0.13 atm) to

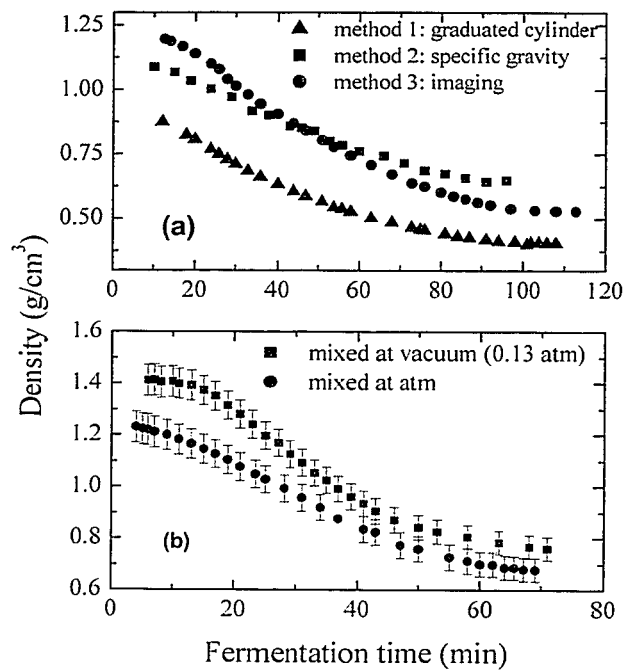


Figure 4.16. (a) The density of fermenting dough measured using three different techniques. (b) Comparison of the density of fermenting dough mixed under vacuum and atmospheric conditions, as measured using the digital imaging method.

investigate structural changes of the dough at the two extreme pressures (figure 4.16b). These data show that the density of fermenting dough, mixed at both extreme pressures, decreases as a function of fermentation time, as expected. However, at the beginning of fermentation, the density of the dough mixed under vacuum is higher than when the dough is mixed at ambient pressure. This is because there are fewer air bubbles occluded into the dough during mixing. There is also a lag in the density at the beginning of fermentation and this lag extends over a longer time in the vacuum-mixed dough. The lag represents the time taken for the yeast to start fermenting the sugars and the time taken for the CO₂ to diffuse through the matrix into the air nuclei. Since at the beginning of fermentation, the vacuum-mixed dough has fewer bubbles per unit volume than the dough mixed at ambient pressure, the diffusion path for CO₂ to reach the air nuclei must be longer. This will cause the vacuum-mixed dough to exhibit a longer lag than its ambient counterpart. In both cases, the density drops by about the same amount with time suggesting that at the end of fermentation roughly the same amount of CO₂ is produced in both cases. The density was measured as a function of fermentation time up to a maximum time of 70 minutes, which corresponds to the time at which the transmitted ultrasonic signal became comparable to the noise level. Another feature that can be seen from figure 4.16b (in comparison with section 4.1.2) is that the density for both mixing pressures at zero fermentation time starts at higher values than for their corresponding unyeasted counterparts, i.e.,

$$\rho_{\text{vacuum, unyeasted}} = 1.271 \text{ g/cm}^3$$

$$\rho_{\text{atm, unyeasted}} = 1.176 \text{ g/cm}^3$$

while

$$\rho_{\text{vacuum, yeast}} = 1.42 \text{ g/cm}^3$$

$$\rho_{\text{atm, yeast}} = 1.24 \text{ g/cm}^3$$

This increase in the dough density as a result of the addition of yeast is due, at least in part, to the yeast consuming the oxygen for its metabolic activity, which in turn shrinks the volume of the air bubbles by 20% and therefore increases the dough density.

The gassing rate of CO₂ as a function of fermentation time can be determined from the rate of change with time of the inverse of the density; this is shown in Figure 4.17. The initial high rate of fermentation activity is attributed to the rapid assimilation by yeast of the free sugars available in the flour. The decline in the rate that follows marks the exhaustion of the supply of this free sugar and the period of adaptation of the yeast to the fermentation of the maltose that is being produced by the action of amylases on the damaged starch in the flour (Harbrecht and Kautzmann, 1968). At later times, the gassing rate of the yeast is expected to rise again, as shown by Harbrecht and Kautzmann (1968), until the maltose also becomes depleted.

4.2.2 Ultrasonic velocity as a function of fermentation time

The ultrasonic velocity for the fermenting dough was measured by placing the sample between two 3-cm-thick acrylic plates, which were exactly the same as those used in the density measurements. Using a set of 1-mm-thick glass slides, the sample thickness was set to the same thickness as that used in the density measurements. On the outer sides of the acrylic plates were the two 54 kHz transducers, see figure 4.14b. Since both temperature and relative humidity are important factors in the fermentation process, the sample was placed in the proofing cabinet (37°C and 83% R.H. as required by the baking methods, Preston *et al.*, 1982).

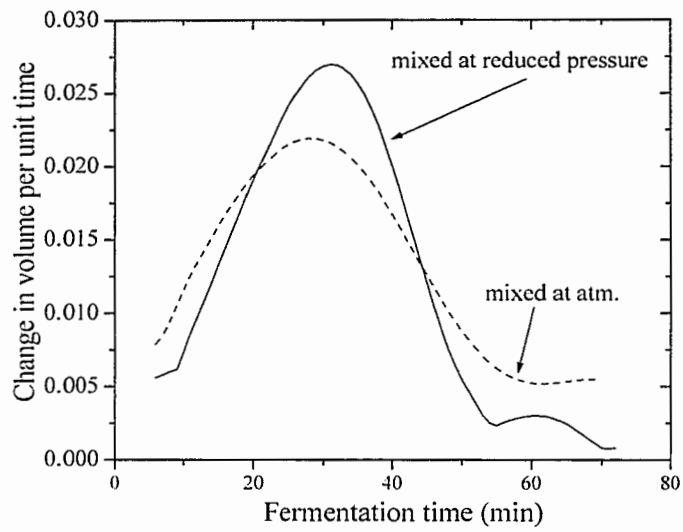


Figure 4.17. The gassing rate of CO₂ as a function of fermentation time. The solid curve represents the rate of CO₂ production in dough mixed under vacuum and the dashed curve represents the rate of CO₂ production in dough mixed under atmosphere pressure.

The ultrasonic velocity of the yeasted dough was found by measuring the transit time as a function of fermentation time while keeping the sample thickness fixed throughout the measurements. This velocity was then determined using $v = d/t$, where d is the fixed sample thickness and t is the transit time. Figure 4.18 shows the results of the ultrasonic velocity as a function of fermentation time for the yeasted dough mixed at ambient pressure and at “vacuum” (0.13 atm). At the beginning of fermentation, these data show that the velocity is substantially greater in the dough mixed under vacuum than its ambient counterpart. This is attributed to the presence of fewer air nuclei in the dough as well as the large increase in the matrix shear modulus that was found to occur when dough is mixed at low pressures (see section 4.1). As the yeast’s metabolic activities produce CO₂ in the dough, a substantial drop in the velocity was observed in the first twenty minutes for doughs mixed under both conditions. At later fermentation times, the velocities converge to approximately the same velocity indicating that the same amount of CO₂ was produced in both doughs and that the matrix moduli are similar. Attempts to correlate the behavior of the velocity to the density decrease show that there is no correlation between the initial drop in the velocity and the density (figure 4.16b), especially for the vacuum-mixed dough at early times where the density did not change by much. This led us to the conclusion that there are additional effects, other than the increase in void fraction, which cause this dramatic drop in velocity.

One possible effect is that the large drop in velocity arises from the increase in internal pressure within the sample as a result of the uniaxial stress caused by confining the sample between the transducers. This stress limits the expansion of the dough to the radial

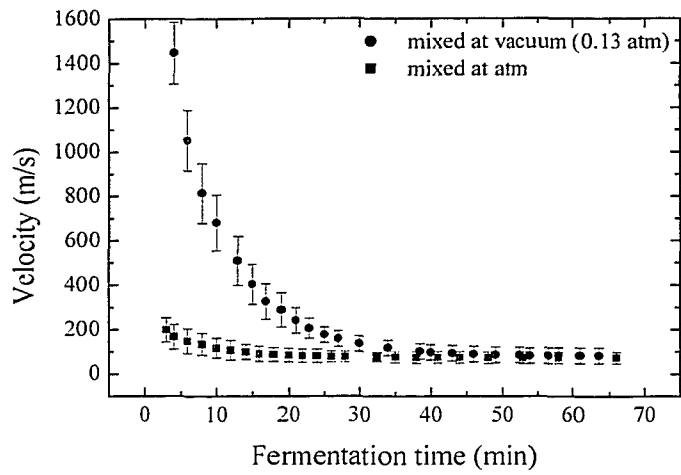


Figure 4.18. The velocity of ultrasound in fermenting dough mixed at vacuum (•) and atmospheric (◻).

direction in the plane of the acrylic plates. To investigate the increase in the internal pressure of the dough as a result of the two transducers squishing the dough, we measured the density and ultrasonic velocity as a function of fermentation time for samples with masses of 2, 4 and 7 grams (doughs were mixed at atmospheric conditions). In these experiments the sample thickness was fixed at 2 millimeters, so that the net effect of changing the mass was to change the amount by which the two transducers stressed the dough sample uniaxially. Since 4 grams was the usual mass used throughout all the other density and ultrasonic experiments on yeasted dough, this range of masses includes one sample with less and one sample with greater initial compressions. Hence the internal pressure within the sample should increase as the mass is increased from 2 to 7 grams. The results of these experiments are shown in figure 4.19 which shows the density and velocity results for the yeasted dough as a function of fermentation time for all three samples. It is clear from figure 4.19 that these data are the same within experimental error. Hence we conclude that the internal pressure introduced as a result of sandwiching the sample between the two transducers does not significantly affect either the density or the velocity results: neither does it hinder the diffusion of CO₂ through the matrix into the air bubbles whose expansion results from the yeast's metabolic activity. Therefore the rapid drop in the velocity at early fermentation times is not caused by the stress introduced by the transducers.

A second possible effect that could influence the decrease in the velocity is the effect of the drop in the pH value of the dough during the first sixty minutes of fermentation (Cooper and Reed, 1968). While some researchers have previously shown that the pH of the dough drops from 5.2 to 4.2 during this time (Cooper and Reed, 1968),

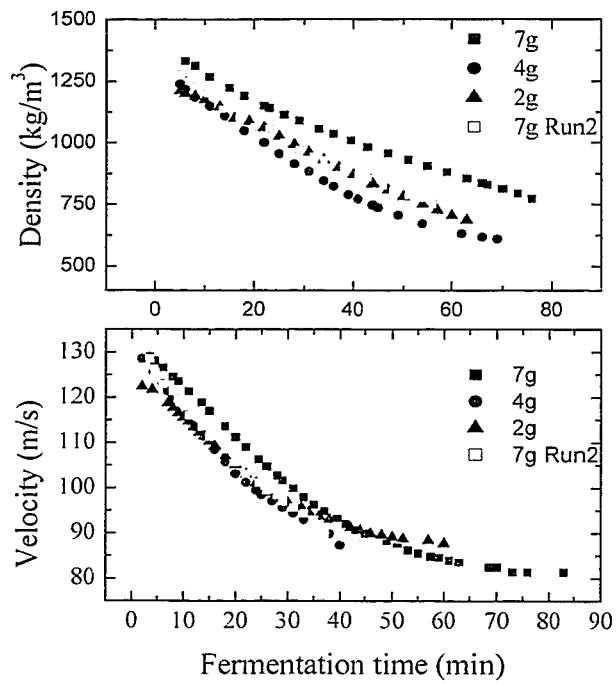


Figure 4.19. (a) The density of fermenting dough measured using dough of masses 2, 4 and 7 grams. (b) The velocity measured for the samples in a.

others have reported a drop in the pH of dough to as low as 3.8 (Holmes and Hosney, 1987). Before we discuss the results of our experiments to investigate the effect of the drop in pH on the ultrasonic velocity, I will briefly discuss the increase in protein charge repulsion and how the pH of the dough affects its elasticity. The pH of the dough is determined by the wheat proteins through the dissociation of charged amino acid side chains. The dough, which has a considerable buffer capacity, has an initial pH of about 5.5 (Eliasson and Larsson, 1993), which drops as a function of fermentation owing to the saturation of carbon dioxide in the aqueous phase. In general, the repulsion over the aqueous zone in the gluten structure will increase with increasing protein charges (Eliasson and Larsson, 1993). Therefore the swelling of the gluten will increase as we move away from the isoelectric point for the dough (most of the gliadin-type proteins have isoelectric point values above 6.5 (Eliasson and Larsson, 1993)), and therefore the mechanical strength of the gel will be reduced. Dropping the pH value is expected to increase ion concentration within the matrix, and we therefore expect the pH drop to influence the physical properties of the dough and its characteristics in particular (Cooper and Reed, 1968). In the following paragraph we describe the ultrasonic velocity measurements done on the dough at two pH values of 5.2 and 4.3.

To reduce the pH of the dough, we performed one mix of the dough using HCl solutions with pH values varying from 0.5 to 6.0. Due to the dough buffering capacity, these solutions produced doughs with pH values of 1 to 5.3, see figure 4.20. It should be pointed out that these experiments were performed on dough with no yeast to eliminate complications that arise from the yeast activities. The ingredients were then mixed with

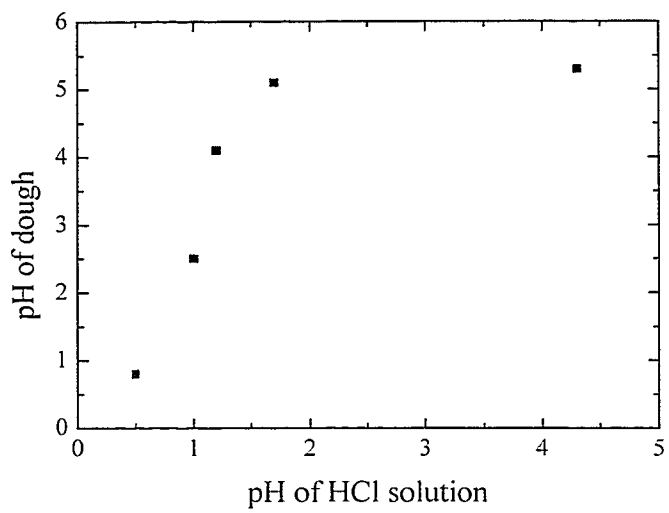


Figure 4.20. Dough buffer capacity as shown by the pH of the dough vs. the pH of the solution.

Table 4.1. Summary of pH experiment performed on dough.

Pressure	pH of the dough	Velocity (m/s)
Ambient	5.2	96
Ambient	5.2	99.3
Ambient	5.2	105.3
		Ave. 100.2
Ambient	4.3	176.7
Ambient	4.3	168.2
Ambient	4.3	147.3
		Ave. 164.1
Vacuum	5.2	1947.7
Vacuum	5.2	1916
Vacuum	5.2	2000
		Ave. 1954.6
Vacuum	4.3	1434
Vacuum	4.3	1585
Vacuum	4.3	1416.7
		Ave. 1478.6

solutions to give a dough pH of 4.3 and 5.3 respectively. The results for the two extreme mixing pressure values are summarized in table 4.1. From these results we see that the velocity behaves differently for the two mixing pressures (atm. and vacuum). When the pH value was dropped to 4.3, the velocity for the dough mixed at ambient pressure increased by about 64% of its original values. Conversely, at the same pH value, 4.3, the velocity of the dough mixed at vacuum decreased by 25% of its original value. Qualitatively, these two "opposite" effects may be explained in terms of charge repulsion as follows:

Mixing at reduced pressure: (very few air bubbles present in the dough)

i) at high pH:

There are lots of chain links (albeit weak) in the dough and hence sound is effectively transmitted.

ii) at low pH:

As the chains are protonated, they repulse each other and chain links get broken, the matrix is softened, therefore, sound does not propagate as effectively. A small drop in dough density should accompany the drop in pH value.

Mixed at atmospheric: (air bubbles are present in the dough)

ii) at high pH:

the air bubbles have the dominant influence on sound propagation properties. Ultrasonic velocity is low.

ii) at low pH:

as the chains are protonated, they repulse each other and chain links get broken and a drop in the density of the dough matrix results. Because of the presence of voids, the repulsion will cause the air bubbles to shrink, resulting in two competing effects: the weakening of the matrix and the shrinkage of the air bubbles. Since the velocity is largely determined by the air bubbles at this low frequency, the shrinkage of the bubbles will prevail as the dominant factor, resulting in an increase in velocity.

To quantify this description of the velocity results and their dependence on the elasticity of the dough matrix, it would be highly desirable to apply the effective medium model used in section 4.1. However, we have not been able to do this because of experimental difficulties in determining the absolute attenuation, α , and void fraction, ϕ . Because the absolute attenuation is large, both the real and imaginary parts of the longitudinal modulus must be calculated, i.e., β' and β'' (see equations 4.31 and 4.32). The difficulty in calculating the absolute void fraction, ϕ , lies in the fact that we were not able to measure the gas free density of the yeasted dough because the yeast cells start their activities as early as the later stages of hydration during mixing (Pylar, 1988). Despite these problems, we can use our knowledge of the behavior of unyeasted dough to qualitatively interpret the behavior of the velocity of the yeasted dough as a function of fermentation time. Just as in the unyeasted dough, the parameters that largely control the change in the velocity are the shear moduli of the matrix, and they must decrease very markedly to account for the drop in the velocity with fermentation time. In particular, the initial sharp decrease in the velocity must indicate that the matrix shear modulus values are lowered considerably as CO_2 becomes dissolved in the matrix. Even though these qualitative arguments provide an explanation of the behavior of the velocity, further

experiments are needed to study the changes in the internal structure of the matrix as a result of the chemical interactions that occur during fermentation, with more emphasis on the first twenty minutes where the yeast is most active.

4.2.3 Ultrasonic attenuation coefficient as a function of fermentation time

In section 4.1.3, the absolute attenuation coefficient, α , was determined by measuring the signal amplitude as a function of sample thickness and fitting the result to an exponential decay. The attenuation coefficient was then calculated directly from the decay length. This method requires measuring the signal amplitude for samples taken from the same dough as a function of sample thickness. For the yeasted dough this procedure was not possible because the fermenting samples evolved too rapidly for ultrasonic measurements to be made on different thicknesses of the same sample. An alternative approach is to determine the relative attenuation rather than the absolute one, i.e., measure the change in the attenuation coefficient, $\Delta\alpha$, relative to the attenuation coefficient at the onset of fermentation. The relative attenuation $\Delta\alpha$ still provides information that is valuable for understanding the changes in the structure of the dough as a function of fermentation. The expression for $\Delta\alpha$ can be derived from the amplitude decay equation, i.e. $A(t) = A_0 \exp(-\alpha L/2)$, where $A(t)$ and A_0 are the signal amplitudes at times t and $t = 0$ respectively, L is the sample thickness and α is the attenuation coefficient. Taking the signals at $t = 0$ and at a later time t we get,

$$A(0) = A_0 \exp(-\alpha_0 L/2), \quad \text{at } t = 0$$

and

$$A(t) = A_0 \exp(-(\alpha_0 + \Delta\alpha)L/2), \quad \text{at } t = t_1$$

so that,

$$\frac{A(t)}{A(0)} = \exp\left(-\frac{\Delta\alpha}{2} L\right) \quad (4.33)$$

Hence,

$$\Delta\alpha = \frac{-2}{L} \ln\left(\frac{A(t)}{A(0)}\right) \quad (4.34)$$

Using this equation, $\Delta\alpha$ may be calculated from direct measurements of the amplitude as a function of fermentation time with $A(0)$ as the signal amplitude at the onset of fermentation¹. Figure 4.21 shows the relative attenuation coefficient as a function of fermentation time for the two extreme pressure values, ambient and vacuum (0.13 atm). Figure 4.21 shows that for the dough mixed under vacuum, the data show a linear increase in the change of the attenuation coefficient for times between 5 and 30 minutes. After that, the signal amplitude becomes very small and the signal-to-noise ratio approaches one. Similar behavior can be seen by the data mixed at ambient pressure, with the exception that the increase in $\Delta\alpha$ is not linear at early fermentation times. To interpret these results, we needed to express the change in attenuation in terms of the change in the void fraction, $\Delta\phi$, which will enable us to relate the behavior of $\Delta\alpha$ to the inflation in the air bubbles as a dough was found by fitting a fifth order polynomial to the density data in figure 4.16b, thus enabling the density and hence the change in void fraction to be calculated for any

¹ Note that in equation (4.34), no account has been taken of the possible change in transmission coefficient due to the change in acoustic impedance of the sample. For fermenting dough, where the velocity and density both decrease with time, equation (4.34) will overestimate $\Delta\alpha$. Nonetheless, equation 4.34 will still suffice to establish the qualitative trends in the change of attenuation in fermenting dough.

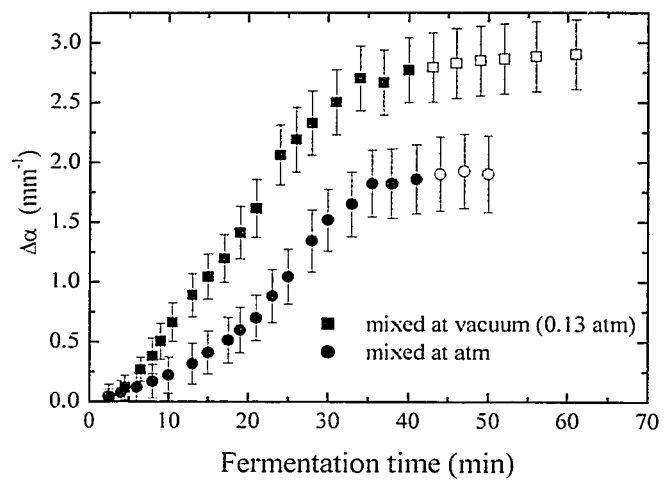


Figure 4.21. The change in the attenuation coefficient for fermenting dough mixed at vacuum (□) and atmospheric (●). The open symbols represent the data at which the signal becomes very small and comparable to the noise level. These data points are less accurate.

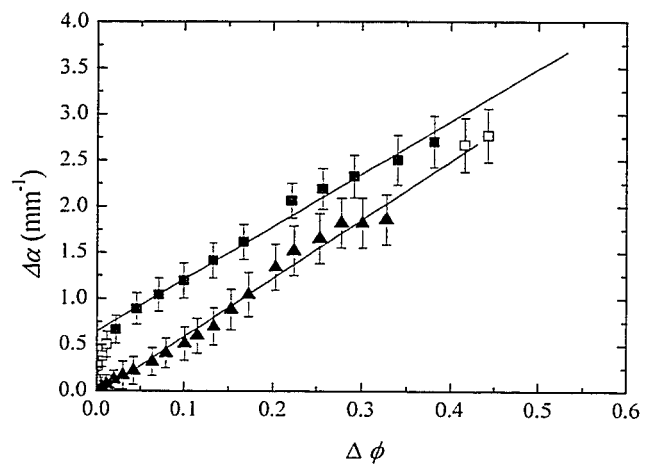


Figure 4.22. The change in the attenuation coefficient as a function of the change in void fraction for the dough mixed at vacuum (▲) and atmospheric (●). The open symbols are not included in the linear fit.

value of the fermentation time. The change in void fraction was then calculated using the equation, $\Delta\phi = 1 - \rho/\rho_{t_0}$, where t_0 is the zero fermentation time, which starts at the end of mixing, and the values $\rho_{t_0} = 1.24$ and 1.42 for the dough mixed at ambient and vacuum, respectively. These values were determined by extrapolating the density data back to zero fermentation time (section 4.2.1).

The change in the attenuation was then plotted as a function of void fraction, as shown in figure 4.22. The change in attenuation coefficient increases with void fraction for both samples mixed at either pressure. However, the way in which $\Delta\alpha$ changes is different as the void fraction increases. At early fermentation times, where the yeast is actively fermenting the sugars and aqueous CO_2 is diffusing through the matrix, the data show an increase in $\Delta\alpha$ even though the void fraction has not changed by much. This suggests that the diffusion of CO_2 affects the matrix in a way that increases the absorption of the ultrasonic signal. The change in $\Delta\alpha$, which is not due to the increase in void fraction, is represented by the open symbols in figure 4.20. In the region, $0.05 \leq \phi \leq 0.4$, the void fraction is changing rapidly because CO_2 has reached the air nuclei, and $\Delta\alpha$, for both mixing pressures, increases approximately linearly as a function of void fraction. A comparison of these results with those found in section 4.1 for the uncasted dough, shows:

$$\Delta\alpha = 0.643 + 5.695\phi, \text{ for the yeasted dough mixed at vacuum.}$$

$$\Delta\alpha = -0.0431 + 6.328\phi, \text{ for the yeasted dough mixed at ambient, and}$$

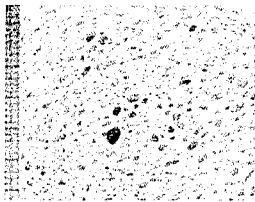
$$\alpha = 0.245 + 9.8\phi, \text{ for the uncasted dough.}$$

Thus we see that the rate of change in attenuation with void fraction $\Delta\alpha/\Delta\phi$ is similar in magnitude for both yeasted and unyeasted dough. (In fact, $\Delta\alpha/\Delta\phi$ is likely to be even closer than suggested from these relationships since $\Delta\alpha$ for the yeasted samples is probably overestimated because of the change in acoustic impedance with void fraction – see footnote 1 on page 130).

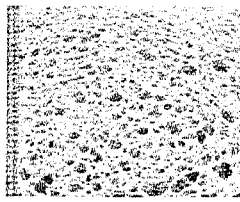
Chapter 5

Results and discussion part II: Evaluation of the mechanical properties of freeze-dried breadcrumb

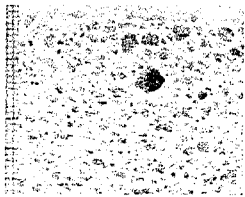
In this chapter, I discuss the results of the ultrasonic experiments performed on freeze-dried breadcrumb samples. In Section 5.1, the results of the experiments performed on the breadcrumb as the proofing time was varied will be presented. The purpose of these experiments was to investigate the mechanical properties of the breadcrumb as the size and concentration of the air cells is varied by varying the proofing time. First, the behavior of the density of the breadcrumb as a function of proofing time will be discussed. After that, the results for the ultrasonic phase velocities and the elastic constants of the samples will be calculated. These results will be compared to existing theoretical models. In section 5.2, the results of the ultrasonic experiments done on compressed samples will be presented. The purpose of these experiments was to investigate the effect of gas cell anisotropy on the mechanical properties of the breadcrumb. The anisotropy effects were investigated by probing the compressed samples in directions parallel and perpendicular to the compression direction. In section 5.3, the attenuation results for the compressed and noncompressed samples will be presented.



0 minutes



35 minutes



53 minutes



70 minutes



87 minutes



108 minutes

Figure 5.1. Digital images of breadcrumb proofed at various times varying between 0 and 108 minutes. Each small division on the scales corresponds to 1 mm.

5.1 Mechanical properties of freeze-dried breadcrumb proofed at different proofing times

5.2 Density of breadcrumb as a function of proofing time

Using the imaging procedure described in section 4.2.1, the density of the freeze-dried bread samples was measured for samples proofed for times ranging from 0 minutes to 108 minutes. This measurement was done before the samples were bonded and glued to the sample holders. The cellular structure of the samples proofed at different proofing times is shown pictorially in figure 5.1. In these images, the evolution of the gas cells at the different proofing times is clearly visible. As the samples are proofed for longer times, the air cells increase in size. As a result, the number of air cells per unit volume decreases and the cell walls become thinner. Therefore, we expect the density of the freeze-dried breadcrumb samples to decrease as a function of proofing time. The results for the density as a function of proofing time are shown in figure 5.2, which confirms this hypothesis. Figure 5.2 also compares the fresh (moist) results to those of Zghal *et al.* (1999), who used a digital image analysis technique to predict the density of samples prepared under the same conditions and using the same flour, i.e. CWRS. We find that our results are in good agreement with their measured densities, which are represented by the open symbols in figure 5.2. Zghal *et al.* (1999) have also used image analysis to measure parameters such as void fraction, number of cells per unit area, cell size, cell median, cell area and the cell wall thickness. Even though these parameters were measured for moist and partially air-dried breadcrumb samples, they will nevertheless be useful for us in the following sections to interpret the ultrasonic results. Both methods of

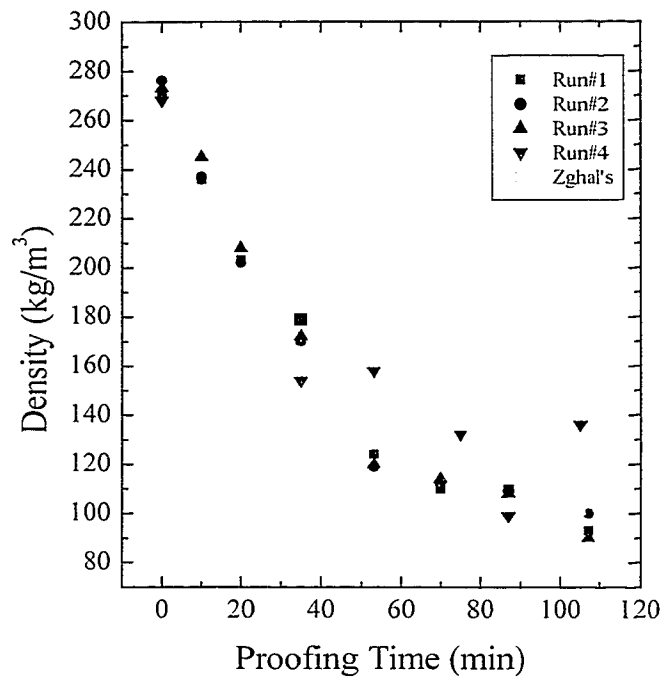


Figure 5.2. Density of freeze-dried breadcrumb as the proofing time is varied (closed symbols). For comparison, the results obtained by Zghal *et al.* (1999) are shown by the open symbols.

Table 5.1. Effect of proof time on breadcrumb structure (Zghal, 2000)

Parameter	Proofed for 35 min.	Proofed for 70 min. (optimum)	Proofed for 105 min.
Density (g/cm ³)	0.190	0.131	0.101
Number of cells per Unit area (cm ²)	113	96	80
Average cell size (mm)	0.712	0.795	0.885
Average cell area (mm ²)	0.400	0.500	0.622
Median cell area (mm ²)	0.033	0.034	0.041
Cell wall thickness (mm)	0.647	0.792	0.813

drying the samples preserve the original breadcrumb structure, the only difference between the freeze-drying and air-drying lying in the fact that much less moisture is present in the freeze dried sample. Zghal's relevant results are summarized in table 5.1.

5.1.2 Phase velocity

The phase velocity was measured in a similar way to that discussed in section 4.1.4, in which the transit time t (the time taken for the ultrasonic signal to travel through the sample) was found by measuring the arrival time difference between the sample signal and the reference signal. The velocity was then determined from the simple formula $v=d/t$, where d is the sample thickness. This procedure was done for all samples baked at different proofing times. The results of the velocity as a function of proofing time are shown in figure 5.3. The graph shows that the velocity decreases as a function of proofing time, indicating that the velocity is strongly affected by the size of the air cells, with its velocity decreasing markedly as the air cells become bigger.

To better understand these results, we first plotted the velocity data as a function of density using the density *versus* proofing time results from the previous section. These results are plotted in figure 5.4, which show that the velocity increases as the sample density increases. The $\rho^{1/2}$ dependence (dotted curve in figure 5.4) was included to show the best power law that fits the data. To gain quantitative understanding of these results, the data will be examined in light of the theoretical models that have been developed for similar cellular structures and porous materials. Two of these models to which we will compare our results are the cellular structure model developed by Gibson and Ashby (1982a,b) and a tortuosity model.

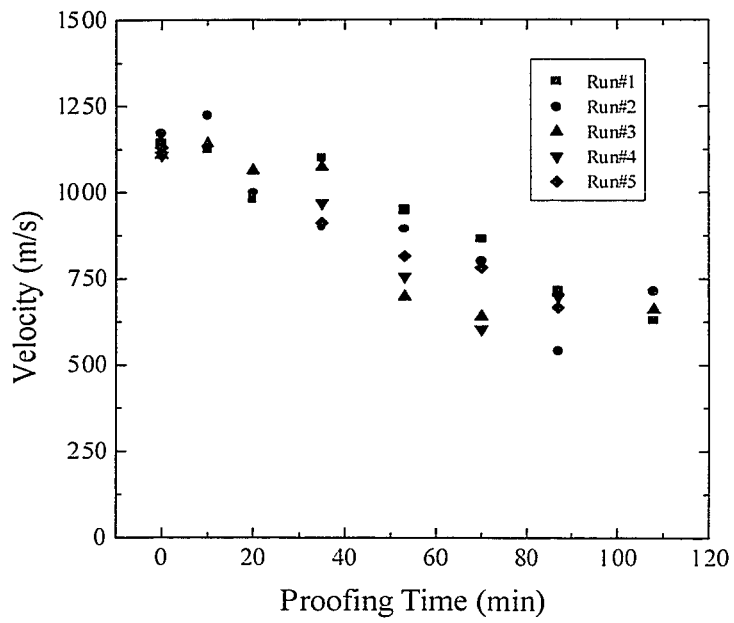


Figure 5.3. The phase velocity of breadcrumb proofed at different proofing times.

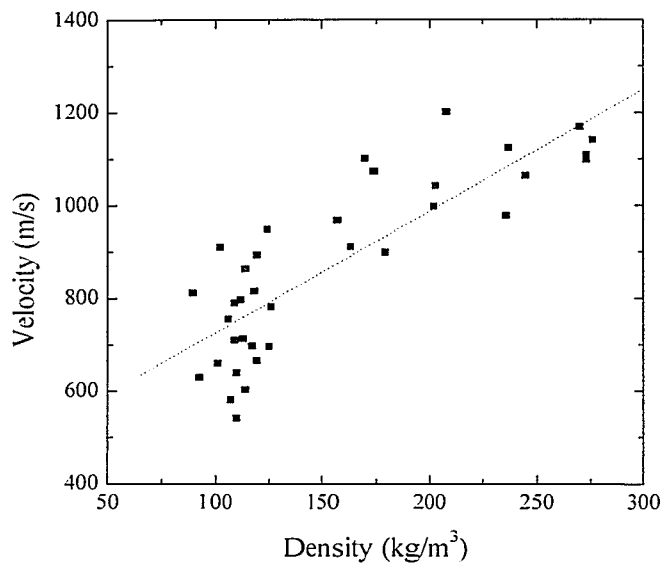


Figure 5.4. The velocity as a function of the density of the breadcrumb. The solid symbols represent the experimental data, while the dotted line is a fit to an expression with $\rho^{1/2}$ dependence.

5.1.3 Interpretation of the mechanical properties of freeze-dried breadcrumb

5.1.3.1 Gibson and Ashby's cellular structure model

In this model, the system is treated as a cellular solid structure, like that of a foam. For a comprehensive review of Gibson and Ashby's model, the reader is referred to the following references: Gibson and Ashby (1997), Gibson and Ashby (1982a,b). At the simplest level, an open-cell foam structure is modeled as a cubic array of beams of length l and square cross section of side t ; see figure 5.5a. Adjoining cells are staggered so that their members meet at their mid points. The deformation of such a cellular structure may be understood using dimensional arguments which omit all proportionality constants arising from the specific cell geometry. The relative density of the foam is related to the dimensions t and l by.

$$\frac{\rho}{\rho_s} = \left(\frac{t}{l}\right)^2 \quad (5.1)$$

Where ρ_s is the density of the cell wall material. Young's modulus for this foam-like structure is calculated from the linear elastic deflection of the beam of length l at its mid point. When a uniaxial stress is applied to the foam, each cell edge transmits a force F that bends each beam to cause a deflection, δ , which is given by

$$\delta = \frac{l^3 F}{4t^3 E_s} \quad (5.2)$$

Here E_s is Young's modulus of the beam. From the relationship between the stress and the strain $\epsilon = \delta/l$, Young's modulus for such a foam structure can be related to the foam density by

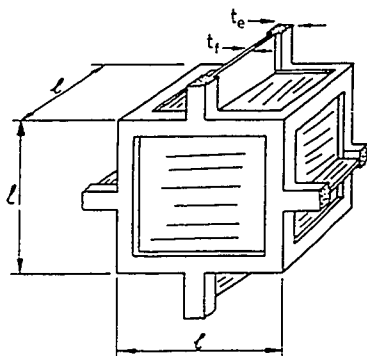
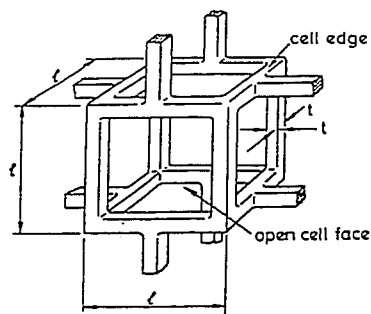


Figure 5.5. Cubic-cell model used in Gibson and Ashby's open cells model (a), where l is the edge length, t is the edge thickness, and closed cells model (b) where t_e and t_f are edge thickness and the face thickness respectively. Taken from Gibson and Ashby (1997).

$$\frac{E}{E_w} = C \left(\frac{\rho}{\rho_w} \right)^2 \quad (5.3)$$

Where E is Young's modulus. C is constant (experimental data showed that $C \approx 1$) and ρ is the density of the foam. The subscript w refers to properties of the walls of the cellular solid.

For a closed cell foam structure (the statement whether the cell walls are open or closed is determined by the wall's permeability to gas and/or liquid), a fraction Φ of the solid is contained in the cell edges, which have cell thickness t_e . The remaining fraction $(1 - \Phi)$ is in the faces, which have thickness of t_f . Such structure is shown in figure 5.5b.

The prediction of Gibson and Ashby's model for Young's modulus becomes:

$$\frac{E}{E_w} = \Phi^2 C_1 \left(\frac{\rho}{\rho_w} \right)^2 + (1 - \Phi) C_2 \left(\frac{\rho}{\rho_w} \right) + C_3 (1 - \Phi)^3 \left(\frac{\rho}{\rho_w} \right)^3 \quad (5.4)$$

Where C_1 , C_2 and C_3 are constants (experimental data showed that $C_1, C_2, C_3 \approx 1$).

To test the Gibson and Ashby model, we first calculate the longitudinal modulus, β , using the formula $\beta = \rho v^2$, where ρ is the density of the breadcrumb and v is the longitudinal ultrasonic velocity through the material. In Gibson and Ashby's model for foam, Young's modulus is equal to the longitudinal modulus. This can be easily seen from the following argument. For an isotropic material, $\epsilon_3 = s_{33} \sigma_3 = \frac{1}{E} \sigma_3$, where s is the elastic compliance. Young's modulus is given by the following expression as derived by Nye (1972).

$$\frac{1}{E} = \frac{s_{11} + s_{12}}{(s_{11} - s_{12})(s_{11} + 2s_{12})} \quad (5.5)$$

The Gibson and Ashby model assumes that $s_{12} = 0$, since there is no ϵ_1 or ϵ_3 generated by σ_3 (Poisson's ratio = 0). Therefore, for this foam model $\beta = E$.

Figure 5.6 shows the longitudinal modulus for breadcrumb as a function of relative density. The relative density was calculated using $\rho_w = 1601 \text{ kg/m}^3$, as measured for freeze-dried breadcrumb (Zghal, 2000). This value was used to enable us to represent the data as a function of relative density; any uncertainty in this number will introduce a small systematic effect that does not affect the exponent found in a power law fit to the data. The error bars shown on the graph were calculated by grouping the data into four windows of relative densities. The width of each window was 0.04 starting at a relative density of 0.05. The β values in each window were then averaged and the standard deviation was calculated. The reason for performing such an operation was the difficulty in obtaining samples of the same density. This occurred because of the intrinsic inhomogeneities of the samples, i.e. samples cut from the same loaf of bread have different densities. The predictions of the Gibson and Ashby model are shown on the graph by the solid line (open cell model) and dotted line (closed cell model). For the closed cell model, Φ was assumed to be independent of the density (Gibson and Ashby, 1997) and its value was determined from the least square fit to the data to be 0.96. We see that from figure 5.6 that the closed cell model gives a slightly better fit to the experimental results. This is not surprising since there is one additional fitting parameter. The open cell model gives very good agreement with the experimental data over the entire relative density range as well. The difference in the two fits is probably not significant.

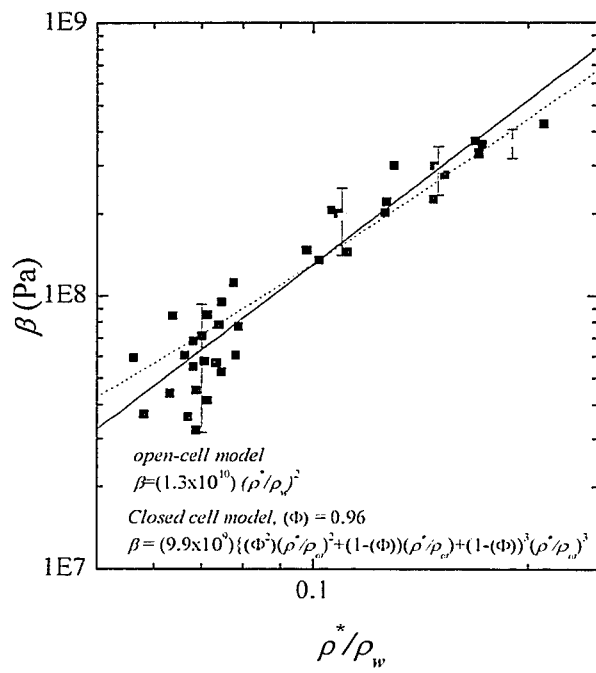


Figure 5.6. Longitudinal modulus: experimental results- black symbols: Gibson and Ashby's open cells model- solid line: closed cells model- dotted line.

Despite the considerable simplification of the structure, the Gibson and Ashby simple beam model for both open and closed cells appears to fit the data very well. This is an acceptable result since the breadcrumb has a finite permeability inferring that the cell walls are not completely closed. However, close inspection of the breadcrumb structure show that a plausible model is one where the structure is dominated by the large cells, which have an appearance of “closed” quasi-spherical cells with porous cell walls due to small cells. An extension of Gibson and Ashby’s model was attempted by Zghal *et al.* (2001), in which they accounted for the missing cell walls (MCW) that arise from the fact that at higher proofing times some adjacent cells will coalesce. MCW represent the fraction of cell walls present at every stage of proofing time that become missing as a result of coalescence. The result of coalescence is the formation of fewer, but bigger cells, leading to a reduction in the modulus. (Silva and Gibson, 1997). Zghal *et al.* (2001) also considered the effect of strain hardening (van Vliet *et al.*, 1992) in the gas cell walls as a result of gas cell expansion during proofing. This mechanism has the opposite effect to the MCW by causing the modulus to stiffen. These two effects are accounted for by multiplying the Gibson and Ashby result by additional factors as follows.

$$E = E_w \left(\frac{\rho}{\rho_w} \right)^2 \left(1 - \frac{MCW}{\phi} \right) \left(\frac{r}{r_0} \right)^p. \quad (5.6)$$

Where the exponent p is the strain hardening exponent, ϕ is a constant taken from the finite element results of Silva and Gibson (1997), and r_0 and r are the radius of the cells at the lowest proofing time and at a later time t , respectively. The challenge in testing to see if this model gives a better fit to the data lies in the need to accurately measure the parameters r and MCW as a function of proofing time, requiring a detailed image analysis

of samples proofed at the various proofing times. Such analysis is beyond the scope of this thesis, but would be an interesting project for future research .

5.1.3.2 Tortuosity model

In the previous section, the data were compared to the predictions of the Gibson and Ashby model in which the elastic properties of the material were described using a static approach. In this section, the data will be compared to the predictions of a model that is based on a wave propagation approach, which we call the tortuosity model. The basic idea behind the model is that in a porous material, the wave may be confined to one of the constituents, and thus be forced to follow a tortuous path through the material. This model has been applied most extensively to treat the velocity of the slow compressional waves seen in some porous materials filled with a fluid, one example being the model referred to as "fourth sound" for liquid helium confined to a porous medium (Johnson and Plona, 1982; Johnson and Sen, 1982); Schwartz and Johnson, 1984). This slow compressional wave is confined almost exclusively to the liquid in the pores and has the characteristic effect that its velocity is considerably slower than the acoustic velocity in the backbone. Johnson and Sen (1981) have shown from the wave equation that the speed of the compressional wave can be written as

$$v = \left(\frac{K}{\rho_{eff}} \right)^{1/2} \quad (5.7)$$

where K is the bulk modulus and ρ_{eff} is an effective density reflecting the inertial drag on the fluid due to the presence of the solid pore walls. Using the fact that the differential equation and boundary conditions governing the motion of an incompressible fluid in the

pore space is identical with those of the electrical conduction through the sample if the pores are filled with a conducting fluid. Brown (1980) shown that

$$\rho_{eff} = FP\rho_f \quad (5.8)$$

where F is the ratio of the electrical conductivity of the pore fluid to the conductivity of the sample as a whole, P is the porosity and ρ_f is the bulk fluid density. Thus the velocity of the slow compressional wave is given by

$$v = \left(\frac{K}{FP\rho_f} \right)^{1/2} = \frac{v_f}{\sqrt{FP}} \quad (5.9)$$

where v_f is the velocity of the wave in the bulk fluid. Thus the velocity can be expressed in terms of an acoustic refraction index, n , as

$$v = \frac{v_f}{n} \quad (5.10)$$

where $n^2 = FP$.

One important conclusion from this result is that the index of refraction, n , is independent of the fluid characteristics (density and modulus) and is purely a geometrical quantity. As a result, for a system consisting of a dilute concentration of nonconducting ellipsoid inclusions embedded in a conducting medium, the expression for the index of refraction can be written in terms of the depolarization factors, L_i , as,

$$n^2 = \frac{1 - PL_i}{1 - L_i} \quad (5.11)$$

where the subscript i labels the axes of the ellipsoid. Since the depolarization factor can be calculated explicitly in terms of the particle shapes and dimensions, this relation is useful for determining the acoustic index of refraction in terms of the microstructure of the porous material. For example, Johnson and Sen (1981) give a detailed derivation of

the L_i expressions for different shapes of inclusions. For a sphere, where $a_x = a_y = a_z$, (where the a 's are the axes of the ellipsoid), $L_x = L_y = L_z = 1/3$. To extend equation 5.10 to account for the behavior when the concentration of the inclusions is high, Johnson and Sen (1981) have proposed a self-similar model for dielectric properties. They obtained the following expression (Johnson and Sen, 1981)

$$F = P^{-m} \quad (5.12)$$

where $m = \frac{1}{1-L_i}$ is a constant that is related to the depolarization factor which describes the shape of the inclusions. Thus for any concentration of spherical inclusions,

$$n = (FP)^{1/2} = (PP^{-m})^{1/2} = P^{\frac{1-m}{2}} \quad (5.13)$$

Therefore, the velocity of the slow wave is

$$v = v_f P^{\frac{m-1}{2}} \quad (5.14)$$

This result developed for the slow compressional wave in a fluid-filled porous material may be used to interpret our data for breadcrumb with air-filled pores by exploiting the following analogy. In our system, the concentration contrast between the solid matrix (breadcrumb) and air is large, so that the wave is largely confined to the backbone. Thus the wave propagation through the solid matrix backbone will experience similar geometric tortuosity constraints to the fluid-confined slow wave, except that the roles of the pores and the solid matrix are reversed. Therefore, by substituting $(1-\phi)$ for the porosity in the above equation, and $m=3/2$ for spherical inclusions, we get

$$v = v_m (1-\phi)^{0.25} \quad (5.15)$$

Where v_m is the velocity in the solid matrix material and ϕ is the void fraction, which is defined by

$$\phi = 1 - \frac{\rho}{\rho_v} \quad (5.16)$$

Figure 5.7 shows the velocity as a function of ϕ along with the tortuosity prediction (solid line) for spherical inclusions. The tortuosity prediction for the velocity shows a similar behavior as the experimental data at the low void fraction values. However, at high ϕ values, the experimental data falls more rapidly with ϕ than the prediction of the tortuosity model. From the fit, the velocity of sound through the matrix is found to be about 1700 m/s. For comparison purposes, Gibson and Ashby's prediction for open cell foam, $v = v_m(1 - \phi)^{0.5}$, is shown in figure 5.7 by the dash curve. The Gibson and Ashby model does appear to show better overall agreement with the experimental data.

5.2 Compression experiments: Investigating the effect of anisotropy

5.2.1 Introduction

To further increase the density and to study the effects of elastic anisotropy on the mechanical properties of the freeze-dried breadcrumb, the samples were compressed uniaxially in the following steps. A graphical description of these steps is shown in figure 5.8. First the samples were cut from the freshly baked loaf of bread, with the long-axis parallel to the bottom plate of the baking pan and placed between two 9-millimeter-thick acrylic plates. The samples were then mounted in a custom-made uniaxial compression apparatus and a weight of approximately 10 Newton was applied to the top

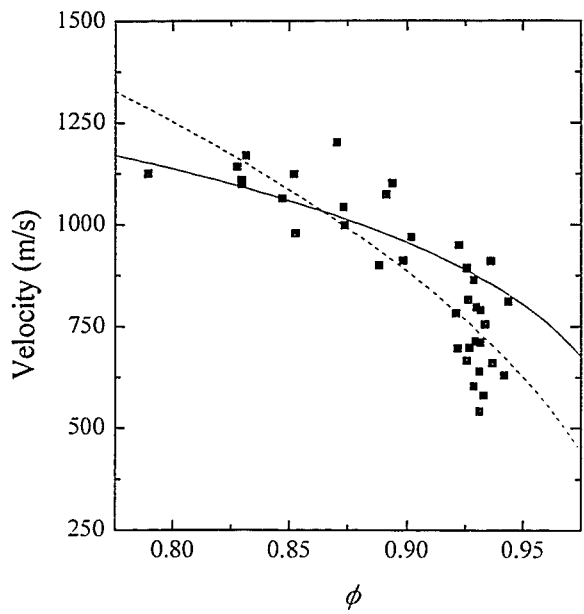
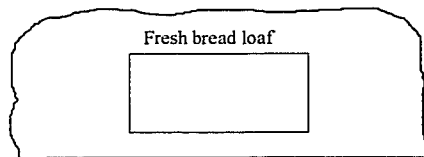
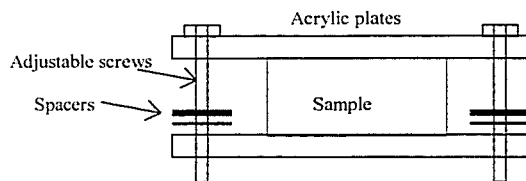


Figure 5.7. Velocity as a function of void fraction: as predicted by the tortuosity model (solid line) and Gibson and Ashby open cell model (dash line).

Step 1: the sample is cut from the fresh bread loaf



Step 2: the sample is placed between the acrylic plates



Step 3: the sample is placed in the compression apparatus

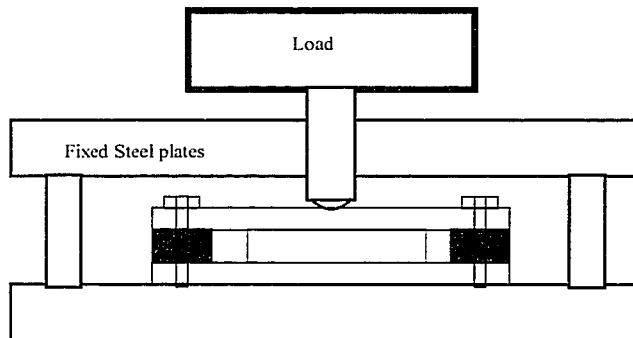
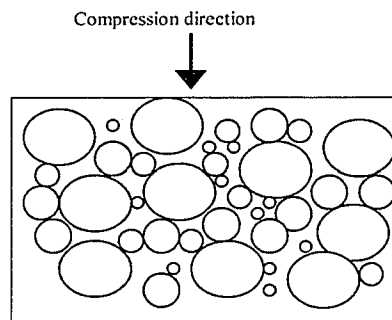


Figure 5.8. Steps involved in compressing the freshly baked breadcrumb samples.

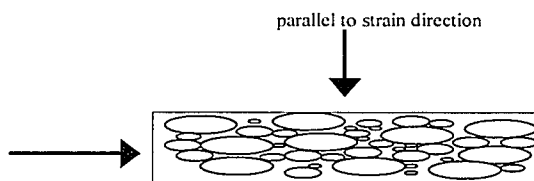
plate. The separation between the plates was preset using one, two and three millimeter spacers, depending on the final desired sample thickness. After compressing the sample, it was fixed between the two acrylic plates using four screws, one in each corner, and transferred to the freeze drier.

Using this method, we were able to increase the density of the samples up to five times the non-compressed samples, allowing ultrasonic investigation to be undertaken over a wider range of densities. However, the structure of the samples is now different to that of the non-compressed samples. In particular, the air cells are no longer spherical and the cell walls are bent and compressed in the direction parallel to the strain direction. Schematically this is shown in figures 5.9a,b and c. Figure 5.9d shows digital images of the compressed samples as the strain is increased. The immediate observation that comes out of this schematic description of the compressed samples is that the structure of the material is now anisotropic and the ultrasonic parameters will depend on the direction at which the sample is probed. The direction in which we probe the sample is important, because of the difference in structure as a result of the air cell compression. Hence, independent measurements of the velocity both parallel and perpendicular to the strain allow the effect of these differences in the structure to be investigated. It should be noted that the final thickness of the compressed sample was set to be the same for all samples and the same load is used for compressing every sample. Because Poisson's ratio is essentially zero for the as-baked bread, the density increase is therefore determined by the decrease in original sample thickness only.

(a) before compression: approximately spherical air cells



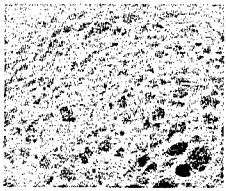
(b) after compression: pancake-like air cells



(c) propagation paths.



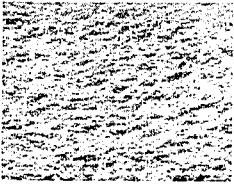
Figure 5.9. Changes in sample structure as a result of the uniaxial compression and the resulting propagation paths in both directions.



Zero strain



0.2 strain



0.25 strain



0.44 strain

Figure 5.9d. Digital images of compressed samples as a function of increasing strain.

In the remainder of this section, we will discuss the results of the experiments done on the compressed samples for which we will investigate the anisotropy effects over a range of uniaxial compressions. Hence, the sample anisotropy will be investigated by probing the sample in the parallel and perpendicular directions to the strain direction.

The density of the compressed samples, which was determined in the same way as described in the previous section, will be presented as a function of strain rather than proofing time. The results are plotted in figure 5.10, which shows how the density of the compressed samples increases as the strain is increased. This result is expected since the net effect of straining the sample is to “squish” the spherical air cells, resulting in the elongation of these cells in the direction perpendicular to the strain direction, see figures 5.8 and 5.9. Furthermore, since the density is defined as the mass divided by the volume and the mass of the sample does not change as a result of the compression, the change in the density reflects the change in the sample volume as the thickness of the sample is decreased. If Poisson’s ratio is zero, then the density, ρ , of the compressed samples will increase as follows.

$$\rho(\varepsilon) = \frac{M}{V} = \frac{M}{V_0 - \Delta V} = \frac{M}{V_0 \left(1 - \frac{\Delta V}{V_0}\right)} = \frac{M}{V_0 (1 - \varepsilon)} = \frac{\rho_0}{1 - \varepsilon} \quad (5.17)$$

where M is the mass of the sample, V is the sample volume after it has been decreased by ΔV from its original volume V_0 , $\varepsilon = \frac{\Delta l}{l} = \frac{\Delta V}{V}$ is the strain, l and Δl are the length of the sample and its change in the compression direction, and $\rho_0 = \frac{M_0}{V_0}$ is the original density.

The solid curve in figure 5.10 shows this prediction for the strain-dependent density. The

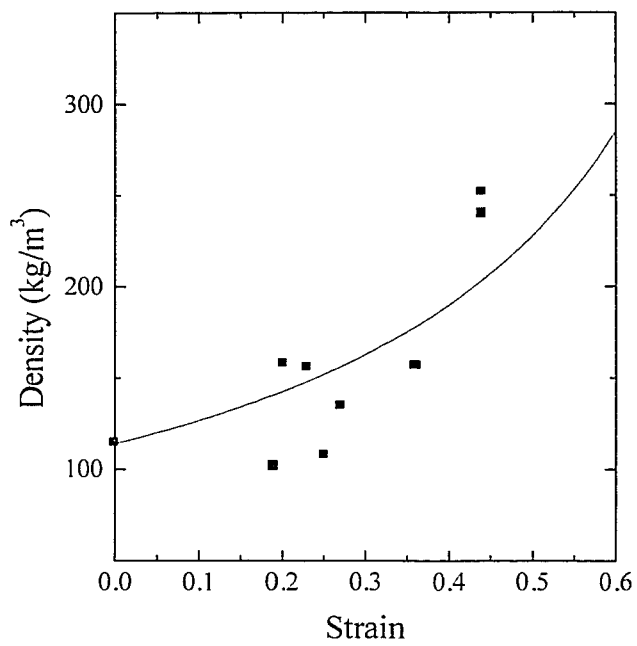


Figure 5.10. Density as a function of strain resulting from uniaxially applied stress. Solid symbols represent the experimental data and solid line is given by $\rho(\epsilon) = \rho_0 / (1 - \epsilon)$ (see text).

good agreement between this prediction and the data confirms that Poisson's ratio is essentially zero for bread. Rohm *et al.* (1997) report that Poisson's ratio for bread ranges between 0.17 to 0.25 for small strain and 0.07 to 0.15 for large strain.

To illustrate the substantial difference in the velocity as a result of the change in structure brought about by the uniaxial stress, we will first compare the ultrasonic velocity parallel to the compression direction in the compressed samples with the velocity in the compressed samples found by varying the proofing time, section 5.1.2. Figure 5.11 shows the velocity results for these two sets of measurements as a function of density. We see that the velocity dependence on the density of the compressed freeze-dried bread samples behaves differently to that of the non-compressed samples. The velocity for both sets of samples starts at the same value at low densities, but their behavior thereafter is opposite. While the velocity of the non-compressed samples increases with density, the velocity of the compressed samples decreases. In particular, the velocity of the compressed samples drops off dramatically as the air cells depart from their approximately spherical shapes and the cells attain a pancake-like structure. At higher densities, $\rho > 250 \text{ kg/m}^3$, the phase velocity levels off at a minimum value which is about 300 m/s. The different behavior of the phase velocities for the compressed and noncompressed samples is a clear indication that the structure of the samples is altered as a result of the induced strains. Two points which are important and need to be emphasized are: 1) all compressed samples are proofed for 70 minutes, which is the optimum proofing time as determined by the Canadian Short Processing Method which was discussed in chapter 2; 2) the phase velocities presented in figure 5.11 were

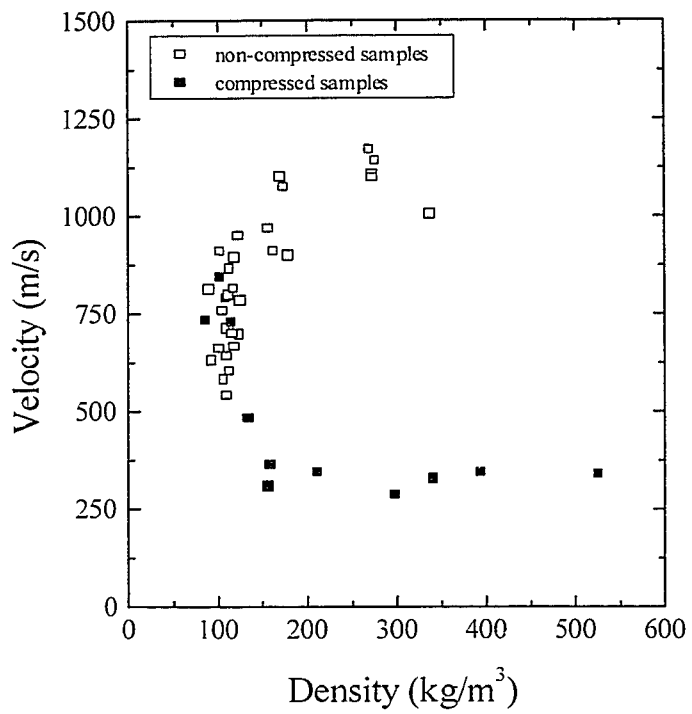


Figure 5.11. Velocity of compressed breadcrumb samples (solid symbols), propagated along the direction parallel to the strain direction, and non-compressed samples (open symbols).

measured along the parallel direction to the strain. This is the same direction at which the non-compressed samples were probed relative to the baking pan.

5.2.2 Investigating the anisotropy effects on the mechanical properties of the breadcrumb by probing the samples along the two orthogonal directions

The structural differences between the parallel and perpendicular directions to the strain and their effect on the velocity were examined by cutting slab-shaped samples of thickness 4-6 mm perpendicular to both directions. These samples were cut from compressed loaves from the same batch. The phase velocity was measured for both sets of samples separately. The results for the phase velocity as a function of the density are plotted in figure 5.12, which shows that the velocity density relationship is indeed different for the two propagation directions. For samples probed along the direction perpendicular to the strain, the velocity shows a significant decrease of about 30% over the range of densities over which the measurements were performed. For samples probed along the direction parallel to the strain, the decrease is even more pronounced: the velocity starts at 700 m/s at zero strain and decreases sharply to a velocity of 250 m/s as the density is increased. To gain a quantitative understanding of these results, we will examine these data in light of the Gibson and Ashby model and the tortuosity model, which were previously applied to the noncompressed samples where the air cells were approximately spherical.

5.2.2.1 Modified Gibson and Ashby's cellular structure approach to anisotropy

The Gibson and Ashby foam model discussed in the previous section can be extended to account for an anisotropic system in which the foams are approximately

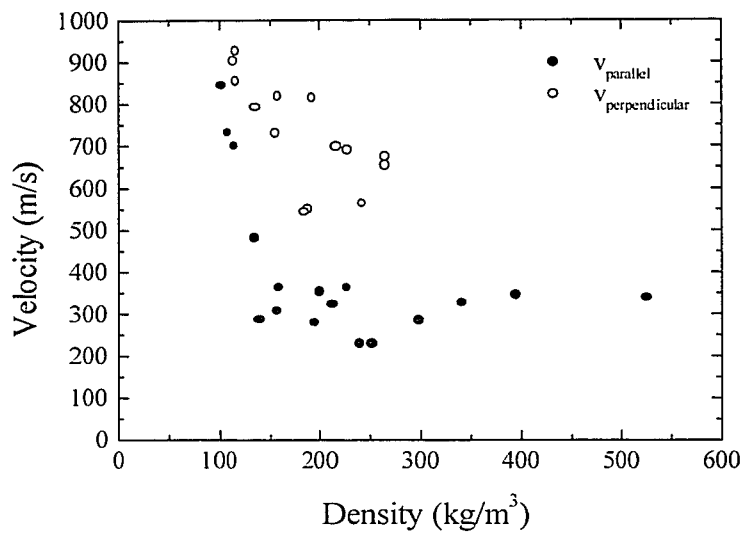


Figure 5.12. Phase velocity of ultrasonic waves propagating parallel to the strain direction (solid circles) and perpendicular to the strain direction (open circles).

axisymmetric (Gibson and Ashby, 1982b,1997). In this model, the anisotropy is characterized by the ratio of the cell dimensions parallel (h) and perpendicular (l) to the uniaxial stress, which is called the shape-anisotropy ratio R . Figure 5.13 shows a typical cell used in the Gibson and Ashby anisotropic model. The anisotropy of the elastic properties of the cellular structure is determined by calculating the ratio of Young's modulus in the two orthogonal directions and expressing this ratio in terms of the anisotropy parameter R . However, our experimental situation is different to the situation described by Gibson and Ashby in that our experiments were performed in compression whereas they treat uniaxial extension. Hence for our data, $R \leq 1$. They derive the following expression for Young's modulus in the two directions.

$$E_{par} = CE_w \left(\frac{l}{l}\right)^4 \left(\frac{h}{l}\right) \quad (5.18)$$

$$E_{per} = \frac{CE_w}{2} \left(\frac{l}{l}\right)^4 \left(\frac{l}{h}\right) \left(1 + \left(\frac{l}{h}\right)^3\right) \quad (5.19)$$

In the Gibson and Ashby model for an anisotropic material, both Young's modulus and the shear modulus, G , have similar scaling behavior with similar scaling factors. Therefore, the longitudinal modulus, β , for the foam exhibits the same behavior as Young's modulus because the longitudinal modulus is proportional to both the Young's modulus and the shear modulus. Hence, the ratio of the moduli is

$$\frac{\beta_{par}}{\beta_{per}} = \frac{E_{par}}{E_{per}} \frac{2R^2}{1+1/R^3} \quad (5.20)$$

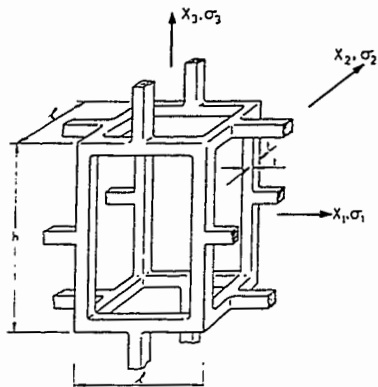
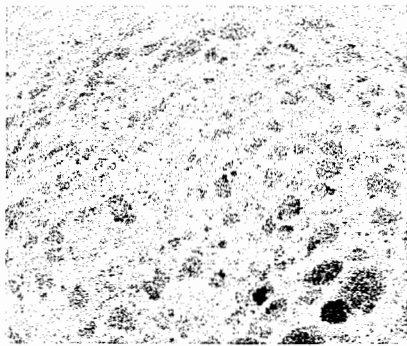


Figure 5.13. Anisotropic open cell used in Gibson and Ashby's model. Taken from Gibson and Ashby, (1997).

For the closed cell model, Gibson and Ashby find that an additional term, $(1-\phi)\frac{2R}{1+1/R}$, is added to the ratio of $\frac{E_{par}}{E_{per}}$. Therefore, for the closed cell model, the ratio of longitudinal moduli is,

$$\frac{\beta_{par}}{\beta_{per}} = \Phi \frac{2R^2}{1+1/R^3} + (1-\Phi) \frac{2R}{1+1/R} \quad (5.21)$$

where $\Phi = \frac{V_{edge}}{V_{total}}$, is the fraction of the volume of the edges, which was taken to be 0.96, see section 5.1.3.1. To test this model against our data, we first need to calculate the anisotropy ratio, R . To do that, digital images for each of the samples were taken from which a mean value for l and h were determined as follows. Using the Scion Image software program, the perimeter of the cells was traced and an ellipse was fit to each cell. An example of the images used in these analyses is shown in figure 5.14. One observation that can be seen from this figure is that some cells were not traced in the figure due to imperfect lighting conditions in the original photograph. To get a true representation of the breadcrumb cells in the image, it was essential to a voids counting cells for which the cell walls were so close to touching that they appeared to touch after thresholding. This was achieved by setting the threshold in such a way so that the small cells were delineated. This procedure was repeated for different threshold settings and found to give comparable measurements for the average value of l and h . From these fitted ellipses, the area of the cells, the major and the minor axes and the angle of orientation of the individual ellipses were calculated for each ellipse. To calculate R , both l and h were projected using the orientation angle, θ . Figure 5.15 illustrates this



(a)



(b)

Figure 5.14: A typical digital image of bread samples which were used in the calculation of the anisotropy ratio, R . (a) the original digital image of the sample, (b) the traced ellipses used in the calculations for determining the anisotropy ratio R , the orientation angle θ and the area of gas cells.

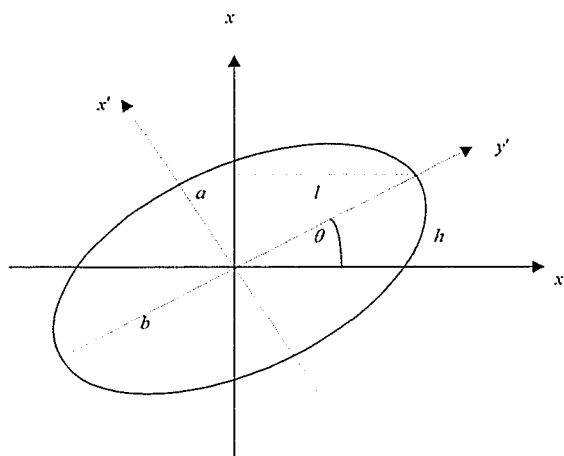


Figure 5.15. Projecting the axes a and b using the coordinate transformation $x = x' \cos \theta - y' \sin \theta$ and $y = x' \sin \theta + y' \cos \theta$. Using the equation of an ellipse: $\frac{x'^2}{a^2} + \frac{y'^2}{b^2} = 1$, the projected axes are defined as follows: $l = \sqrt{\frac{1}{\cos^2 \theta + \sin^2 \theta}}$, and

$$h = \sqrt{\frac{1}{\sin^2 \theta + \cos^2 \theta}}$$

point and the relevant projection formulas used. After that, the average values for the major and minor axes as well as the angle of orientation were calculated for each ellipse. Once both projected lengths l and h were calculated, R is then simply given by the ratio of the two, i.e. $R = \frac{h}{l}$.

The second calculation that had to be done before we compare our experimental results to the prediction of Gibson and Ashby's model, is the determination of the ratio of the experimental results for the longitudinal modulus in the two propagation directions. This is not a straightforward operation because the density of the samples oriented parallel and perpendicular to the compression direction was not the same. This problem occurred because of the intrinsic inhomogeneities in the samples. To get around these problems, the ratio of the longitudinal moduli (in the perpendicular and parallel propagation directions) was calculated from the two independent measurements of the moduli as follows: first, both sets of velocity data were truncated at a density of 300kg/m^3 , see figure 5.16. The reason for truncating the data is that we do not have data for the perpendicular velocity beyond this density and it only eliminates three readings. The data is then binned into intervals of 50kg/m^3 on the density scale. The data in each interval were then averaged and the deviation for each point in the interval was used to calculate the errors in each point. The average velocities along with their error bars are plotted on the graph using the open symbols. Using this method, the longitudinal modulus ratio was calculated directly from

$$\frac{\beta_{per}}{\beta_{par}} = \left(\frac{\bar{v}_{per}}{\bar{v}_{par}} \right)^2 \quad (5.22)$$

where \bar{v} is the average velocity in a given density bin.

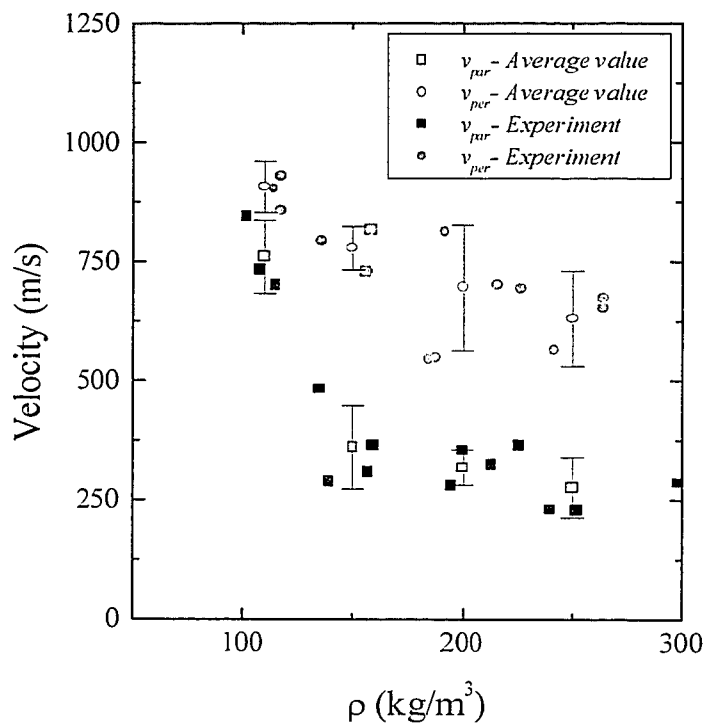


Figure 5.16. The parallel and perpendicular phase velocities. The open symbols are the mean values of the velocities averaged over an interval of 50 kgm⁻³ on the density scale.

Our experimental results for the longitudinal modulus are compared with the prediction of Gibson and Ashby's open and closed cell models in figure 5.17. The experimental results agree with both the open and closed cell models in the range $0.6 < R < 1$. However, at lower values of R , the data are larger than this theoretical prediction. The prediction of the Gibson and Ashby's closed cell model has an odd feature that at $R = 1$, the ratio is bigger than 1.

5.2.2.2 Tortuosity model

In section 5.1.3.2, it was established that the velocity of a wave which is confined to the backbone (solid matrix) is given by equation 5.14. For an oblate spheroid, with axes, $a_x < a_y = a_z$, and eccentricity, $e = \left(\frac{a_x^2}{a_y^2} - 1 \right)$, the depolarization factors are expressed by (Johnson and Sen, 1981).

$$\begin{aligned} L_x = L_x &= \frac{1+e^2}{e^3} (e - \tan^{-1} e); \\ L_y = L_z &= \frac{1}{2} (1 - L_x) \end{aligned} \quad (5.23)$$

Using our results for the of the anisotropy ratio R from the section 5.3.2.1, m can easily be determined from the depolarization factors and hence the dependence of the ultrasonic velocity in both direction was calculated, allowing a comparison to the experimental data. The results of such calculations are shown in figure 5.18a. The solid and dashed curves in this figure represent the velocity in the parallel and perpendicular propagation directions for oblate spheroids. Also, plotted on figure 5.18a by the dotted curve, is the velocity for spherical inclusions where $a_x = a_y = a_z$. The velocity in the perpendicular

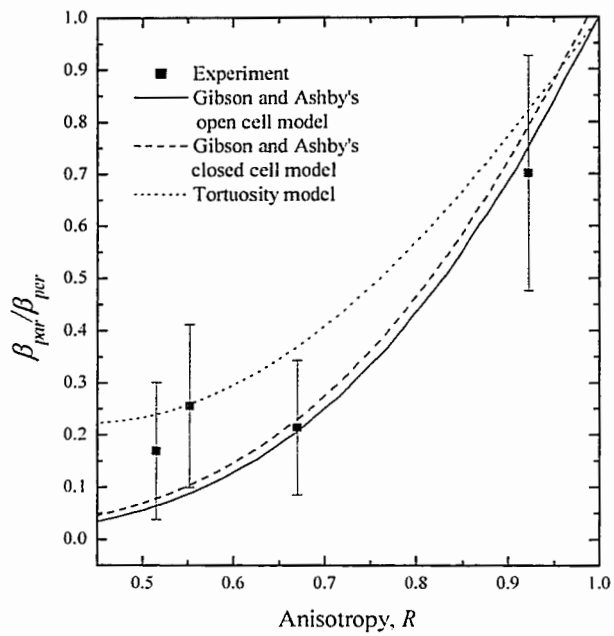


Figure 5.17. The ratio of the longitudinal modulus in the two propagation directions. Solid line represents Gibson and Ashby's open cells model; dotted line represents Gibson and Ashby's closed cells model; the dashed line represents the tortuosity prediction, to be discussed in section 5.3.2.2, and the solid symbols represent our experimental results.

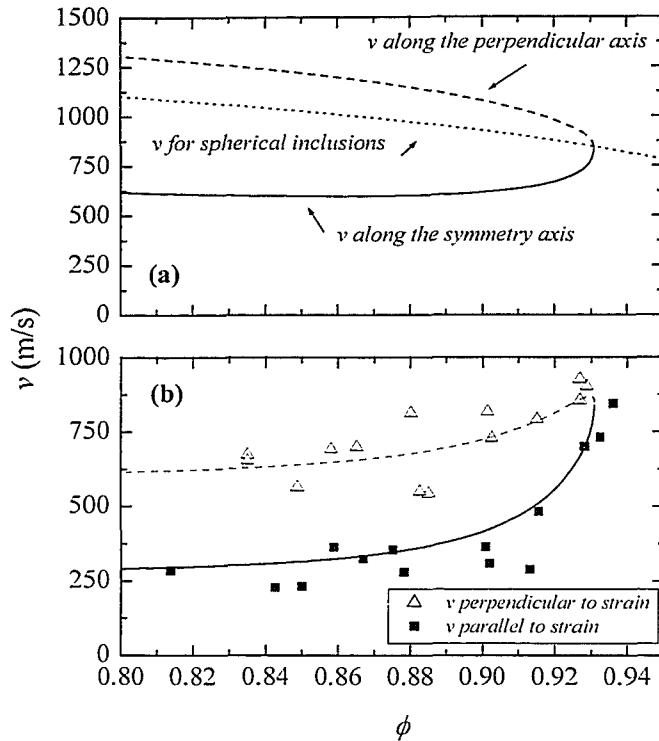


Figure 5.18. (a) Predictions of the tortuosity model with oblate elliptical inclusions for parallel (bottom curve) and perpendicular (top curve) propagation directions relative to the compression direction. For comparison, the prediction for spherical inclusions are shown by the dotted curve. (b) Our experimental results for parallel and perpendicular ultrasonic phase velocities. The dashed and solid lines in (b) represent the tortuosity model for perpendicular and parallel directions multiplied by $(1 + \epsilon)^{-1.5}$, where ϵ is the strain.

direction increases as the void fraction is lowered, consistent with the hypothesis that sound travels through shorter distances as the anisotropy increases. The opposite conclusion can be drawn from the velocity behavior in the parallel direction, namely that v decreases with increasing anisotropy. The experimental results for the phase velocity along the directions parallel and perpendicular to the strain are plotted in figure 5.18b. While the behavior of the measured parallel velocity is qualitatively similar to the theoretical prediction in figure 5.18a (solid symbols), the measured perpendicular velocity decreases as ϕ is decreased (open symbols), an effect that is not predicted by the tortuosity model alone. This suggests that there is an additional weakening of the cell walls due to compression. We account for this effect phenomenologically by multiplying the predictions of the tortuosity model by the factor $(1 + \epsilon)^{-1.5}$, giving the solid and dashed curves in figure 5.18b. As can be seen from this figure, the tortuosity prediction multiplied by this factor gives an excellent description of the data, with a matrix velocity, v_m , of 1650 m/s which is consistent with the value v_m for both directions of 1700 m/s found in section 5.1.3.2.

The prediction of the tortuosity model for the effects of the anisotropy on the elasticity of bread can also be examined by calculating the ratio of the longitudinal modulus along the two directions, given by the ratio of the squares of the velocities. These data are shown in figure 5.17. Although the tortuosity model appears to overestimate the effects of anisotropy for R close to 1, it gives better agreement with our data at low R . Overall, the tortuosity model gives a quite satisfactory explanation of our experimental measurements of the anisotropy in the velocity and caused by uniaxial compression of the bread samples.

5.3 Attenuation results

For the freeze-dried samples, it was not possible to cut samples that have exactly the same density. This is true for samples cut from the same loaf. This is due to the intrinsic inhomogeneities within the sample. In fact for samples proofed for the same time, the density variation was found to be as high as 0.01 g/cm^3 . Such density fluctuations make it difficult to make measurements for a range of sample thicknesses and hence unambiguously determine the attenuation coefficient. (c.f. section 4.1.3 for dough where α was measured). As a result, the attenuation results will be expressed in terms of the amplitude of the propagating signal in samples of fixed thickness of 6.3 mm, rather than by the attenuation coefficient. This still allows the qualitative trends in the density dependence of the attenuation to be inferred from our measurements, thus providing information on the changes in the size of air cells and their concentration.

We first examine the signal amplitude as a function of density as found by varying the proofing times. This is shown in figure 5.19. In this figure, the signal amplitude increases as the density increases. In other words, for the more dense samples, in which the air bubbles are smaller and the cell walls are thicker, the signal suffers less loss due to either absorption or scattering. In fact this interpretation is consistent with our interpretation of the attenuation results in section 4.2.3 for the dough, even though the nature of the samples are different.

For the compressed samples (note that all compressed samples are of the same thickness which was 4.2 mm), the behavior of the signal amplitude is different. The results of the ultrasonic signal amplitude for both samples are shown in figure 5.20 for

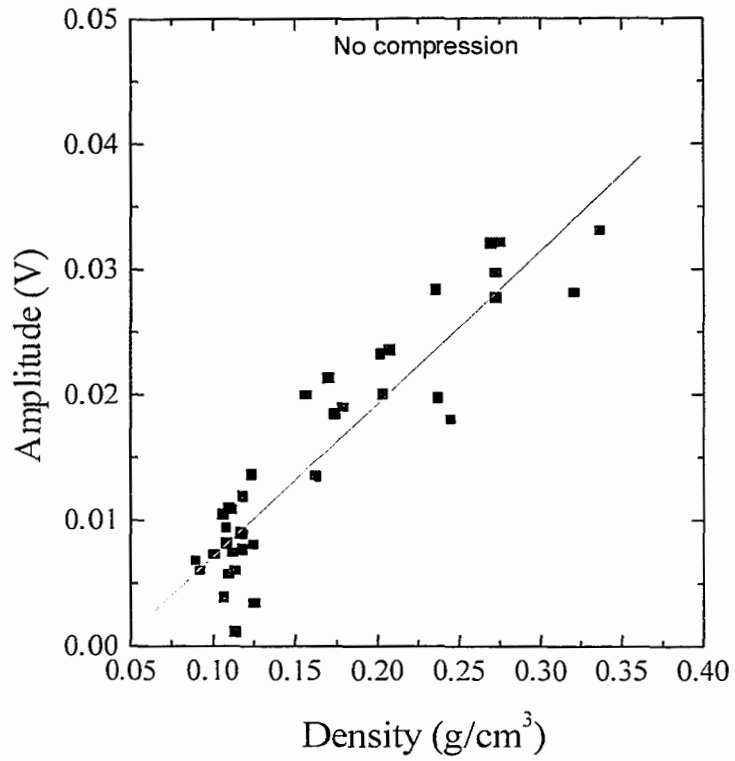


Figure 5.19. The amplitude of the ultrasonic signal as the density of breadcrumb is varied by varying the proofing time. The solid line is a linear fit to the data.

which all samples were proofed for the same time, namely 70 minutes. Thus the increase in the density is due to the application of the uniaxial stress. In figure 5.20, the signal amplitudes start at the same value as the noncompressed samples, see figure 5.19. However, as the density is increased, as a result of compression, there is a slight increase in the signal amplitude for the perpendicular samples and a slight decrease in the signal amplitude in the parallel samples. In both cases the signal amplitude stays substantially smaller than that of the uncompressed samples at comparable density values. To explain the increase and decrease in the signal amplitude with the density for the perpendicular and parallel samples respectively, we have to look back at the structure of the compressed samples, shown in figure 5.9a,b. The only difference is in the amount by which the samples were compressed, i.e. the relevant factor that we have to account for is the amount of the strain.

For the parallel sample, the cross section of the gas cells remains about the same, but the number of cells per unit length is thus directly increased ($\propto \epsilon$), so that a strain of 0.5 gives twice as many cells per unit length. Therefore, the amount of scattering is expected to increase, with a corresponding decrease in the signal amplitude. For the perpendicular samples, the average cross section of air cells decreases, but the number of cells per unit length is similar to the noncompressed one. Thus, the tortuous path is shorter and hence the signal will encounter less scattering. Therefore, the signal amplitude is bigger.

These tortuosity/scattering arguments suggest that for the parallel strain, the amplitude is expected to be less than the uncompressed samples, but that for the

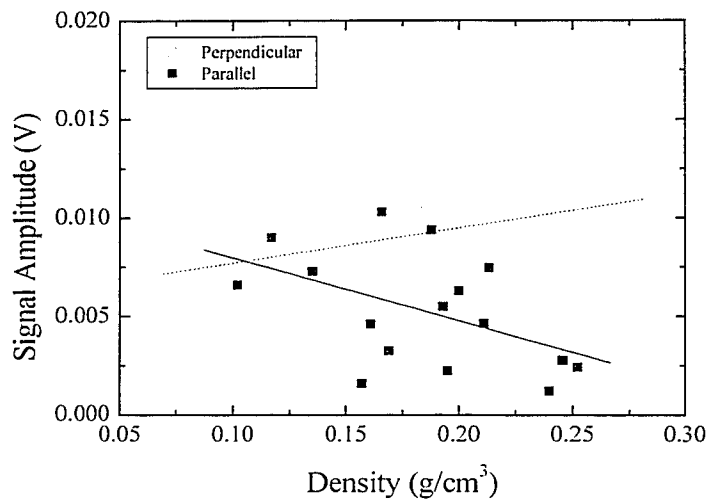


Figure 5.20. The amplitude of the ultrasonic signal as the density of breadcrumb is varied by applying uniaxial stress to the sample. The solid symbols represent the amplitude of the signal propagating along the direction parallel to the strain, and the open symbols represent the signal amplitude as the signal propagates along the direction perpendicular to the strain. The solid and dotted line represent linear fits to the parallel and perpendicular data respectively.

perpendicular strain, the amplitude should be bigger. However, this is not the case, as the amplitudes in both directions are considerably less. This suggests that there is an additional mechanism that causes the average ultrasonic attenuation to increase with strain. This mechanism is likely the same as the one that reduces the average velocity and weakens the matrix. One possible mechanism would be ruptured cell walls.

Chapter six

Summary and conclusions

The work presented in this thesis may be divided into two areas: 1) investigating the roles of air bubbles and the surrounding matrix in determining the mechanical properties of the dough, both at the end of mixing and during fermentation, and 2) investigating the effect of gas cells on the mechanical properties of breadcrumb. In both areas, low frequency (54 kHz) ultrasonic velocity and attenuation measurements were used to investigate the mechanical properties. The motivation for this work is the need to better understand the key role played by air cells in breadmaking and to develop new ultrasonic techniques for characterizing the physical properties of these systems. The significance of gas cells in determining the quality of bread products has been highlighted by Campbell *et al.* (1998), who articulated the view that breadmaking is essentially a series of aeration processes that must be understood and optimized to produce a well aerated loaf with an attractive volume and textural attributes. The bubbles are incorporated into the dough during mixing and act as nucleation sites for carbon dioxide produced by the yeast metabolism during proofing. The development of the dough structure allows these bubbles to be inflated with carbon dioxide without excessive coalescence or loss of gas. However, the effect of the air bubbles on the mechanical properties is not a well-understood subject. The lack of knowledge of this subject is mainly due to two factors, the complexity of the material, and the lack of tools to probe the samples non-destructively and delineate the contribution of the air bubbles to dough

elasticity. Breadcrumb is also a complex material, and while several researchers have studied the mechanical properties of this cellular solid, much remains to be learned about the role of the air cells in determining its mechanical properties. The results presented in this thesis demonstrate the potential importance of using ultrasonic techniques to characterize this food system, opening the door for possible future applications where non-destructive ultrasound techniques can be employed to monitor one of the most important attributes of bread quality.

6.1 Investigating the effect of air bubbles on the mechanical properties of dough at the end of mixing and during fermentation

Our experimental results have shown that both ultrasonic velocity and attenuation are sensitive to the presence of gas bubbles in dough. We exploited this phenomenon to investigate the effect of the air bubbles on its mechanical properties. First, experiments were performed to vary the amount of air incorporated into unyeasted dough by changing the mixing pressure. We found that the attenuation coefficient increased as the amount of air occluded within the sample was increased, so that the change in the attenuation coefficient is proportional to the amount of air within the sample. This observation suggests that the attenuation can be modeled by a background matrix value plus a contribution due to scattering and absorption from the bubbles, given by the product of the number density of bubbles and the ultrasonic scattering/absorption cross section. While further measurements as a function of frequency are still needed to further test this hypothesis and investigate the frequency dependence of the cross section, this simple physical interpretation of these attenuation measurements does suggest an important

potential application: it might be possible to use ultrasonic measurements to determine both the concentration and the size distribution of air bubbles in dough once definitive measurements of the cross section have been performed.

For the same samples, the velocity of longitudinal ultrasonic waves was also found to change considerably as the amount of air within the sample was varied, with the velocity varying by more than an order of magnitude as the void fraction ϕ was varied from 0.01 to 0.07. To understand this dramatic change in the velocity, a different theoretical approach was used, based on an effective medium model for the (static) elastic moduli of a heterogeneous system with dispersed inclusions. This model allowed us to show that, in addition to an explicit dependence on the void fraction, much of the variation of the velocity results from a surprisingly large change in the shear modulus of the dough matrix as ϕ is varied. These results point to another potential application of the ultrasonic velocity measurements, namely providing a means of probing changes in the intermolecular bonding in the dough matrix as the mixing environment is manipulated.

When yeast was added to the dough, thus allowing fermentation to take place, we found that both the ultrasonic velocity and attenuation were sensitive to the resulting increase in the size of the air bubbles. To gain a better understanding of the effect of the bubble expansion, the dough was mixed at the two extreme mixing headspace pressures, i.e., at ambient pressure and at 0.13 atm. The ultrasonic velocity was found to decrease as the bubbles expanded, with a much larger decrease in the case where the dough was mixed at vacuum. By relating the change in the velocity to the corresponding change in the density during fermentation, it was found that there are two distinct mechanisms that

contribute to the large changes in the velocity found experimentally. The first is the direct dependence on the size and number density of the bubbles already alluded to above. The second mechanism is especially important at early fermentation times and arises from changes in the shear moduli of the matrix. These changes occur as the dissolved CO₂ molecules diffuse through the matrix, causing a drop in the pH and an associated weakening of the intermolecular interactions due to protein chain charge repulsion effects. Thus, our experiments demonstrate the important interplay between the effects of gas bubbles and matrix interactions in determining the mechanical properties of dough during fermentation, and suggest a new way of measuring these important changes quantitatively.

6.2 The effect of air cells on the mechanical properties of breadcrumb

The second area of research that was covered in this thesis was the investigation of the role of the air cells in determining the mechanical properties of freeze-dried breadcrumb, using the same low frequency ultrasonic technique. Freeze-dried breadcrumb samples were used since freeze-drying greatly facilitates the ability to carry out ultrasonic experiments reliably while accurately preserving the breadcrumb structure. The cell size was varied by varying the proofing time, allowing us to demonstrate that both the velocity and attenuation are quite sensitive to these changes. The attenuation coefficient was found to decrease as the gas cells got smaller, i.e., as the density increased, consistent with the simple physical picture that scattering and absorption is decreased when the sizes of the cells become smaller relative to the ultrasonic wavelength. By contrast, the ultrasonic velocity was found to increase as the density of

the breadcrumb was increased, varying approximately as the square root of the density. These velocity data were interpreted using two complementary approaches: a model for the static elasticity of foams, due to Gibson and Ashby (1997), and a tortuosity model, developed by Johnson and Sen (1981). In contrast to the Gibson and Ashby model, the tortuosity model is based on a wave propagation picture, which is valid in cases of extreme acoustic contrast between constituent materials, where the wave is confined to the tortuous pathways along only one of the materials. Both models gave a satisfactory description of the experimental velocity data, although the Gibson and Ashby model for open cell foams does appear to give a better account of the density dependence. Nonetheless, it is difficult to make a connection at the microscopic level between the observed structure of breadcrumb and the simple beam bending arguments on which the predictions of the Gibson and Ashby model are based.

To study the effects of anisotropy on the mechanical properties of breadcrumb, we performed a set of experiments in which the samples were compressed uniaxially, thereby changing the shape of the voids to partially oriented, pancake-shaped ellipsoids. Large differences were found in the ultrasonic velocity depending on the direction of propagation relative to the compression direction, although the signal amplitude was found to be rather insensitive to the anisotropy. Our velocity data were compared with the predictions of both the Gibson and Ashby model and the tortuosity model, by plotting the ratio of the longitudinal moduli parallel and perpendicular to the compression direction as a function of the anisotropy parameter R . We found that for weak anisotropy, the Gibson and Ashby model gives better agreement with our data for the elastic anisotropy ratio, while the tortuosity model appears to work better at large

anisotropies. One advantage of the tortuosity model is that it is relatively straightforward to calculate not only the elastic anisotropy ratio but also the void fraction dependence of the velocity both parallel and perpendicular to the strain direction. This allowed us to infer that there must be an additional weakening of the cell walls caused by the uniaxial compression, over and above the effects resulting from anisotropy in the structure alone. These experiments show that useful information can be obtained on the change in both size and shape of the air cells in breadcrumb using ultrasonic velocity and attenuation measurements.

In conclusion, I have demonstrated that ultrasound can be used to investigate the effect of the air bubbles on mechanical properties of the dough and the effect of the air cells on the mechanical properties of the breadcrumb. The sensitivity of this non-destructive technique to such changes provides the food science community with a tool that can supply valuable information about the mechanical and structural properties of these systems.

6.3 Recommendations for future work

The results presented in this thesis have demonstrated that ultrasound techniques have enormous potential for learning about the mechanical properties of aerated cellular food materials. Some examples of future work that are suggested by our experimental findings are as follows:

- 1) One important extension of the current experiments is to perform similar experiments on doughs prepared using a variety of flours. The main differences between different types of flours are their "strengths", which are related to their protein content and

manifest in different degrees of interaction between the gluten molecules. Because, as we have shown, the ultrasonic velocity in dough can be strongly influenced by the nature of the intermolecular interactions, these experiments may provide a new way of probing dough “strength” and hence aid in predicting flour quality.

2) A second experiment is to perform experiments on dough over a wide range of frequencies, in order to measure the frequency dependence of the velocity and attenuation associated with resonant scattering and absorption by the bubbles. By analogy with the behavior of air bubbles in water, we expect the bubble resonances to occur at higher frequencies than those used in the experiments reported in this thesis. While these experiments will no doubt be challenging technically, their successful execution along with the development of a quantitative model for bubble resonances in a viscoelastic medium, would enable the bubble size distribution to be measured using ultrasonic techniques.

3) A third experiment is to measure the ultrasonic velocity and attenuation at $\phi = 0$, which will require mixing the dough under real vacuum conditions. Since we have not been able to reduce the pressure below about 0.1 atm, using the mixer available for the current experiments, this experiment has not been feasible so far in our laboratory. The results of this proposed experiment will provide additional information about the matrix contribution to the velocity and attenuation and confirm the analysis of the ultrasonic data using the effective medium model.

4) For the yeasted dough, the most important next step is to determine the void fraction just after mixing is completed. This will probably best be achieved using image analysis techniques.

5) For yeasted dough, it will also be important to devise a way of reliably measuring the absolute attenuation, so that a quantitative analysis of ultrasonic velocity and attenuation will be possible using the effective medium theory. This should give reliable information on the expected changes in the shear moduli of the matrix, and how they are affected by dissolved CO₂ molecules. Such experiments should give important new information on the mechanical properties of the fermenting dough at early times, when the density of the dough is hardly changing.

6) For the second material studied in this thesis, breadcrumb, several experiments are also recommended. One experiment is to use detailed image analysis to investigate the effects of missing cell walls resulting from coalescence due to bubble inflation. As for dough, a second recommended experiment is to use different flours to obtain breadcrumb samples of different strengths, and to investigate how this affects the structure of breadcrumb using our ultrasonic techniques.

References

- AACC. (1983). In *Approved Methods of the American Association of Cereal Chemists Vol. II* (8th ed.) American Association of Cereal Chemists, Inc. St. Paul, Minnesota.
- Agricultural Research Council (1982). Report of ARC Working Party on Transducers. HMSO. London.
- Ablett, S., Attenburrow, G.E. and Lillford, P.J. (1986). In *Chemistry and Physics of Baking*. Ed. by J.M.V. Blanshard, P.J. Frazier, and T. Galliard. The Royal Society of Chemistry, Nottingham. UK.
- Anderson, H.L. (1989) *A Physicist's Desk Reference* American Institute of Physics, New York. USA.
- Anderson, S., Hyde, S.T., Larsson, K. and Lidin, S. (1988). *Chem. Rev.*, **88**:221.
- Bailey, C.H. (1944). *The Constituents of Wheat Cereals and Wheat Products*. Reinhold Publishing Co., New York.
- Baker, J.C. (1941). *Cereal Chem.* **18**:34.
- Baker, J.C. (1957). *The Bakers Digest* **31** (5):64.
- Baker, J.C. and Mize, M.D. (1937). *Cereal Chem.* **14**:721.
- Baker, J.C. and Mize, M.D. (1939). *Cereal Chem.* **16**:213.
- Baker, J.C. and Mize, M.D. (1941a). *Cereal Chem.* **18**:19.
- Baker, J.C. and Mize, M.D. (1941b). *Cereal Chem.* **18**:34.
- Baker, J.C., Parker, H.K. and Mize, M.D. (1946). *Cereal Chem.* **23**:16.
- Bietz, J.A. (1974). *The Bakers Digest* **48**(1):265.
- Bietz, J.A. and Wall, J.S. (1975). *Cereal Chem.* **52**:145
- Bloksma, A.H. (1962). *Rheol. Acta* **2**:217.
- Bloksma, A.H. (1971). *Elasticity, Plasticity and the Structure of Matter*. Ed. by R. Houwink and H.K. de Decker, p.391.
- Bloksma, A.H. (1972). *J. Texture Studies* **3**:3.
- Bloksma, A.H. (1974). *The Bakers Digest* **38**(4):53.
- Bloksma, A.H. (1981). *Cereal Chem.* **58**:481.
- Bloksma, A.H. (1990a). *Cereal Foods World* **35**:237
- Bloksma, A.H. (1990b). *Cereal Foods World* **35**:244

- Bloksma, A.H.** and Meppelink, E.K. (1973). *J. Texture Studies* 4:145.
- Bohlin, L.** and Carlson, T. (1981). *Colloids Surf.* 2:59.
- Booth, M.R.** and Melvin, M.A. (1979). *J. Sci. Food Agric.* 30:1057.
- Brown, R.J.S.** (1980). *Geophysics* 45:1269.
- Bushuk, W.** (1987). In *Rheology of Wheat Products* Ed. by H. Faridi. American Association of Cereal Chemists. St. Paul Minnesota, USA.
- Bushuk, W.** and Mehotra, V.K. (1977). *Cereal Chem.* 54:320.
- Bushuk, W.**, and Tsen, C.C. (1968). *The Bakers Digest* 42(4):36.
- Campbell, G.M.**, (1991). *The Aeration of Bread Dough During Mixing* Ph.D. Thesis. University of Cambridge, England.
- Campbell, G.M.**, Rielly, C.D., Fryer, P.J. and Saad, P.A. (1998). *Cereal Foods World* 43:163
- Campbell, G.M.** and Shah, P. (1999). In *Bubbles in Food*, Ed. by G.M. Campbell, C. Webb, S.S. Pandiella and K. Niranjan. American Association of Cereal Chemists. St. Paul, Minnesota. p. 11.
- Campbell, L.E.**, and Schoenleber, L.G. (1994). *Agric. Eng.* 57:239
- Carlson, T. L.G.** (1981). *Law and Order in Wheat Flour Dough. Colloidal Aspects of Wheat Flour Dough and its Lipid and Protein Constituents in Aqueous Media.* Ph.D. Thesis. Lund University, Lund.
- Carlson, T.** and Bohlin, L. (1978). *Cereal Chem.* 55:539.
- Cauvain, S.P.** (1999). In *Technology of Breadmaking*, Ed. by S.P. Cauvain and L.S. Young. Aspen Publisher, Inc. Gaithersburg, MD pp. 18-44.
- Cauvain, S.P.** Whitworth, M.B., Alava, J.M. (1999). In *Bubbles in Food*, Ed. by G.M. Campbell, C. Webb, S.S. Pandiella and K. Niranjan. American Association of Cereal Chemists, St. Paul, Minnesota.
- Chen, P.**, Whitney, L.F. and Peleg, M. (1994). *J. Texture Studies* 25:299.
- Chuah, S.L.**, and Scanlon, M.G. (2001). *IFT Annual Meeting*. IFT, New Orleans.
- Chui, D.S.** and Mark, J.E. (1977). *Colloid. Polym. Sci.* 255:644.
- Collatz, F.A.** (1943). *Association of Official Agricultural Chemists* 26 No.1:107.
- Cordonier, M.** (1999). *World Grain* 42(3):44.
- Cornell, H.J.** and Hoveling, A.W. (1998). *Wheat Chemistry and Utilization*, Technomic

Publishing Company, Inc., Pennsylvania. U.S.A.

- Cornford, S.J., Axford, D.W.E., and Elton, G.A.H. (1964). *Cereal Chem.* 41:216.
- Coulton, G.G. (1925). *The Medieval Village*. University Press, Cambridge. pp. 55-58.
- Coulson, C.A. (1955). *Waxes* Oliver and Boyd, Edinburgh. Chapter 6.
- Cowan, M.L., Beaty, K., Page, J.H., Liu, Z. and Sheng, P. (1998). *Phys. Rev. E.* 58: 6626.
- D'Appolonia, B.L., Gilles, K.A. and Medcalf, D.G. (1970) *Cereal Chem.* 147:194.
- Dubois, D.K. and Vetter, J.L. (1987). *White, whole wheat and multi-grain bread, a survey of formula and processes*. AIB Bull. 9:2.
- Eliasson, A. and Larsson, K. (1993), *Cereals in Breadmaking: A Colloidal Approach*. Marcel Dekker Inc., New York, USA.
- Elion, E. (1940). *Cereal Chem.* 17:573.
- Elmer, J.C. and Reed, G. (1968). *The Bakers Digest* 42(6):22
- Encyclopedia Britannica, Encyclopaedia Britannica, Inc. William Benton, Chicago. (1979). Vol. II. pp. 247.
- Fairley, P. (1992). *Ultrasonic Studies of Food Containing Air*. Ph.D. Thesis. Leeds University, U.K.
- Faubion, J.M., Dreese, P.C. and Diehl, K.C. (1985). In *Rheology of Wheat Products* Ed. by H. Faridi. American Association of Cereal Chemists. St. Paul, Minnesota, USA.
- Finney, K.F. (1943). *Cereal Chem.* 20:20.
- Finney, K.F. (1984). *Cereal Chem.* 61:20
- Finney, K.F. and Shogren, M.D. (1972). *The Bakers Digest* 46(2):32.
- Flory, P.J. and Rehner, J. (1943). *J. Chem. Phys.* 11:521.
- Fogler, H.S. and Goddard, J.D. (1970). *Phys. Fluids* 13:1135.
- Freilich, J. (1949). *The Bakers Digest* 33(3):27.
- Funt Bar-David, C.B. and Lerchenthal, C.H. (1975). *Cereal Chem.* 52:154.
- Gaunaurd, G.C. and Uberall, H. (1981). *J. Acoustic Soc. Am.* 69(2):362.
- Garver, J.C., Navarini, I. and Swanson, A.M. (1966). *Cereal Sci. Today* 11(9):410.
- Gent, A.N. and Tobias, R.H. (1982). *J. Polym. Sci., Polym. Phys. Ed.* 20:2051.
- Gibson, L.J., and Ashby, M.F. (1997). *Cellular Solids: Structure and Properties* (2nd Ed.) Cambridge: University Press.
- Gibson, L.J., and Ashby, M.F. (1982a). *Proc. R. Soc. Lond., Series A* 38:25.

- Gibson, L.J., and Ashby, M.F. (1982b). *Proc. R. Soc. Lond, Series A* **38**:43.
- Glass, R.L. (1960) *Cereal Sci. Today* **5**(3):60.
- Gross, H., Bell, R.L. and Redfern, S. (1966). *Cereal Science Today* **11**: 419.
- Halton, P. and Scott Blair, G.W. (1936). *J. Phys. Chem.* **40**:561.
- Harbrecht, A., and Kautzmann, R. (1968). *The Bakers Digest.* **46**(5): 22
- Hibberd, G.E. and Parker, N.S. (1979). *Cereal Chem.* **56**:232.
- Hlynka, I. (1970). *The Bakers Digest* **44**(2):125.
- Hlynka, I. (1972). *The Bakers Digest* **46**(2):44.
- Holmes, J.T. and Hosney, R.C. (1987). *Cereal Chem.* **64**:343.
- Hosney, R.C. (1986). *The Principles of Cereal Science and Technology*. American Association of Cereal Chemists. Inc. St. Paul, Minnesota, U.S.A. pp. 69.
- Hosney, R.C. and Finney, P.L. (1974). *The Bakers Digest* **48**(1):22.
- Hosney, R.C., Finney, K.F., Pomeranz, Y. and Shogren, M.D. (1969). *Cereal Chem.* **46**:606.
- Hosney, R.C., Finney, K.F., Pomeranz, Y. and Shogren, M.D. (1971). *Cereal Chem.* **48**:191.
- Irvine, G.N. and McMullen, M.E. (1960). *Cereal Chem.* **37**:603.
- Ishimaru, A. (1978). *Wave Propagation and Scattering in Random Media*, Vol. I and II. Academic Press, New York.
- Johnson, D.L. and Plona, T.J (1982). *J. Acoust. Soc. Am.* **72**:556.
- Johnson, D.L., Plona, T.J. and Scala, C. (1982). *Phys. Rev. Lett.* **29**:1840.
- Johnson, D.L. and Sen, P.N. (1981). *Phys. Rev. B* **24**:2486.
- Junge, R.C., Hosney, R.C., and Varriano-Marston, E. (1981). *Cereal Chem.* **58**:316.
- Kasarda, D.D., Bernardin, J.E. and Nimmo, C.C. (1971). *Adv. Cereal Sci. Technol.* **1**:158.
- Kent, N.L. (1983). *Technology of Cereals*, 3rd Ed. Pergamon Press Ltd., Tarrytown, New York, USA. Ch.8.
- Kent, N.L. and Evers, A.D. (1994). *Kent's Technology of Cereals*, 4th Ed. Elsevier Science Ltd., Tarrytown, New York.
- Kilborn, R.H. and Dempster, C.J. (1965) *Cereal Chem.* **42**:432.
- Kilborn, R.H. and Tipples, K.H. (1972). *Cereal Chem.* **49**:34.

- Kilborn, R.H. and Tipples, K.H. (1981a). *Cereal Foods World*. 26:624.
- Kilborn, R.H. and Tipples, K.H. (1981b). *Cereal Foods World*. 26:628.
- Kinsler, L.E., Coppens, A.B., and Sanders, J.V. (1982). *Fundamentals of Acoustics*. 3rd Ed. John Wiley, New York.
- Kulp, H. (1991). In *Handbook of Cereal Science and Technology*. Ed. by K.J. Lorenz and K. Kulp. Marcel Dekker, New York, p. 639.
- Lambert, W. (1982). *Chemical Engineering*, August/September, 320.
- Launay, B. and Bure, J. (1974). *Cereal Chem.* 51:151
- Launay, B. and Bure, J. (1987). in: *Physical Properties of Foods 2*. Ed. by R. Jowitt, E. Escher, M. Kent, B. McKenna and M. Roques. Elsevier Applied Science, London. p.455.
- Lasztity, R. (1980). *J. Texture Studies* 11:81.
- Lee, H.O., Luan, H. and Daut, D.G. (1992). *J. Food Eng.* 16:127.
- Leighton, T.G. (1997). *The Acoustic Bubble*, Academic Press, Inc., San Diego.
- Letang, C., Piau, M. & Verdier, C. (1996). *Les Cahiers de Rheologie* 15:319.
- Lister, D. (1984). *Measurements of Body Composition in Meat Animals*. Applied Science Publishers, London. Ch. 3.
- Longton, J. and LeGrays, G.A. (1981). *Starch/Starke* 33:410.
- MacRitchie, F. J. (1976). *Cereal Chem.* 53:318.
- Manners, D.J. and Matheson, N.K. (1981). *Food Res. Int.* 90:99.
- Mason, T.J., and Lorimer, J.P. (1989). *Sonochemistry: Theory, Application and Uses of Ultrasound in Chemistry*. Ellis, Horwood, Chichester, UK.
- Marston, P.E. and Wann, T.L. (1976). *The Bakers Digest* 50(4):24.
- Matsumoto, H., (1973). *The Bakers Digest* 48(5): 40.
- Matsumoto, H. and Nishiyama, J. (1973). *Cereal Chem.* 50:363.
- Matsumoto, H., Nishiyama, J. and Hlynka, I. (1971). *Cereal Chem.* 48:669.
- McClements, D.J. (1994). *Colloids and Surfaces A: Physicochemical and Engineering Aspects* 90:25.
- McClements, D.J., Povey, M.J.W. and Dickinson, E. (1993) *Ultrasonics* 31:433.
- McGee, H. (1984). *On Food and Cooking*. George Allen & Unwin (Publishers) Ltd., London.

- Mifflin, B.J., Field, J.M. and Shewry, P.R. (1983). In *Seed Protein*, Ed. by J. Daussant and J. Vaughan. Soc. Eur. Symp. Ser. No. 20, Academic Press. London, p. 255.
- Miller, B.S. and Johnson, J.A. (1946). *The Bakers Digest* 21(5):38.
- Moore, W.R. and Hosney, R.C. (1985). *Cereal Foods World* 30:791.
- Moorjani, R. (1984). *An Investigation into the Acoustics of Bread Doughs*. Master of Science Thesis, University of Leeds, Leeds, UK.
- Moss, R. (1974). *Cereal Sci. Today* 19:557.
- Morse, E, Rivers, J. and Houghan, A. (1988). *The family Guide to Food and Health* Barrie and Jenkins Ltd., London.
- Muller, H.G. (1969). *Cereal Chem.* 46:443.
- Nelson, J.H., Glass, R.L. and Geddes, W.F. (1963) *Cereal Chem.* 40: 343.
- Nussinovitch, A., Roy, I. And Peleg, M. (1990). *Cereal Chem.* 67:101.
- Nye, J.F. (1972). *Physical Properties of Crystals* University Press, Oxford, UK.
- Page, J.H, Sheng, P., Schriemer, H.P., Jones, I., Jing, X. and Weitz, D.A. (1996) *Science*. 271:634
- Payne, P.I., Jackson, E.A. and Holt, L.M. (1984). *J. Cereal Sci.* 2:73.
- Peleg, M. (1997). *Food Sci. Technol., Int.* 23:127.
- Persaud, J.N., Faubion, J.M. and Ponte, J.G.Jr. (1990). *Cereal Chem.* 67:92.
- Piazza, L. and Masi, P. (1995). *Cereal Chem.* 72:320.
- Pomeranz, Y., Chung, O.K. and Robinson, R.J. (1966). *J. Am. Oil Chemists Soc.* 43:45.
- Pomeranz, Y., Meyer, D., and Seibel, W. (1984). *Cereal Chem.* 61:53.
- Pomeranz, Y., Rubenthaler, G. and Finney, K.F. (1966). *Food Technol.* 20(3):95.
- Ponte, J.G.Jr. and Faubion, J.M. (1987). In *Rheology of Wheat Products* Ed. by H. Faridi. The American Association of Cereal Chemists, Inc. St. Paul, Minnesota, pp. 241.
- Ponte, J.G.Jr. and Ovadia, D.Z. (1996). In: *Baked Goods Freshness*. Ed. by: R.E. Hebeda and H.F. Zobel. Marcel Dekker, Inc., New York, pp. 151-170.
- Potter, N.N. (1986) *Food Science* The Avi Publishing Company, Inc. Westport, USA, pp 247
- Powers, J.M. (1967). *Eucharistic Technology*; Header and Header, New York, pp. 13.
- Povey, M.J.W. (1998). In: *Ultrasound in Food Processing*. Ed by M. J. W. Povey and T. G. Mason. Chapman and Hall, London, UK, p 31.
- Povey, M.J.W. (1997). *Ultrasonic Techniques for Fluid Characterization*. Academic Press, San Diego.

- Preston, K.R., Kilborn, R.H. and Black, H.C. (1982). *Can. Inst. Food Sci. Technol. J.* 15(1):29.
- Pylar, E.J. (1967). *The Bakers Digest* 41(3):55.
- Pylar, E.J. (1988). *Baking Science and Technology*. Sosland Publishing Comp., Merriam, Kansas, USA.
- Rohm, H., Jaros, D., and deHann, M. (1997). *J. Texture Studies*, 28:245.
- Sapirstein, H.D. (1999). In *Bubbles in Food*, Ed. by G.M. Campbell, C. Webb, S.S. Pandiella and K. Niranjana. American Association of Cereal Chemists, St. Paul, Minnesota.
- Satin, M. (1988). *New Sci.*, 56:59.
- Scanlon, M.G., Fahloul, D. and Sapirstein, H.D. (1997). *Cereal Chem.* 74:612.
- Scanlon, M.G. and Zghal, C.M. (2001). *Food Res. Int.* In press.
- Schofield, D. (1986). In *Chemistry and Physics of Baking*. Ed. by J.M. Blanshard, P.J. Frazier and T. Galliard. The Royal Society of Chemistry, London, England, p. 14.
- Schofield, R.K. and Scott Blair, G.W. (1932). *Proc. R. Soc. Lond. Series.A* 138:707
- Schofield, R.K. and Scott Blair, G.W. (1933a). *Proc. R. Soc. Lond. Series.A* 139:557
- Schofield, R.K. and Scott Blair, G.W. (1933b). *Proc. R. Soc. Lond. Series.A* 141:72
- Schofield, R.K. and Scott Blair, G.W. (1937). *Proc. R. Soc. Lond. Series.A* 160:87.
- Schriemer, H.P., Cowan, M.L., Page, J.H., Sheng, P., Liu, Z. and Weitz, D.A. (1997). *Phys. Rev. Lett.* 79: 3166.
- Schwartz, L.M. and Johnson, D.L. (1984). *Phys. Rev. B* 30:4302.
- Siffering, K. and Bruinsma, B. L. (1993). *Cereal Chem.* 70:351.
- Shimiya, Y. and Nakamura, K. (1997). *J. Texture Studies* 28:273.
- Sheng, P (1988). In *Homogenization and Effective Moduli of Materials and Media*, ed. by J.L. Ericksen, D. Kinderlehrer, R. Kohn and J.-L. Lions. Springer, p. 196.
- Silva, M.J. and Gibson, L.J. (1997). *Int. J. Mech. Sci.* 39:549.
- Singh, N.K., Donovan, G.R., Batey, I.L. and MacRitchie, F. (1990). *Cereal Chem.* 67(2):150.
- Smith, R.E.F. (1977). *Peasant Farming in Muscovy*. University Press, Cambridge p. 74.
- Soulaka, A. B., and Morrison, W.R., (1985). *J. Sci. Food Agric.* 36:709.
- Thorn, J.A. and Ross, J.W. (1960). *Cereal Chem.* 37:415

- Tipples, K.H.** (1960). *The Bakers Digest* 34(3):49.
- Treloar, L.R.G.** (1958). *The Physics of Rubber Elasticity*, 2nd Ed., Clarendon Press, Oxford, UK.
- Tsen, C.C.** (1973). *The Bakers Digest* 47(6):50.
- Urlick, R.J.** (1947). *J. Appl. Phys.* 18:983.
- van Dam, H.W.** (1986). In: *Chemistry and Physics of Baking*. Ed. by J.M. Blanshard, P.J. Frazier and T. Galliard. The Royal Society of Chemistry, London, England. p.117.
- Veyne, P.** (1990). *Bread and Circuses*. Translated by Pearce, B. The Penguin Group, London. pp. 97-100 and 236-245.
- Vliet, T. Van, Janssen, A.M., Bloksma, A.H. and Walstra, P.** (1992). *J. Texture Studies* 23:439.
- Walden, C.C.,** (1959). *The Baker's Digest* 33(1):24.
- Wassermann, L.** (1973). In *Food Texture and Rheology*. Ed. by P. Sherman. Academic Press Inc., London, UK.
- Webb, T., Heaps, P.W., Russell Eggitt, P.W. and Coppock, J.B.M.** (1970). *J. Food Technol.* 5: 65.
- Wehrli, H.P., and Pomeranz, Y.** (1970). *Cereal Chem.* 47:160.
- Westerlund, E. Theander, O. and Aman, P.** (1989). *J. Cereal Sci.* 10:139.
- Whitworth, M. B. and Alava, J.M.** (1999). In *Bubbles in Food*. Ed. by G.M. Campbell, C. Webb, S.S. Pandiella, and K. Niranjana. American Association of Cereal Chemists, St. Paul, Minnesota.
- Wolforn, M.L. and Elkhadem, H.** (1975). In *Starch: Chemistry and Technology*, Vol. 1. Ed. by R. L. Whitler and E.F. Paschall. Academic Press, New York. p.251
- Wood, A.B.** (1941). *A Textbook of Sound*, G. Bell and Sons, London. p.361.
- Yoneyama, T. Suzuki, I., and Murohashi, M.** (1970). *Cereal Chem.* 47:27.
- Zhang, Z.Q., Jones, I.P., Schriemer, H.P., Page, J.H., Weitz, D.A. and Sheng, P.** (1999). *Phys. Rev. E* 60, 4843
- Zghal, C.M.,** (2000). *The Relationship Between Bread Physical Texture and its Structure Determined by Digital Image Analysis*. Master of Science Thesis, University of Manitoba, Canada.
- Zghal, C.M., Scanlon, M.G. and Sapirstein, H. D.** (1999). *Cereal Chem.* 76:734.

Zghal, C.M., Scanlon, M.G. and Sapirstein, H. D. (2001). Submitted to *J. Cereal Sci.*